THE STUDY OF LOCALISED SOLUTION IN LASER PLASMA SYSTEM

By

DEEPA VERMA

PHYS06201104010

INSTITUTE FOR PLASMA RESEARCH, GANDHINAGAR

A thesis submitted to the
Board of Studies in Physical Sciences

In partial fulfillment of requirements

for the Degree of

DOCTOR OF PHILOSOPHY

of

HOMI BHABHA NATIONAL INSTITUTE

January 2017

Homi Bhabha National Institute[1]

Recommendations of the Viva Voce Committee

As members of the Viva Voce Committee, we certify that we have read the dissertation prepared by **Deepa Verma** entitled **"The Study of localized solutions in laser plasma system"** and recommend that it may be accepted as fulfilling the thesis requirement for the award of Degree of Doctor of Philosophy.

Chairman : Prof. Subroto Mukherjee		**Date:** 21/8/17
Guide / Convener : Prof. Amita Das	Amita Das	**Date:** 21-8-17
Co-guide :		**Date:**
Examiner : Prof. M. Krishnamurthy		**Date:** 21/8/17
Member : Prof. Abhijit Sen		**Date:** 21.8.17
Member : Prof. Sudip Sengupta		**Date:** 21/08/2017

Final approval and acceptance of this thesis is contingent upon the candidate's submission of the final copies of the thesis to HBNI.

I hereby certify that I have read this thesis prepared under my direction and recommend that it may be accepted as fulfilling the thesis requirement.

Date:

Place: Gandhinagar

Amita Das

Guide: Amita Das

STATEMENT BY AUTHOR

This dissertation has been submitted in partial fulfillment of requirements for an advanced degree at Homi Bhabha National Institute (HBNI) and is deposited in the Library to be made available to borrowers under rules of the HBNI.

Brief quotations from this dissertation are allowable without special permission, provided that accurate acknowledgement of source is made. Requests for permission for extended quotation from or reproduction of this manuscript in whole or in part may be granted by the Competent Authority of HBNI when in his or her judgment the proposed use of the material is in the interests of scholarship. In all other instances, however, permission must be obtained from the author.

Deepa Verma

DEEPA VERMA

DECLARATION

I, hereby declare that the investigation presented in the thesis has been carried out by me. The work is original and the work has not been submitted earlier as a whole or in part for a degree/diploma at this or any other Institution or University.

Deepa Verma

DEEPA VERMA

List of Publications arising from the thesis

Journals:

- **The study of electromagnetic cusp solitons**,
  Deepa Verma, Amita Das, Predhiman Kaw, and Sanat Kumar Tiwari
  Physics of Plasmas (22), 013101 (2015)

- **The stability of 1-D soliton in transverse direction**,
  Deepa Verma, Ratan Kumar Bera, Amita Das, and Predhiman Kaw.
  Physics of Plasmas (23), 123102 (2016);

- **Observation of 1-D time dependent non propagating laser plasma structures using Fluid and PIC codes**,
  Deepa Verma, Ratan Kumar Bera,Atul Kumar, Bhavesh Patel and Amita Das
  Physics of Plasmas (POP52936), Under Communication

- **Observation of 1-D time dependent propagating laser plasma structures using Fluid and PIC codes**,
  Deepa Verma, Ratan Kumar Bera, Bhavesh Patel and Amita Das
  To be submitted

Conferences:

International Participation

- Localized solutions in laser plasma coupled system with periodic time dependence (**Poster presentation**)
  Deepa Verma, Amita Das, Bhavesh Patel and Predhiman Kaw Asia Plasma And Fusion Association (APFA), 14-18 DEC 2015, Gandhinagar, India.

- Formation and dynamical evolution of relativistic electromagnetic cusp soliton in plasma (**Poster presentation**)
  Deepa Verma, Amita Das, Predhiman Kaw and Sanat Kumar Tiwari
  ASHULA-2015, 20-21 January, 2015 Lonavala, Maharashtra, India.

- Relativistic electromagnetic solitons in cold plasmas (**Poster presentation**)
  Amita Das, Sita Sundar, Deepa Verma and Predhiman Kaw
  Laser and Plasma Accelerator Workshop, 1-6 Sep, 2013 in Goa, India.

National Participation

- Characterization of relativistic electromagnetic soliton in plasma (**Poster presentation**)
  Deepa Verma, Amita Das, Predhiman Kaw and Sanat Kumar Tiwari
  PSSI-2014, 8-11 Dec 2014, Kottayam, Kerala, India.

- Study of cusp solitons in plasma (**Poster presentation**)
  Deepa Verma, Amita Das and Predhiman Kaw
  8th CNSD, IIT, Indore, India, 11-14 December 2013.

- A study of black hole (**Talk**)
  Deepa Verma
  9th PLANEX Workshop, Rajasthan University, Jaipur, 2009.

Schools:

- Observation of time dependent 1-D localized structures in laser plasma system (**Poster presentation**)
  Deepa Verma, Amita Das, Bhavesh Patel and Predhiman Kaw
  International School on Ultra-Intense Lasers (ISUIL), 4-9 October 2015, Russia

- DST SERC School on Tokamaks and Magnetized Plasma Fusion.
  25-15 Mar 2013, Institute for Plasma Research, Gandhinagar, India

Deepa Verma

DEEPA VERMA

Dedicated to

My family and friends

ACKNOWLEDGEMENTS

Here I take the opportunity to acknowledge people whose support kept me moving during the period of my Ph.D. First and foremost I would like to express my sincere gratitude to my thesis supervisor Prof. Amita Das for her guidance. I am also thankful to my review committee members Prof. Predhiman Kaw, Prof. Abhijit Sen and Prof. Sudip Sengupta for providing their useful suggestions during reviews which helped me to improve my thesis.

I wish to thanks Dr. Sudip Sengupta, Dr. Prabal Chattopadyay, Dr. Joydeep Ghosh, Dr. Subrato Mukharji, Dr. R. Ganesh, Dr. Mrityunjay Kundu, Dr. Shantanu Kumar Karkari, Dr. Devendra Sharma, Dr. G. Ravi and Dr. Surya P. Pathak for their endurance while teaching us during the 1st year course work.

I would also like to convey my sincere thanks to computer center staff, library staff and the administration staff at the IPR for always being cooperative. Thanks to all my seniors (Dr.) Pintu, Ritu, Maya, Vikrant, Shekhar, Sharad, Jugal, Satya, Sita, Gurudatt, Vikram, Ujjwal, Ashwin, Kshitish, Deepak, Prabal, Sanat, Sushil, Rameswar, Pravesh, Sayak, Manjeet, Soumen, Aditya, Vikram Jr., Rana for their wonderful company in the hostel and their co-operation whenever needed. I would like to thanks, Akanksha, Vidhi, Vara, Neeraj, Roopendra, Bibhu, Mangilal, Harish, Megharaj, Sameer, Chandrasekhar, Veda, Sandeep, Dushyant and all my juniors for providing me a homely atmosphere in hostel and the institute.

Special thanks to (Dr.) Bhavesh Patel, Sanat Kumar Tiwari and Vikram Singh Darodhi for their support and patience while teaching me numerical techniques. I thank Avadhesh for all his technical and other official support as it helped me to focus primarily on my research work. My colleagues and friends from theory room Sanat Kumar Tiwari, Vikram Dharodi, Chandrasekhar, Avadhesh, Ratan, Atul, and Sandeep are always special to me. They were around me in all ups and down during my Ph.D. tenure.

I would like to make a special mention of Anjali, Bindu, Monika, Swati, Akanksha,

Vidhi, Meenakshi and Prabhakar for the numerous discussions, encouragement, care and for always listening to me with all their patience.

I take this opportunity to thank my teacher Mrs. Alka Rastogi for motivating me to pursue higher studies. My heartfelt gratitude to my parents, and brother Deepak, for their goodwill and support all through my life. I would like to thank Vijay Verma, Sanjay Verma and Baby Verma, whose continuous support and faith in me motivated me to pursue a research career.

Contents

Synopsis iv
List of Figures xi
List of Tables xv

1 Introduction **3**
1.1 Background and Motivation 4
1.2 Laser Plasma Interaction: An introduction 5
1.3 Review of earlier works 10
1.4 Content and organization of the thesis 12
1.4.1 Study of electromagnetic Cusp Solitons 12
1.4.2 Dynamical study of 1-D soliton in transverse direction . . . 13
1.4.3 Observation of the time-dependent 1-D localized structures in laser plasma system with fluid simulations 14
1.4.4 Observation of time-dependent 1-D localized structures in laser plasma system with Particle in cell simulations 15
1.5 Conclusion and future scope of the thesis 16

2 Study of Electromagnetic Cusp Solitons **17**
2.1 Introduction 17
2.2 Governing equations 20
2.3 Exact and Analytical Cusp solutions with Ion dynamical response . 23
2.4 Dynamical Evolution of Cusp Solution and its instability 30
2.4.1 Numerical simulation 31
2.4.2 Evolution of Cusp Solution and instability 31
2.5 Summary 37

3 The stability of 1-D soliton in transverse direction **39**
3.1 Introduction 39
3.2 Fluid simulation on 2-D study of electromagnetic solitons 40
3.3 Numerical observations of transverse instability 42
3.3.1 Single peak structures 42
3.3.2 Paired solitonic structures 46
3.3.3 Multiple peak structures 48

3.4 Comparison of analytical and numerical growth rates 51
3.5 Nonlinear development of the instability 54
3.6 Summary 56

4 Observation of time-dependent 1-D localized structures in laser plasma system with fluid simulations 59
4.1 Introduction 60
4.2 Numerical simulation technique 62
4.3 Evolution of spontaneously formed structures 63
4.4 Evolution of significantly perturbed stable structures 67
4.4.1 Evolution of perturbed static structures 68
4.4.2 Evolution of perturbed propagating structures 77
4.5 Summary and Discussion 83

5 Time-dependent 1-D localized structures in laser plasma system: Insight from particle-in-cell simulations 85
5.1 Introduction 86
5.2 Description of PIC Simulation for 1-D study 87
5.3 Results 89
5.3.1 Time dependent observations for stationary localized structure in Particle-in-cell simulation 92
5.3.2 Time dependent observations for moving localized structure in Particle-in-cell simulation 99
5.4 Summary 104

6 Conclusion and future work 107
6.1 Salient features of the thesis 108
6.1.1 **Cusp solitary structure** 108
6.1.2 **Stability of 1-D soliton in transverse direction** 109
6.1.3 **Observation of time-dependent localized structures in a one-dimensional laser plasma system.** 110
6.1.4 **Kinetic studies of time-dependent localized structures in a one-dimensional laser plasma system.** . . . 111
6.2 Future directions 112

Bibliography **113**

SYNOPSIS

Plasma is an ensemble of charged particles which is neutral macroscopically. These charged particles respond to the self-consistent and external electric and magnetic fields in a collective manner. The disparate masses of the two species and the nature of electromagnetic interaction leads to the existence of many collective modes in plasma at distinct spatial and temporal scales. The plasma is thus a complex medium which supports a plethora of waves and instabilities where the nonlinearity of the medium manifests in terms of the existence of diverse coherent structures as well as turbulence fluctuations.

The interaction of plasma with electromagnetic radiation leads to interesting effects which are of interest both from fundamental and applied points of view. The electric and magnetic field of the radiation essentially interact with the charged species of plasma. The electron species, which has a smaller mass than ions, responds predominantly to the oscillating electric and magnetic fields at the light frequencies. With the advent of powerful lasers, the new physical regime has been opened up wherein electron quiver velocity in the light field becomes relativistic. A one-dimensional fluid model along with the complete set of Maxwell's equations has been found extremely useful in predicting the formation and the evolution of nonlinear coherent electromagnetic structures in a laser-plasma system. One dimensional localized structures were predicted analytically [1–4] and further explored using full nonlinear set of fluid-Maxwell equations in the simulation studies as well [5–11]. Experimental and PIC studies also show formation of localized structures [12–14]. They also suggest that a significant amount of laser energy (25-30 %) gets trapped into the plasma in the form of these coherent structures. Clearly, such localized structures would then have an important role in many applications such as particle acceleration and inertial confinement fusion. Keeping their importance in view, the solutions have been characterized in considerable detail by various authors in the λ (laser frequency) and β (group velocity) plane [6, 8–10]. Six different varieties of solitonic structures have been identified. These are, (i) single peak (corresponding to radiation in the plasma density cavity) (ii) multi-peak (iii) paired structures (iv) flat top (v) cusp and (vi) high amplitude. The dynamical evolution studies of some of these structures have also been carried out which have illustrated that solutions which have a single light peak trapped inside the plasma cavity are stable [6], while those having multiple radiation peaks and the flat top structures with ion response have been found to be unstable to Raman forward [7] and Brillouin backscattering instabilities [9] respectively.

This thesis focusses on the study of the coherent localized solutions in considerable detail. In particular, we have provided an analytical description of the cusp solitonic structure, which shows a good match with the numerical profile. The cusp structures have been shown to be unstable to the forward Raman scattering process. The 2-D evolution studies of several 1-D structures have also been performed which show that even those structures which are stable in 1-D are unstable to filamentation instability. Furthermore, certain time-dependent localized structures have been identified in the thesis which shows the interesting interplay between field and kinetic energies. Question on the formation of such structures in the aftermath of a wave breaking process has been probed in detail by employing both fluid and Particle-In-Cell (PIC) codes.

The thesis covering discussions on these specific issues comprises of six chapters. The chapter wise summary of the thesis has been provided below:

- **Chapter - I:** In this chapter an introduction to the laser plasma (LP) interaction process and the physics of the formation of localized exact solutions are discussed in detail. The energy trapped in these solutions can be naturally transported as the structures often move with a group speed and may have interesting implications to problems such as particle acceleration [15–19] and inertial confinement fusion [20, 21] etc. A detailed review of the earlier studies on the exact solutions of the coupled laser plasma system has been provided. This includes the characterization of the variety of solutions and their dynamical evolution in 1-D. A brief introduction to the proposed study in this thesis have been presented and the future challenges have been outlined.

- **Chapter - II:** The incorporation of ion dynamical response leads to an increased number of possible solitonic structures in the coupled laser plasma system. The single peak and multiple peak solitonic structures show a clear split in two distinct branches of low and high amplitude structures. The bifurcation occurs beyond a particular group velocity after which two solutions, one with a small and other with high amplitude is possible. Certain solutions with new and distinct profiles are also possible, such as flat top and cusp structures. As the names suggest the flat top solutions have a profile which remains flat at the high value of all the fields. The cusp structure, on the other hand, has a discontinuity in the derivative of scalar potential at the center. This happens as a result of ions achieving the wave breaking

condition at the center resulting in a sharp peak of ion density there. In this chapter, the cusp solitons are discussed in detail. These solitonic structures form in the presence of ion response when the ions reach the wave breaking limit at the center of the solitonic structures. An analytical approximate form of these solitonic structures has been obtained which is shown to agree with the numerically obtained structures. The dynamical evolution of these structures have also been studied and it is shown that the cusp structures are unstable to the forward Raman scattering instability.

- **Chapter - III:** Several studies [2, 4–11, 22–24] have been conducted on the evolution of one-dimensional solitary structures. The 1-D studies have shown that out of the three varieties of solutions, (in the case where only electron response is considered) the single peak and paired peak are solutions stable whereas the multiple peak solutions are unstable to forward Raman scattering instability. In the presence of ion response, the evolution of flat top [9] and cusp structures [24] have been investigated, showing them to be unstable to Brillouin backscattering and forward Raman scattering instabilities respectively. In this chapter, we have considered the evolution studies in 2-D by including the second dimension in the numerical code. The LCPFCT package of flux corrected subroutines with time-splitting technique has been adopted for the purpose of integrating into the second dimension. We have considered the evolution of three solutions (which are permitted in the presence of only the electron response) in 2-D. The numerical studies show that the single peak, paired peak and multiple peak 1-D structures are unstable to transverse perturbations. It is shown that the transverse instability is the filamentation instability. The 1-D solitons thus break up as light filaments. For the multiple peak structures which were unstable in 1-D, the forward Raman scattering instability appears earlier which is then followed up by the filamentation instability in 2-D.

- **Chapter - IV:** In the fourth chapter of this thesis, we present our observations of certain time-dependent localized structures which invariably form either by ejection from unstable structures or as an aftermath of collisional interactions amidst certain solitonic structure. These time-dependent structures are observed to be considerably robust and are seen to preserve their identity for hundreds of plasma period. Typically the structures show the interplay of oscillations amidst density and radiation fields and often have compact support. To gain a better understanding we have introduced ex-

cess radiation in the density cavity of exact solutions, thereby disturbing the precarious balance of forces of the structure. The radiation pressure being high, it pushes the electron density and triggers a plasma oscillation. An interesting interplay of out of phase oscillations between the field and kinetic energies are observed. This continues for hundreds of plasma periods. However, the electron density in the plasma oscillations keeps getting steeper and ultimately approaches the wave breaking limit. In the fluid simulations, the density spike approaches the grid scale and one observes a slight dip in the total energy. The simulation thereafter continues with spiky density structures with radiation trapped inside it. In the next chapter, PIC studies have been carried out to confirm the wave breaking process and the evolution thereafter.

- **Chapter - V:** In this chapter we employ Particle - In - Cell (PIC) codes to reproduce the results that have been obtained in Chapter IV by fluid simulations. The PIC studies capture the observations associated with the time-dependent structures with fluid simulations very accurately till the wave breaking point. The oscillations in the field and kinetic energies are captured exactly. Though the fluid simulations show a dip in energy at the time of wave breaking, in PIC the energy remains conserved all throughout. However, after wave breaking one observes an increase in the random thermal part of the kinetic energy. The PIC studies compare well qualitatively with fluid observations even after wave breaking. the main conclusion of the studies conducted in chapter IV and V are that even when the precarious balance required in the exact solutions are disturbed the localized structure retains its identity for a sufficiently long time. The imbalance triggers plasma oscillations and the inhomogeneity of the electron density lead to the wave breaking of these oscillations ultimately as a result of which density spikes are formed. Radiation trapped between the density spikes invariably form interesting time-dependent structures with compact support which last for a considerable time. Thus such time-dependent compact structures are expected to be observed invariably.

- **Chapter - VI:** This chapter summarizes the thesis work recapitulating its salient points. Future prospects in terms of the form of the solutions in higher three dimensions and the process of thermalization of the plasma through the wave breaking process triggered in unstable solutions as well as those in which the delicate balance between electrostatic and ponderomotive

forces are disturbed are projected.

The detailed investigations made in this thesis thus contribute significantly to the theoretical understanding of formation and stability of localized structures in a system where lasers interact with the plasma.

---

[1] T. Tajima. A triple soliton accelerator. *Nature*, 1987.

[2] P. K. Kaw, A. Sen, and T. Katsouleas. Nonlinear 1d laser pulse solitons in a plasma. *Phys. Rev. Lett.*, 68:3172–3175, May 1992.

[3] A. G. Litvak V. A. Kozlov and E. V. Suvorov.

[4] H. H. Kuehl and C. Y. Zhang. One-dimensional, weakly nonlinear electromagnetic solitary waves in a plasma. *Phys. Rev. E*, 48:1316–1323, Aug 1993.

[5] T. Zh. Esirkepov, F. F. Kamenets, S. V. Bulanov, and N. M. Naumova. Low-frequency relativistic electromagnetic solitons in collisionless plasmas. *Journal of Experimental and Theoretical Physics Letters*, 68(1):36–41, 1998.

[6] Vikrant Saxena, Amita Das, Abhijit Sen, and Predhiman Kaw. Fluid simulation studies of the dynamical behavior of one-dimensional relativistic electromagnetic solitons. *Physics of Plasmas*, 13(3), 2006.

[7] Vikrant Saxena, Amita Das, Sudip Sengupta, Predhiman Kaw, and Abhijit Sen. Stability of nonlinear one-dimensional laser pulse solitons in a plasma. *Physics of Plasmas*, 14(7), 2007.

[8] S. Poornakala, A. Das, P. K. Kaw, A. Sen, Z. M. Sheng, Y. Sentoku, K. Mima, and K. Nishikawa. Weakly relativistic one-dimensional laser pulse envelope solitons in a warm plasma. *Physics of Plasmas*, 9(9), 2002.

[9] Sita Sundar, Amita Das, Vikrant Saxena, Predhiman Kaw, and Abhijit Sen. Relativistic electromagnetic flat top solitons and their stability. *Physics of Plasmas*, 18(11), 2011.

[10] D. Farina and S. V. Bulanov. Relativistic electromagnetic solitons in the electron-ion plasma. *Phys. Rev. Lett.*, 86:5289–5292, Jun 2001.

[11] Daniela Farina and Sergei V Bulanov. Dynamics of relativistic solitons. *Plasma Physics and Controlled Fusion*, 47(5A):A73, 2005.

[12] M. Borghesi, S. Bulanov, D. H. Campbell, R. J. Clarke, T. Zh. Esirkepov, M. Galimberti, L. A. Gizzi, A. J. MacKinnon, N. M. Naumova, F. Pegoraro, H. Ruhl, A. Schiavi, and O. Willi. Macroscopic evidence of soliton formation in multiterawatt laser-plasma interaction. *Phys. Rev. Lett.*, 88:135002, Mar 2002.

[13] M. Borghesi, D. H. Campbell, A. Schiavi, M. G. Haines, O. Willi, A. J. MacKinnon, P. Patel, L. A. Gizzi, M. Galimberti, R. J. Clarke, F. Pegoraro, H. Ruhl, and S. Bulanov. Electric field detection in laser-plasma interaction experiments via the proton imaging technique. *Physics of Plasmas*, 9(5), 2002.

[14] Timur Esirkepov, Katsunobu Nishihara, Sergei V. Bulanov, and Francesco Pegoraro. Three-dimensional relativistic electromagnetic subcycle solitons. *Phys. Rev. Lett.*, 89:275002, Dec 2002.

[15] T. Tajima and J.M. Dawson. Laser electron accelerator. *Phys. Rev. Lett.*, 43, 1979.

[16] Thomas Katsouleas. Accelerator physics: Electrons hang ten on laser wake. *Nature*, 431:515–516, Sep2004.

[17] C. G. R. Geddes et al. High-quality electron beams from a laser wakefield accelerator using plasma-channel guiding. *Nature*, 431:538–541, Sep2004.

[18] J. Faure et al. A laser-plasma accelerator producing monoenergetic electron beams. *Nature*, 431:541–544, Sep2004.

[19] S. P. D. Mangles et al. Monoenergetic beams of relativistic electrons from intense laser-plasma interactions. *Nature*, 431:535–538, Sep2004.

[20] V. Malka et al. *Nat. Phys.*, 4, 2008.

[21] M. Honda, A. Nishiguchi, H. Takabe, H. Azechi, and K. Mima. Kinetic effects on the electron thermal transport in ignition target design. *Physics of Plasmas*, 3(9):3420–3424, 1996.

[22] Maurizio Lontano, Matteo Passoni, and Sergei V. Bulanov. Relativistic electromagnetic solitons in a warm quasineutral electron-ion plasma. *Physics of Plasmas*, 10(3), 2003.

[23] R. N. Sudan, Y. S. Dimant, and O. B. Shiryaev. One-dimensional intense laser pulse solitons in a plasma. *Physics of Plasmas*, 4(5), 1997.

[24] Deepa Verma, Amita Das, Predhiman Kaw, and Sanat Kumar Tiwari. The study of electromagnetic cusp solitons. *Physics of Plasmas*, 22(1), 2015.

List of Figures

1.1 Schematic of soliton formation. 9

2.1 λ-β spectrum indicating the existence region for possible soliton solutions in movable ion case viz. the flat-top solutions, single peak solutions, single peak solutions with higher amplitudes, paired solutions, multi peak and cusp solutions tagged with 'A', 'B', 'C','D', 'E' and 'F' respectively. The profile of vector potential R (black dashed line), scalar potential ϕ (blue solid line) plotted along right y-axis and electron density n_e (green solid line) and ion density n_i (red dashed line) is on right y axis respectively. 25

2.2 Analytic (solid line) and exact (dashed line) cusp solutions for ϕ field with electrons and ions both considered as dynamical species. The parameters λ and β have been choosen as 0.4570000953 and 0.8 respectively for present case. 30

2.3 Evolution of vector potential (R) and scalar potential (ϕ) in left and right columns respectively at different times t=0, 20, 40, 60 electron plasma periods (ω_{pe}^{-1}). The parameters have been choosen as $\beta = 0.42$ and $\lambda = 0.6289599$. 32

2.4 Evolution of electron density n_e(blue solid line) and ion density n_i(red solid line) with $\beta = 0.42$ and $\lambda = 0.6289599$ at four different times t=0, 20, 40, 60 electron plasma periods (ω_{pe}^{-1}). 33

2.5 Parametric instability feedback loop. 34

2.6 Evolution of Vector potential (R) at (a) 20 electron plasma period (ω_{pe}^{-1}) and (b) 60 electron plasma period (ω_{pe}^{-1}). R_0(black solid line) is vector potential at t=0, R(red dashed line) is vector potential after time t evolution and R_{pert}(green dotted-dashed line) is the perturb vector potential for $\beta = 0.42$ and $\lambda = 0.6289599$. 35

2.7 Growth rate(blue diamonds) comparison with simulation growth rate(pink stars) for (a) backward Raman instability and (b) forward Raman instability. 36

3.1 1-D plot of a vector potential R, scalar potential (ϕ) and electron density (n) of a single peak soliton moving with group velocity β=0.05 and λ=0.93 at different times. 43

3.2 A surface plot of vector potential (R) and corresponding profile of electron density (n) shown in "$x-y$" plane at $z = -2$ for single peak soliton moving with group velocity β=0.05 and λ=0.93 at different times. 44

3.3 Plot of a perturbed field energy vs. time for a single peak soliton moving with group velocity β=0.05 and λ=0.93. 45

3.4 1-D plot of a vector potential R, scalar potential (ϕ) and electron density (n) of a paired peak soliton moving with group velocity β=0.2 and λ=0.938455 at different times. 46

3.5 A surface plot of vector potential (R) and corresponding profile of electron density (n) shown in "$x - y$" plane at $z = -2$ for paired peak soliton moving with group velocity β=0.2 and λ=0.938455 at different times. 47

3.6 Plot of a perturbed field energy vs. time for a paired peak soliton moving with group velocity β=0.2 and λ=0.938455 48

3.7 1-D plot of a vector potential R, scalar potential (ϕ) and electron density (n) of a multi peak soliton moving with group velocity β=0.5 and λ=0.714457 at different times. 49

3.8 A surface plot of vector potential (R) and corresponding profile of electron density (n) shown in "$x - y$" plane at $z = -2$ for multi peak soliton moving with group velocity β=0.5 and λ=0.714457 at different times. 50

3.9 Plot of a perturbed field energy vs. time for a multiple peak soliton moving with group velocity β=0.5 and λ=0.714457. 51

3.10 Surface plot of vector potential R for single peak soliton moving with group velocity β=0.05 and λ=0.93 at different times. 55

3.11 Analytical and simulation growth rate plot vs width (w) of the solitonic structures for (A)Single peak soliton (B) Paired soliton and (C) Multipeak soliton. 56

4.1 Vector potential (R) and density (n) for moving soliton at group velocity (β=0.4) for multi peak soliton. 63
4.2 Vector potential (R) profile at different time t=0, 12, 24, 30. 64
4.3 Collision of two single peak of soliton moving at group velocity $\beta = -0.01$ and $\beta = 0.05$. 66
4.4 Single peak soliton with group velocity $\beta = 0$ and $A_0 = 1$. 68
4.5 Vector potential (R) for stationary ($\beta = 0$) single peak soliton of amplitude $R = 1.1R0$ at different times. 69
4.6 Desnity (n) profile for stationary ($\beta = 0$) single peak soliton of amplitude $R = 1.1R0$ at different times. 70
4.7 Density peak n_{peak} oscillation as a function of time t. 71
4.8 Kinetic energy (KE), field energy (FE), total energy (TE) as a function of time t for fluid. 72
4.9 Vector potential (R) for stationary ($\beta = 0$) single peak soliton of amplitude $R = R0 + 1.1\sin(kx)$ at different times. 74
4.10 Desnity (n) profile for stationary ($\beta = 0$) single peak soliton of amplitude $R = R0 + 1.1\sin(kx)$ at different times. 75
4.11 Density peak n_{peak} oscillation as a function of time t after incorporation of asymmetric perturbation of $R = R0 + 1.1\sin(kx)$ in vector potential. 76
4.12 Kinetic energy (KE), field energy (FE), total energy (TE) as a function of time t for for asymmetric perturbation. 76
4.13 Vector potential (R) profile of moving single peak soliton with group velocity ($\beta = 0.3$) with excess perturbation in vector potential of form $R = 1.1R_0$ at different times. 77
4.14 Density (n) profile of moving single peak soliton with group velocity ($\beta = 0.3$) with excess perturbation in vector potential of form $R = 1.1R_0$ at different times. 78
4.15 Density peak n_{peak} oscillation as a function of time t after incorporation of symmetric perturbation $R = 1.1R0$ in vector potential. 79
4.16 Kinetic energy (KE), field energy (FE), and total energy (TE) as a function of time t for moving single peak soliton with group velocity ($\beta = 0.3$) after trapping of excess radiation of the form $R = 1.1R_0$. 79

4.17 The Localized structure get accelerated from $\beta = 0.3$ to $\beta_{new} = 0.301$, $R = 1.1R_0$. 80
4.18 Frequency spectrum for the moving localized structure, $\beta = 0.3$. . . 82

5.1 Vector potential (R) for stationary (β=0) single peak soliton of amplitude $A_0 = 1$ at different times. 89
5.2 Density (n) for stationary (β=0) single peak soliton at different times. 90
5.3 Kinetic energy, Field energy, Total energy as a function of time t for fluid(marker)and PIC(solid line) for stable stationary single peak soliton. 90
5.4 Distribution function for stable soliton solution at time $t = 0$ and $t = 200$. 91
5.5 Vector potential (R) for stationary (β=0) single peak soliton of amplitude $R = 1.1R_0$, confine an excess radiation 10% of R_0 in electron density cavity at different times. 92
5.6 Plot of density (n) for stationary (β=0) single peak soliton associated with an excess radiation of amount 10% of R_0 at different times. 93
5.7 Kinetic energy (KE), Field energy (FE) and total energy (TE) for the confinement of a symmetric excess radiation (of amount 10%) of stable vector potential in electron cavity as a function of time t from fluid(marker with dashed) and PIC(solid line). 94
5.8 Distribution function of the particles for the confinement of a symmetric excess radiation (of amount 10%) of stable vector potential in electron cavity at time $t = 0$ and $t = 225$. 94
5.9 Vector potential (R) profile having an asymmetricity of 10% in the laser pulse from its stable solution. 96
5.10 Density (n) for stationary ($\beta = 0$) single peak soliton associated with an asymertic radiation at different times. 96
5.11 Kinetic energy (KE), Field energy (FE) and total energy (TE) for the confinement of a asymmetric excess radiation (of amount 10%) of stable vector potential in electron cavity as a function of time t obtained from fluid(marker with dashed)and PIC(solid line). 97

5.12 Distribution function of the particles for the confinement of a asymmetric excess radiation (of amount 10%) of stable vector potential in electron cavity at time $t = 0$ and $t = 212$. 98
5.13 Vector potential (R) for moving single peak soliton for group velocity $\beta = 0.3$ and $\lambda = 0.94$ having an 10% excess radiation confinement in electron density cavity at different times. 99
5.14 Density (n) for moving single peak soliton for group velocity $\beta = 0.3$ and $\lambda = 0.94$ having an 10% excess radiation confinement in electron density cavity at different times. 100
5.15 Kinetic energy (KE), Field energy (FE) and total energy (TE) for the confinement of a symmetric excess radiation (of amount 10%) of stable vector potential in electron cavity for moving single peak soliton with group velocity $\beta = 0.3$ and $\lambda = 0.94$ as a function of time t for fluid(marker with dashed)and PIC(solid line). 101
5.16 Distribution function of the particles for the confinement of a symmetric excess radiation (of amount 10%) of stable vector potential in electron cavity at time $t = 0$ and $t = 290$. 102
5.17 Vector potential for self generated compact localized solution moving in -ve x direction. 103
5.18 Kinetic energy, field energy and total energy as a function of time for localized compact structure. 104

List of Tables

2.1 Numerically observed growth rates comparison with analytically estimated growth rates. 37

3.1 Comparison of numerical and analytical filamentation growth rates for single peak solitary solutions. 52

3.2 Comparison of numerical and analytical filamentation growth rates for paired peak solutions. 53

3.3 Comparison of numerical and analytical filamentation and raman forward scattering growth rates for multi peak solitary solutions. 54

1

Introduction

A typical plasma is a collection of freely moving charges under the influence of a self-consistent and external electromagnetic fields. Such a medium comes into existence by violently imparting energy (in the form of heat, laser, intense electric field, etc.) to ordinary matter. The neutral atoms and molecules of the matter get ionized and release some or all of its electrons. The collection of such an ensemble of charged particles is called plasma provided it satisfies certain criteria, e.g. displaying collective properties, remaining quasi-neutral etc. The majority of the universe (excluding dark matter and dark energy) is in the form of plasma. It is often also referred to as the fourth state of matter.

Understanding the behavior of plasma state of matter under various circumstances remains a topic of considerable interest for the research community. The quest is driven by both fundamental understanding and the host of applications which are being and can be garnered through this medium. One such important aspect is the interaction of this medium with the electromagnetic field of the light wave. With the steady improvements in the laser power (and many other attributes

of the laser system) many new challenges and novel features are continuously being uncovered in the interaction of plasma with laser light. For instance, laser plasma interaction forms the basis for the new principle of particle acceleration with a a promise of almost thousand-fold increase in the acceleration gradient [1–9]. Areas such as photon acceleration [10–13], production of X-ray sources [14–17], novel radiation sources of table top sizes hold a lot of promise in the field of medical, security and imaging are all based on light plasma interaction. Furthermore, the inertial confinement fusion (and its variants such as fast ignition etc.,) are all dependent crucially on the interaction of laser with the plasma medium [18–21].

The interaction of laser electromagnetic field with plasmas is beset with many interesting collective phenomena. This involves a variety of collective plasma modes, instabilities and coherent nonlinear structures and their dynamics. In this thesis formation, stability and dynamics of coupled light plasma coherent structures are explored. In the subsequent sections, we will provide the background and motivation behind the thesis work. The basis tenets of the laser-plasma interaction is introduced briefly and the summary of earlier studies have been provided. A brief outline of the studies carried out in the present thesis has also been provided.

1.1 Background and Motivation

A soliton is one of the very interesting coherent nonlinear structure and is ubiquitously found in many natural circumstances. This was first observed and described by John Scott Russell in 1834. He observed solitary wave in the Union Canal, Scotland and named it the "wave of translation". Thereafter these structures have been observed many diverse areas, for example in optical fibers [22], as energy carrying packets in protein and other molecular systems [23], localized

structures in fermionic superfluids [24, 25] and conducting polymers [26], spiky electrostatic structures in the Earths magnetosphere [27] etc. The main properties of such structures are that they propagate unmolested and survive even after mutual collisions. This property of the soliton makes them significant useful entities for the purpose of information and signal transmission. In the context of plasmas also such coherent nonlinear entities have been observed and studied. For example, such localized structures have been observed in the simplest setting of the dusty plasma experiments, where their robustness have been tracked even by naked eyes [28–34]. Other areas where there are evidence of the existence of such structures include space plasma - in the form of a bow shock [35, 36], pulsar radio emission [37], and in the laser-matter interaction [38–42]. In this thesis, we will focus mainly on the behavior of coherent nonlinear entities in the context of laser plasma interaction.

1.2 Laser Plasma Interaction: An introduction

After the invention of the chirped pulse amplification (CPA) technique given by Mourou et al. [43], it has been possible to amplify an ultra-short laser pulse up to the petawatt level. In the CPA method, a short laser low intensity pulse is first stretched in time and then amplified. It is then compressed to obtain an ultra-short pulse of a very high intensity. This technique increases the laser intensities from 10^{16}W/cm^2 to well above 10^{18}W/cm^2. A dimensionless parameter a_0 is used to characterize the strength of a laser pulse

$$a_0 \sim \frac{p}{m_e c} = eE_L/m\omega_e c = 0.85 \times 10^{-9}\lambda[\mu m]\sqrt{(}I[\mathrm{W/cm^2}]),$$

Here, p is the quiver momentum of electrons, and E_L is the laser electric field. When a powerful laser pulse is focused on the matter, a plasma is formed by field ionization. In this state, the electrons are no longer bound to the ions, however, both the charge particles can move freely. As the ions are much heavier compared to the electrons, their response is very slow to the rapidly changing electric field of the laser light. Typically, at the intensities of 10^{18}W/cm^2, ions are assumed to form merely a stationary neutralizing background. The electrons on the other hand quiver at the frequency of the applied light field. The interaction of laser fields with electrons can under various circumstances lead to an irreversible transfer of energy to the electrons. The laser energy gets absorbed by the plasma medium. This energy typically excites electron plasma waves at the frequency of

$$\omega_{pe} = \sqrt{\frac{4\pi n_e e^2}{m_e}},$$

The plasma frequency depends upon mass of the electron m_e and the electron density n_e; where e is the charge of the electron

When the frequency of laser ω_L, incident on plasma, is higher than the plasma frequency ω_{pe} i.e. $(\omega_L > \omega_{pe})$, plasma behaves as an under dense medium for the laser pulse. The electrons oscillate in the electric field of the laser pulse and thus allow the pulse to propagate inside the plasma. On the other hand when $(\omega_L < \omega_{pe})$, plasma act as an over-dense medium for the laser. Therefore, the electrons can completely shield the electric field of the laser pulse and the light gets reflected from a boundary of the plasma surface. However, when an ultra-intense laser pulse ($a_0 \geq 1$ and intensity 10^{18}W/cm^2) is incident on the plasma, electrons quiver velocity v becomes close to the speed of light. Under these circumstances,

The plasma frequency (ω_p) get reduced by the relativistic factor (γ) as,

$$\omega = \frac{\omega_{pe}}{\sqrt{\gamma}}$$

Where,

$$\gamma = \frac{1}{\sqrt{1 - \frac{v^2}{c^2}}}$$

This relativistic factor is associated with the electrons velocity v, and c is the speed of light in free space. In this case, if the laser frequency is higher than the relativistically modified plasma frequency the laser fields can penetrate inside the plasma. Basically, plasma behaves as a locally under dense medium for a high-intensity laser pulse.

In 1979, Tajima et al. [4] has proposed a mechanism to create a longitudinal electrostatic field. This longitudinal electric field is set up by the expulsion of electrons through the ponderomotive pressure of the laser radiation, thereby forming ion cavity which provides an attractive force to electrons. As the laser pulse propagates one is left in an ion cavity surrounded by electrons. The electrostatic force due to the separated charge attracts the expelled electrons. As electrons rush inwards they overshoot and continue to oscillate in the wake of the laser. These wakefields can be utilized for accelerating electrons in the same way as a surfer accelerates on water waves in the ocean [44]. In recent experimental works, Mangles et al. [45], Geddes et al. [46], and Faure et al. [47] reported the generation of the quasi- mono-energetic electron beam of GeV order [48].

The high intense laser pulse can also be used to accelerate photons in plasma. By acceleration of photons, one implies an increase in the frequency of the photons.

One of the governing nonlinear mechanisms to speed up the photons in plasmas is - Raman forward scattering (RFS). In RFS, incident electromagnetic wave of frequency ω_0 scatters into a plasma wave of frequency ω_{pe} with two electromagnetic side-bands of frequencies $(\omega_0 \pm \omega_{pe})$. The photon experiences a frequency shift. Thus the photon with up-shifted frequency has an increased energy proportional to the frequency and can be viewed as photon acceleration [49, 50] in plasmas.

The Inertial Confinement Fusion (ICF) relies entirely on the interaction of laser with plasma. In ICF, which is an important option for controlled thermonuclear fusion (the other being magnetic confinement fusion), where the target is compressed to supersolid densities by laser to achieve the desirable Lawson Criteria for fusion. In ICF laser power is used to compress as well as heat the target. However, it is observed that the process is pretty inefficient as hydrodynamic instabilities mix the hot and cold fuels, making the energy requirements to be pretty high. In 1994, Tabak et al. [18] had proposed high-intensity, ultrashort laser pulse with an intensity of $\sim 10^{19}$W/cm^2 and a duration of about 100ps is used to push the critical surface of the plasma corona closer to the dense core by the ponderomotive force associated with high-intensity laser light. This process is known as hole-boring. In the third and final stage of this scheme, an intense laser pulse($\sim 10^{20}$W/cm^2), which is shorter (about 1 to 10 ps), propagates in this channel and is stopped at the critical density. There a significant part of the laser energy is converted into hot electrons. These high energetic electrons are now able to penetrate deeply into fuel and deposit their energy to heat high compressed ($\sim 10^{25}$/cm^3) core. So, according to the scenario, a part of the fuel, is rapidly heated and ignition of the thermonuclear fuel is initiated. The particular advantages of this concept are high gain and significantly reduced requirements on driver energy. The hot elec-

trons generated by the laser are often source for intense X-ray pulses [51]. Thus laser plasma interactions also lead to possible applications in terms of compact radiations sources.

The plasma response to the laser is in terms of coherent plasma oscillations. With high intensity, the coherent oscillations can be nonlinear and/or have relativistic electron response. Such nonlinear waves display phenomena of wave breaking and phase mixing. The possibility of formation of coherent soliton solutions also exists. When a laser pulse interacts with the plasma, it expels plasma electrons due to ponderomotive force and creates an ion cavity devoid of plasma electrons. The electrons get piled up at the edge which prevents, in turn, the light to escape the cavity. Thus a precarious balance between the ion attraction and repulsion by a ponderomotive pressure of light creates an electron configuration which in turn traps the light field inside to form a soliton structure. Such solitonic structures which can either be moving or stationary have been obtained by the solution of coupled Fluid Maxwell system of equation. The schematic diagram of such laser plasma solitonic structures has been shown in figure (1.1).

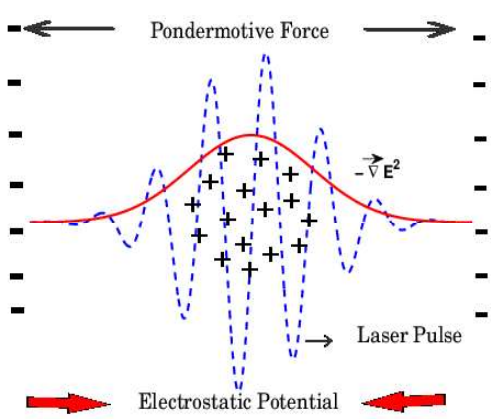

Figure 1.1: Schematic of soliton formation.

1.3 Review of earlier works

Theoretical investigations of the problem of one-dimensional electromagnetic solitons started in the seventies. Both analytical, as well as numerical efforts, were made in this direction. The detailed investigations of these spatially localized solutions with finite ion response were carried out by Kozlov et al. [40] in 1979. They numerically obtained the soliton solution for the propagation of an intense circularly polarized electromagnetic wave in a cold plasma. They analyzed the existence of the continuous spectrum of small amplitude soliton solutions in terms of group velocity (β) and the ratio of the plasma frequency (ω_p) to the laser frequency (ω). They mentioned the transcritical limit $\frac{\omega_p^2}{\omega^2} \sim 5$ of the plasma in their work above which no soliton solution was possible. Further, Kaw et al. [39] studied an exact one-dimensional relativistic soliton solution in cold plasma by considering ions as a stationary entity. They obtained 1-D soliton solutions for various group speeds (β) extending up to the speed of light (c). The relationship between the group velocity (β), the eigenvalue (λ), and the maximum amplitude of the electromagnetic wave for the soliton was provided by them. It was recognized by them that such coherent entities would play an important role in charge as well as photon acceleration. Esirkepov et al. [52] obtained an exact analytical form for stationary solitons and provided a critical value of the maximum amplitude of the vector potential at $R = \sqrt{3}$. In 2001, Farina et al [53] presented the detail investigation of the ion motion on the dynamics of the relativistic soliton solution. They presented the eigenspectra of the effective plasma frequency with the soliton velocity for the single node and multinode (p=2) soliton solution with ion dynamics. They also argued that ion can not be assumed to be at rest when the group velocity of the

soliton is close to zero and very small. At low speed, the ponderomotive force of the laser pulse would start affecting the ion density profile which changes the nature of the eigenspectrum. So, at slow propagation speed and/or sufficiently high electromagnetic field intensities, the dynamical response of ions would also need to be incorporated.

Poornakala et al. [54] and Saxena et al. [55] had presented a characterization of the one- dimensional solitonic structures. The solitons were classified in terms of the single peak, paired peak, and the multipeak structures depending on the number of peaks of the radiation trapped inside the density cavity. Besides, a paired structure is also observed wherein light wave of opposite polarity trapped in two distinct density cavities tunnels across the high electron density at the center to connect with each other and form a single coherent entity. These structures can have group speeds ranging from zero to close to the speed of the light. A complete characterization of the electron dynamics case for one-dimensional soliton solution has been studied in the parameter space of the light frequency (λ) and the group speed (β) given in ref [39,54,55]. These solutions thus represent an envelope of light waves modulated by a large amplitude plasma wave. The time evolution of such solutions has also been studied using the coupled set of fluid Maxwell equations. The simulation studies on the evolution of these solutions in 1-D have shown that the single-peak and paired solutions are stable and remain intact throughout the simulation. The multiple peak structures, on the other hand, have been found to be unstable to the Raman forward scattering instability [56].

However, at slow propagation speed and/or sufficiently high electromagnetic field intensities the dynamical response of ions should also be incorporated. Such studies have been carried out by several authors [53, 57–59]. The incorporation of

ions leads to several new varieties of solutions, viz., (i) flat top, (ii) an additional high amplitude solutions at the similar group speed β and lower frequency λ and (iii) cusp structures where at the center ion speed matches the group speed, and the ions are thus at the limit of wave breaking [53]. The time evolution of the flat top solutions was investigated by Sundar et al [58]. It was shown that the flat top solutions were unstable to the Brillouin's scattering instability.

1.4 Content and organization of the thesis

As we have mentioned in section (1.1), the main aim of this thesis is to investigate the properties of localized structures in the laser plasma coupled system. We discuss in detail the issues that have been covered in the next chapters.

1.4.1 Study of electromagnetic Cusp Solitons

The incorporation of ion dynamics yields additional new varieties of solitons - six kinds of soliton solution are now possible. Along with the single peak, paired peak and multiple peak solutions observed in electron response only case, the ion involvement lead to the high amplitude branch, flat-top and the cusp solitonic structures. The dynamical evolution of single peak and multipeak soliton structures have been investigated by Saxena et al. [55, 56]. Sita et al., [58] considered the evolution and analytical description of the flat-top soliton.

In chapter (2) we have focussed towards providing an analytical description of the cusp solitons which are found at the ion wave breaking point. We show that the analytical form of the scalar potential obtained under the assumption of ion wave breaking matches well with the solutions obtained numerically from the

eigenvalue search. In the second part of this chapter, we have focussed on the dynamical evolution of the cusp soliton with the help of the coupled fluid-Maxwell equations. The study shows that the cusp soliton is unstable during the evolution. This instability is identified as the Raman forward scattering instability.

1.4.2 Dynamical study of 1-D soliton in transverse direction

The coupled light plasma system has been studied seeking 1-D coherent solutions. The attempts of seeking 2-D structures have been rare. Some approximate analysis to obtain 2-D solutions have been provided in the work by [60, 61].

Furthermore, earlier evolution studies have also concentrated only on 2-D evolution characteristics of the exact solutions wherein it was shown that while the single peak and paired solutions are stable, the multiple peaks are unstable to Raman forward scattering instability and the flat top solution is unstable to Brillouin instability in 1-D. It is, however, of interest to see whether the stable structures remain stable or get destabilized in higher dimensions. In the case of 2-D destabilization, it is of interest to see whether the nonlinear development of the instability takes it towards coherent 2-D structures or disintegrates the solutions altogether.

In this chapter, we concentrate on studying the 2-D evolution of various solitonic structures. This includes single and paired peak structures which are stable in 1-D; and also the multiple peak solutions which are known to be unstable even in 1-D. As this is a first attempt towards studying the transverse dynamics of a coupled laser plasma system, we restrict to the case of electron dynamical response only. The ions are assumed to be massive for any response. The fluid code is generalized in the second dimension using the time-splitting technique. The simulations show that the structures survive for few hundred of plasma periods and, thereafter,

become unstable. This instability emerges due to the modulation in the transverse direction and finally suffers destabilization by the transverse filamentation instability [62–67]. The numerical growth rates obtained from simulations shows good agreement with the analytical values determined from growth rate expression provided by Decker et al. [68]. We observed that multiple peaks solitons first undergo the conventional 1-D forward Raman scattering instability. After the longitudinal destabilization, it suffers transverse filamentation. The growth of perturbed energy shows two episodes of the rise in this case. The first rise in the perturbed energy exhibits Raman forward scattering instability. Whereas the second increase in the perturbed energy comes due to the filamentation instability which occurs at the later stage of the evolution.

1.4.3 Observation of the time-dependent 1-D localized structures in laser plasma system with fluid simulations

In the coupled laser plasma system there exists a wide variety of exact 1-D solutions which are stationary as well as propagating. These solutions require a very precarious balance of various field profile. It, therefore, seems that their formation in the experimental situation will be fraught with complications. We, however, observe that there is another class of localized structures which forms rather spontaneously in simulations which do not require such a delicate balance between various field profiles. These structures are found to be time dependent. In the fourth chapter of this thesis, we focus on the study of these time-dependent structures with the help of fluid simulations. It is observed that these structures form as a result of collision amongst certain exact solutions and/or are the emitted remnants from the unstable exact 1-D multipeak soliton solutions. These struc-

tures are seen to survive as coherent entities for the long time ($\sim 100\omega_{pe}^{-1}$) and are found to display interesting out of phase interplay between field and kinetic energies. We observe that the dis-balance in the fields (compared to the exact solutions) triggers a plasma wave in the medium. The plasma wave acquires a high amplitude and invariably gets broken. However, even after the plasma wave gets broken and forms density spikes the structure continues to survive as a robust entity.

Various properties of these time-dependent structures are analyzed and investigated in detail.

1.4.4 Observation of time-dependent 1-D localized structures in laser plasma system with Particle in cell simulations

As mentioned in the earlier subsection the time-dependent structures involve broken plasma waves ultimately. The evolution with the fluid equation is then questionable. We have, therefore, investigated the properties of these time-dependent structures through Particle - In - Cell (PIC) simulations in a chapter (5). The PIC simulations compare quantitatively well before the wave breaking phenomena. However, after wave breaking the evolution shows qualitative agreement with fluid observations. The structure continues to exist as a local robust entity for a long time. We also observe the particle thermalization as a result of wave breaking phenomena.

The fluid and PIC studies thus clearly suggest the existence of interesting time-dependent structures which are more versatile than the regular solutions which require a delicate balance.

1.5 Conclusion and future scope of the thesis

In this chapter, we summarize the results of the whole thesis and recapitulate the salient points of this thesis. We also provide the future scope of work in continuation of the study that has been made in the present thesis.

2

Study of Electromagnetic Cusp Solitons

This chapter is devoted to understanding analytically the formation of a cusp structure in the envelope of electromagnetic solitons for an electron-ion plasma at the condition of ion wave breaking point. Analytical form of the cusp structure has been obtained by solving the fluid-Maxwell equation using the condition of ion wave breaking. It is shown to match well with numerically obtained cusp solutions. These cusp structures which form at the ion wave breaking point would be important for the acceleration of ions. In an effort towards studying the dynamical stability of such structures, the time evolution has been carried out which shows that the structure survives for several plasma periods. However, ultimately it breaks apart due to the forward Raman scattering instability.

2.1 Introduction

There are variety of exact nonlinear localized structures that have been observed in the study of the laser plasma interaction process [18, 39, 40, 52–56, 58, 69–72]. As

we have illustrated in the chapter (1), these solutions are primarily of the form of propagating structures with electromagnetic field trapped within an electron density cavity in the plasma. When the laser frequency is high, a class of exact one-dimensional solutions has been obtained wherein the ion response is ignored and the interaction of light with the electron has been considered. The solutions represent envelope solitons of light waves modulated by a large amplitude plasma wave in the medium and fall into three distinct classes. The first variety is characterized by a single peak of the laser field inside the soliton and is found to exist in a band of region characterizing the group speed and laser frequency space. They can have group speeds ranging from zero (static) to that of close to the speed of light. For these structures, the electron density is evacuated in the central portion and it peaks up at the edge. The second variety of solution known as paired peak solitons represents a spatial coupling of two single peaks of light waves of opposite polarity tunneling through an intermediate region of the electron density plasma oscillations. For the third variety of solutions, the laser field has multiple peaks in the near evacuated central region of the soliton. An approximate semi-analytic understanding of their spectrum λ (frequency) vs. β (group speed) has been provided by Kaw et al. [39] for circularly polarized light. For a circularly polarized electromagnetic pulse, the Lorentz factor is time independent and hence the harmonic generation is ruled out, unlike the case of linear polarization [73, 74]. When the group speed of the soliton is very slow and/or the intensity of the laser pulse is sufficiently high, the dynamical response of ions also needs to be incorporated. Such studies have been carried out by several authors [53, 57–59]. After the consolidation of ion dynamics in the system, new varieties of solutions emerge. Altogether, now there are six different varieties of solitons that can form

as shown in Fig. (2.1). These are the three familiar ones single peak, paired peak, multipeak structure; along with the new class of high amplitude, flat top, and cusp solitons. The dynamical properties of the single peak, paired peak [55], multipeak [56] and flat-top soliton [58] solution have already been investigated earlier. However, cusp solitons still remain to be studied.

In this chapter, we focus on the description of cusp solutions and also study their dynamical evolution. These solutions form when the ion density at the central region approaches the ion wave breaking limit. This happens when the ion velocity matches with the propagation speed of the structure. Farina et al. [53] have shown that at the ion wave breaking point, the ion density shoots up and the scalar potential structure in the soliton takes the form of a cusp. Here we provide a semi-analytic description of the cusp structures. We have also presented the temporal evolution of the cusp solution and found that it gets destabilized via forward Raman scattering instability.

The chapter is organized as follows. Section (2.2) contains the relevant governing equations for the 1D cold plasma model in the presence of electron-ion dynamics. In sec. (2.3), we discuss the cusp solutions. The ion density as well as the scalar potential both exhibit a cusp structure at the wave breaking point. The behavior of the cusp has been analyzed using the semi-analytic model description. The analytical result has been shown to match well with the form of the exact cusp solutions obtained numerically. In sec. (2.4), we dynamically evolve this solution. It is observed that the solutions survive for several plasma periods. However, ultimately they break apart due to forward Raman scattering. In sec. (2.5), we summarize and provide a discussion of our results.

2.2 Governing equations

The relativistic fluid-Maxwell equations govern the formation and the evolution of solitons in a laser-plasma system. These equations contain the continuity equation, momentum equation along with the full set of Maxwell's equations. At present, we have considered an intense circularly polarized laser pulse which is propagating along the x-direction inside a plasma. This yields the following complete set of the equation in the normalized variables:

$$\frac{\partial n}{\partial t} + \vec{\nabla} \cdot (n\vec{v}) = 0 \tag{2.1}$$

$$\left(\frac{\partial}{\partial t} + \vec{v}.\vec{\nabla}\right)(\gamma\vec{v}) = -\vec{E} - (\vec{v} \times \vec{B}) \tag{2.2}$$

$$\vec{\nabla} \times \vec{E} = -\frac{\partial \vec{B}}{\partial t} \tag{2.3}$$

$$\vec{\nabla} \times \vec{B} = \vec{J} + \frac{\partial \vec{E}}{\partial t} \tag{2.4}$$

$$\vec{\nabla} \cdot \vec{E} = \rho \tag{2.5}$$

$$\vec{\nabla} \cdot \vec{B} = 0 \tag{2.6}$$

Where, J is the current density, ρ is the charge density, and $\gamma = (1 - v^2)^{-1/2}$ is the relativistic factor associated with the fluid velocity v and the density of the plasma is n. In above equations,$\nabla = (\frac{\partial}{\partial x}, 0, 0)$, v_x, E_x and B_x represent the x-component of velocity ($\vec{v}$), electric field ($\vec{E}$) and the magnetic field ($\vec{B}$) respectively. We can also write, $\vec{E} = -\widehat{x}\frac{\partial \phi}{\partial x} - \frac{\partial \vec{A}}{\partial t}$, and $\vec{B} = \frac{\partial}{\partial x}(\widehat{x} \times \vec{A})$, where ϕ and $\vec{A}$ represent electrostatic potential and vector potential respectively. Normalization is such that, $n \rightarrow \frac{n}{n_0}$, $\vec{v} \rightarrow \frac{\vec{v}}{c}$, $\vec{E} \rightarrow \frac{e\vec{E}}{mc\omega_{pe}}$, $\vec{B} \rightarrow \frac{e\vec{B}}{mc\omega_{pe}}$, $x \rightarrow \frac{x}{\frac{c}{\omega_{pe}}}$, $t \rightarrow t\omega_{pe}$,

$\phi \rightarrow \frac{e\phi}{mc^2}$, $A \rightarrow \frac{eA}{mc^2}$. We have assumed that the change in plasma parameters in a longitudinal direction (x) is large compared to its transverse direction. Therefore we have ignored the variation of plasma parameters (density, velocity, electric field and magnetic field) in y and z direction. The coupled set of fluid-Maxwell equations (2.1-2.6) are the main fundamental equations to study the propagation of electromagnetic radiation inside the plasma. Now, solving equations (2.1-2.6) in terms of vector and scalar potential for electron-ion plasma, we get-

$$\frac{\partial n_e}{\partial t} + \frac{\partial (n_e u_e)}{\partial x} = 0 \tag{2.7}$$

$$\frac{\partial n_i}{\partial t} + \frac{\partial (n_i u_i)}{\partial x} = 0 \tag{2.8}$$

$$\left(\frac{\partial}{\partial t} + u_e \frac{\partial}{\partial x}\right)(\gamma_e u_e) = \frac{\partial \phi}{\partial x} - \frac{1}{2\gamma_e}\frac{\partial {A_\perp}^2}{\partial x} \tag{2.9}$$

$$\left(\frac{\partial}{\partial t} + u_i \frac{\partial}{\partial x}\right)(\gamma_i u_i) = -\alpha\frac{\partial \phi}{\partial x} - \frac{\alpha^2}{2\gamma_i}\frac{\partial {A_\perp}^2}{\partial x} \tag{2.10}$$

$$\frac{\partial^2 \phi}{\partial x^2} = n_e - n_i \tag{2.11}$$

$$\frac{\partial^2 A_\perp}{\partial t^2} - \frac{\partial^2 A_\perp}{\partial x^2} = -\left(\frac{n_i \alpha}{\gamma_i} + \frac{n_e}{\gamma_e}\right) A_\perp \tag{2.12}$$

Where $\alpha = m_e/m_i$.

Relativistic factors for electron and ion (respectively) are:

$$\gamma_e = \sqrt{\frac{1 + A_\perp^2}{1 - u_e^2}}, \gamma_i = \sqrt{\frac{1 + A_\perp^2 \alpha^2}{1 - u_i^2}}$$

We have followed the same step and notations as given by Sita et al [58]. By using the co-ordinate transformation $\xi = x - \beta t$, $\tau = t$ and quasi-static condition

$\frac{\partial}{\partial\tau} = 0$ in a moving frame. Eqs. (2.7-2.10) reduce to the form of ordinary differential equation. After integrating these equation we get,

$$n_e(\beta - u_e) = \beta \tag{2.13a}$$

$$n_i(\beta - u_i) = \beta \tag{2.13b}$$

$$\gamma_e(1 - \beta u_e) - \phi = 1 \tag{2.13c}$$

$$\gamma_i(1 - \beta u_i) + \phi\alpha = 1 \tag{2.13d}$$

Now elemintaing n_e and n_i from Eqs. (2.13a)-(2.13b), poisson equation becomes:

$$\phi'' = \frac{\beta}{\beta - u_e} - \frac{\beta}{\beta - u_i} \tag{2.14}$$

Here, prime($\prime$) denotes the derivative with respect to ξ. For circularly polarized vecotr potential $\vec{A} = [a(\xi)/2][\{\hat{y} + i\hat{z}\}exp(-i\lambda\tau) + c.c.]$. Further, writing $a(\xi) = R\exp(i\theta)$, the wave equation Eq. (2.10) becomes

$$R'' + \frac{R}{1-\beta^2}\left[\left(\lambda^2 - \frac{M^2}{R^4}\right)\frac{1}{1-\beta^2} - \frac{\beta}{\beta - u_e}\frac{1-\beta u_e}{1+\phi} - \alpha\frac{\beta}{\beta - u_i}\frac{1-\beta u_i}{1-\phi\alpha}\right] = 0 \tag{2.15}$$

Where,

$$u_e = \frac{\beta(1+R^2) - (1+\phi)[(1+\phi)^2 - (1-\beta^2)(1+R^2)]^{1/2}}{(1+\phi)^2 + \beta^2(1+R^2)} \tag{2.16}$$

and

$$u_i = \frac{\beta(1+R^2\alpha^2) - (1-\phi\alpha)[(1-\phi\alpha)^2 - (1-\beta^2)(1+R^2\alpha^2)]^{1/2}}{(1-\phi\alpha)^2 + \beta^2(1+R^2\alpha^2)} \tag{2.17}$$

Here, $M = R^2[(1-\beta^2)\theta' - \lambda\beta]$ is a constant of integration and $R^2 = A_y^2 + A_z^2$. In the next sections, we present the exact nonlinear solutions obtained by solving the set of Eqs. (2.14-2.15).

2.3 Exact and Analytical Cusp solutions with Ion dynamical response

The equations mentioned above are defining the coupled electromagnetic field and the electron-ion plasma response. The exact numerical solution which we have obtained by solving equation are differentiated as a flat-top, single peak, high amplitude, paired peak, multipeak, and cusp soliton. These solution are represented by A, B, C, D, E and F in Fig. (2.1). The description of these soliton has given below-

(A) At the lower limit of the group velocity β, a new variety of solitary structures emerge which has the flat profile of the scalar and vector potential at the top of the potential. These soliton named as Flat-top Soliton, represented by solid magenta diamonds in the center subplot of the figure. (2.1).

(B) These solutions have a single peak in both vector R and scalar ϕ potentials. In Fig. (2.1), these structures are represented by solid line with blue square. It shows that the single peak soliton exists below a critical value of group velocity $\beta = \beta_c$. For a given value of β, the amplitude of the soliton increases upon decreasing the value of λ. It has been observed by Saxena et al [55] that the single peak soliton are very stable and robust.

(C) The second branch of the solutions for both single as well as multiple peak structure named as high amplitude soliton. All these structures lies in the second

branch, has higher amplitude of the vector potential for the given values of the group velocity β.

(D) Another variety of solutions depicted in figure(2.1) by brown dots with the line has been termed as Paired structures. In this soliton, two single peak solutions get coupled with opposite polarity of the vector potential. These solitary structures are also found to be stable and robust similar to the single peak soliton.

(E) Three different colors of crosses(black, pink and green), represent a new variety of soliton which is known as the multipeak soliton. These three branches are categorized on the basis of the vector potential peaks which get trapped inside the scalar potential. Here, the black crosses represent the 3 peak trapping of the vector potential whereas the pink represent the 5peak trapping of the vector potential inside the electron density cavity. Detailed study of these soliton has been done by Saxena et al [56]. They have mentioned in his paper [56] that these solitary structures get destabilized during the evolution due to the Raman forward scattering instability.

(F) The new additional variety of solutions which occurs after the incorporation of ion dynamical response is called as "cusp soliton". This soliton emerges at the ion wave breaking point, i.e. where the ion velocity reaches the group speed of the structure. In the figure (2.1), they are represented by red solid circular dots at the end of branch of the multipeak soliton

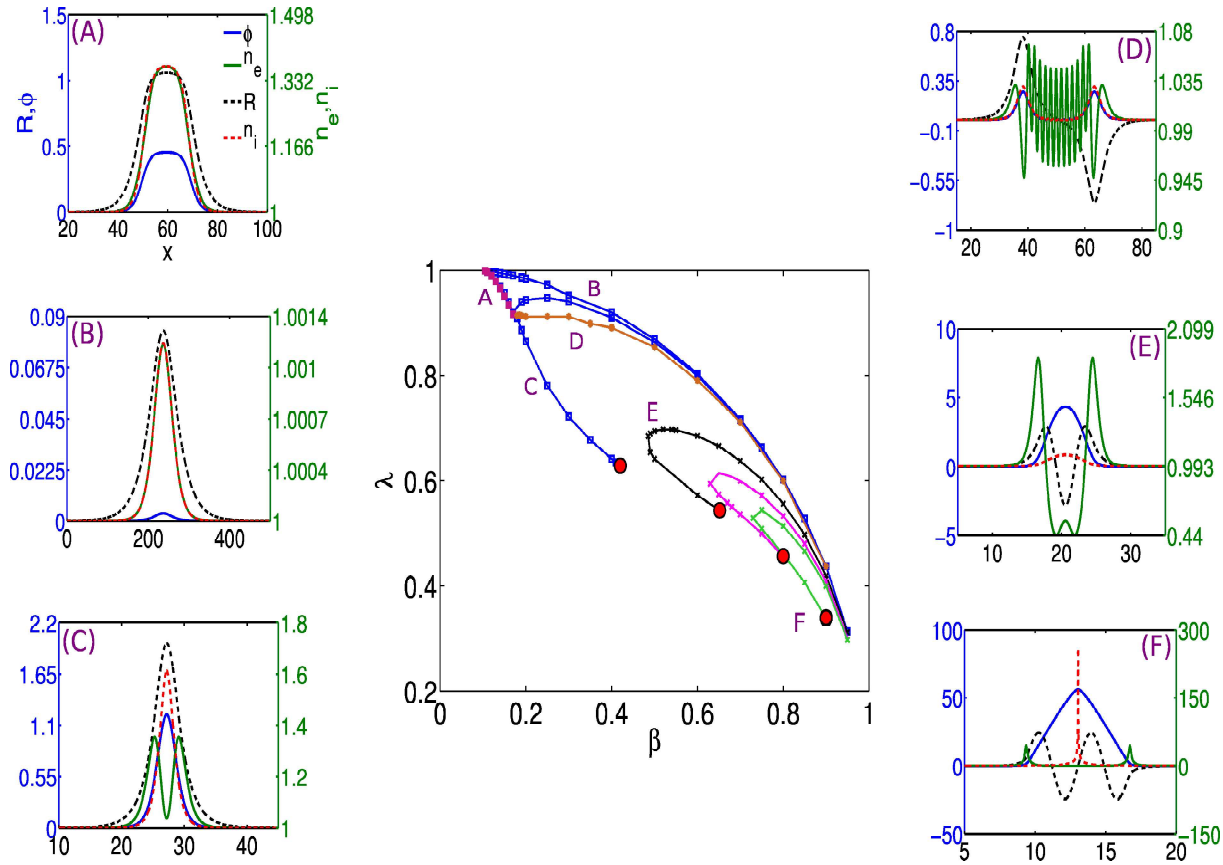

Figure 2.1: λ-β spectrum indicating the existence region for possible soliton solutions in movable ion case viz. the flat-top solutions, single peak solutions, single peak solutions with higher amplitudes, paired solutions, multi peak and cusp solutions tagged with 'A', 'B', 'C','D', 'E' and 'F' respectively. The profile of vector potential R (black dashed line), scalar potential ϕ (blue solid line) plotted along right y-axis and electron density n_e (green solid line) and ion density n_i (red dashed line) is on right y axis respectively.

The single peak, paired peak, and multipeak solution has already been observed and studied by Poornakala et al. [54] and Saxena et al [55, 56] in electron response case for which the ions are assumed to be infinitely massive. On the other hand

when ion mass is taken to be finite three additional varieties of soliton appear. The $\lambda - \beta$ spectrum for ion-electron is presented in Fig. (2.1). The analytical and numerical description of the flat-top solution has done by Sita et al [58]. They have shown that the flat-top soliton solution get destabilize due to Brillouin scattering. However, for the cusp solitons, the ion density approaches infinity at the center of the soliton. Thence, a scalar potential develops a cusp structure. In this chapter, we have presented the brief description of the cusp soliton solution. Their location in the λ vs. β plane has been shown with the red circular dots at the end point of each curve. The form of the cusp structures for each of the circular dots in the λ vs. β plane differ by the number of extremes of the vector potential. For instance the cusp solution plotted in Fig. (2.1), mentioned by (F) consist of four extrema in vector potential and occurs at $\lambda = 0.3402846592$ and $\beta = 0.9$.

A form of the cusp in scalar potential can be obtained by an approximate analytical treatment. In the central region, electron density is taken to be minimal $\sim \beta/(1+\beta)$ for a soliton propagating with a speed of β. This is the minimum value of the electron density in a moving frame. The ion density is finite and assumed to have a spatial dependence. Thus the Poisson equation in the central region of the soliton reduces to:

$$\phi'' = n_e - n_i = \frac{\beta}{\beta + 1} - \frac{\beta}{\beta - u_i} \tag{2.18}$$

Also using the integrated longitudinal component of ion momentum equation viz.,

$\gamma_i(1-\beta u_i)+\phi\alpha = 1$ we have,

$$\frac{1-\beta u_i}{\sqrt{(1-u_i^2)}} = 1-\alpha\phi \tag{2.19}$$

We have ignored $\alpha^2 R^2$ in the expression for the relativistic factor for ions ($\alpha = m_e/m_i$, being small). Eq. (2.19) can further be solved for u_i as

$$u_i = \frac{\beta}{\beta^2+\psi^2} - \sqrt{\frac{\beta^2}{(\beta^2+\psi^2)^2} - \frac{(1-\psi^2)}{\beta^2+\psi^2}} \tag{2.20}$$

Here $\psi = 1-\alpha\phi$. The Poisson equation then can be written as

$$-\phi'' = \frac{\psi''}{\alpha} \quad = \quad -\frac{\beta}{\beta+1} + \frac{\beta(\beta^2+\psi^2)}{\beta(\beta^2+\psi^2-1)+\psi\sqrt{\beta^2+\psi^2-1}} \tag{2.21}$$

We integrate the equation once with respect to ξ to obtain

$$\frac{\psi'^2}{2\alpha} = -\frac{\beta\psi}{\beta+1} + \frac{\beta(\beta\psi-\sqrt{\beta^2+\psi^2-1})}{\beta^2-1} + C_1 \tag{2.22}$$

Here C_1 is the constant of integration. Since the above equation is applicable only in the central region of electron cavitation, the constant C_1 can be obtained, provided one knows the value of ψ and ψ' at a point within this cavitation region. We assume that $\psi = \psi_0$ and $\psi' = \pm\psi_0'$ at the exact central location (say $\xi = 0$) of the structure. These solutions have a peak in ion density at $\xi = 0$ point. This occurs when the ion velocity matches the group velocity of the structure β. This condition defines the ion wave breaking point, and when this happens the structures takes the shape of a cusp. At this breaking point, since $u_i = \beta$ at $\xi = 0$ the value of ψ_0 and C_1 are evaluated in terms of β and can be written as

$$\begin{aligned}\psi &= 1-\alpha\phi = \frac{1-\beta u_i}{\sqrt{(}1-u_i^2)}\\ \psi_0 &= \sqrt{1-\beta^2}\end{aligned}$$

so at centre,

$$\begin{aligned}C_1 &= \frac{\psi_0'^2}{2\alpha}+\frac{\beta}{\beta+1}\sqrt{1-\beta^2}-\frac{\beta^2}{(\beta^2-1)}(\sqrt{1-\beta^2}-0)\\ &= \frac{\psi_0'^2}{2\alpha}+\frac{\beta}{\sqrt{1-\beta^2}}\end{aligned}$$

Since the ion density blows up at the point $\xi = 0$, ϕ'' behaves like a delta function. Thus ϕ' and hence ψ' are discontinuous. The structure, however, being symmetric around $\xi = 0$, the values of both ϕ' and ψ' are unique and finite at this point. Using the expression for C_1 in equation (2.22) we obtain

$$\begin{aligned}\frac{\psi'^2}{2\alpha} &= -\frac{\beta\psi}{\beta+1}+\frac{\beta(\beta\psi-\sqrt{\beta^2+\psi^2-1})}{\beta^2-1}+\frac{\psi_0'^2}{2\alpha}+\frac{\beta}{\sqrt{1-\beta^2}}\\ &= \frac{\beta}{1-\beta^2}(\sqrt{\psi^2-\psi_0^2}-(\psi-\psi_0))+\frac{\psi_0'^2}{2\alpha}\end{aligned} \tag{2.23}$$

Integrating the above equation we have

$$\int\frac{d\psi}{\sqrt{\sqrt{(\psi^2-\psi_0^2)}-(\psi-\psi_0)+(1-\beta^2)\psi_0'^2/2\alpha\beta}} = \int\sqrt{\frac{2\alpha\beta}{1-\beta^2}}d\xi \tag{2.24}$$

$$\sqrt{\sqrt{\psi^2-\psi_0^2}+\psi_0+\frac{\psi_0'^2(1-\beta^2)}{2\alpha\beta}-\psi}\left(-\frac{\psi_0^2}{\left(\psi_0+\frac{\psi_0'^2(1-\beta^2)}{2\alpha\beta}\right)\left(\sqrt{\psi^2-\psi_0^2}-\psi\right)}-2\right)$$
$$+\frac{\psi_0^2\tanh^{-1}\frac{\sqrt{\psi_0+\frac{\psi_0'^2(1-\beta^2)}{2\alpha\beta}}}{\sqrt{\sqrt{\psi^2-\psi_0^2}+\psi_0+\frac{\psi_0'^2(1-\beta^2)}{2\alpha\beta}}-\psi}}{(\psi_0+\frac{\psi_0'^2(1-\beta^2)}{2\alpha\beta})^{3/2}}$$
$$=2\times\left[\sqrt{\frac{2\alpha\beta}{1-\beta^2}}\xi+C_2\right] \quad (2.25)$$

Here C_2 is the second constant of integration. After calculating the value of C_2 near the central region of electron cavitation, the scalar potential (ϕ) is obtained. Fig. (2.2) represent the excellent agreement of the scalar potential (ϕ) obtained from the above expression with the scalar potential of the structure obtained numerically.

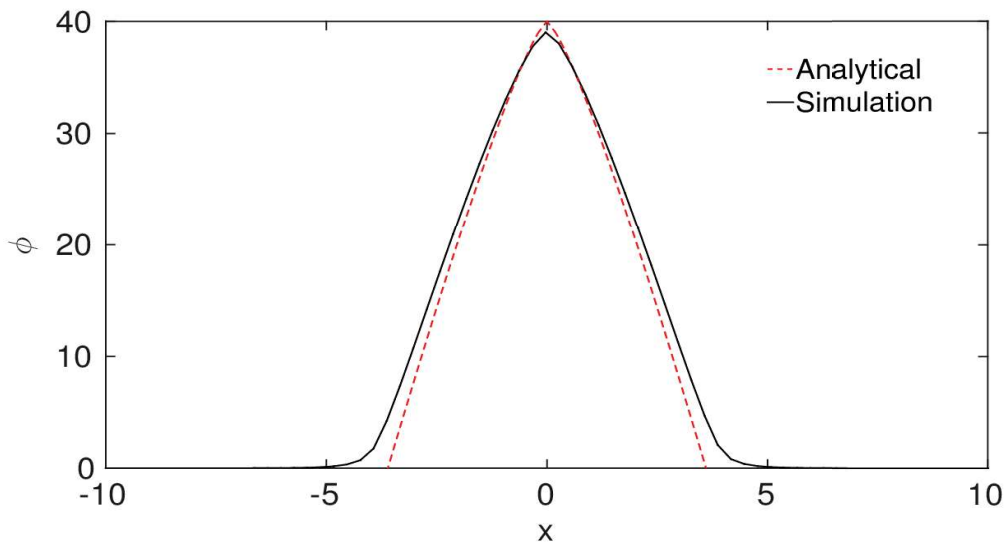

Figure 2.2: Analytic (solid line) and exact (dashed line) cusp solutions for ϕ field with electrons and ions both considered as dynamical species. The parameters λ and β have been choosen as 0.4570000953 and 0.8 respectively for present case.

2.4 Dynamical Evolution of Cusp Solution and its instability

In the above section of this chapter, we have shown the analytical form of the scalar potential which we have obtained by solving equation under the condition of ions approaching wave breaking criteria at the center. We have also shown that our analytical expression compares well for the given set of parameters which we have obtained from exact numerical solution. In the current section, we are going to present the numerical simulation technique used to evolve the exact cusp structure and also presented the results obtained by its dynamical evolution.

2.4.1 Numerical simulation

The set of equations (2.7-2.12) is numerically solved to study the time-dependent problem for the propagation of an intense electromagnetic radiation in a cold plasma for the electron-ion response. These equations are evolved using the Flux-Corrected Transport (FCT) algorithm developed by Boris et al [75]. LCPFCT (Laboratory of Computational Physics, Flux Corrected Transport) is a freely available suite of the subroutines which written in Fortran. This is a standard package whose stability properties has already been established in a variety of contexts by many users [76–79]. Here, we have solved these equations by using periodic boundary conditions along the x-direction. The wave equation (2.12) is a second order equation which is first decomposed in terms of four coupled convective equations. These convective coupled equations evolved by using lcpfct subroutine from the package. On the other hand, the momentum equations have been evolved by using cnvfct subroutine. The Poisson equation is solved using tridiag method. Here, we have used the numerical solutions of the cusp structure for initialization of fields in our simulation to study its dynamical evolution.

2.4.2 Evolution of Cusp Solution and instability

Fig. (2.3) shows the evolution of field variables R and ϕ which have been plotted at four different times $t = 0, 20, 40$ and $t = 60$. here t is normalized with the plasma period (ω_{pe}^{-1}). In the Fig. (2.3) the cusp solutions corresponds to $\beta = 0.42$ and $\lambda = 0.6289599$. The density evolution for electron and ion has also been presented in Fig. (2.4) for the same set of β and λ parameter as shown in Fig. (2.3). Due to lighter mass, electrons expel out from the center region of the laser pulse. However,

ion density is maximum at the center and forms cusp in ion density.

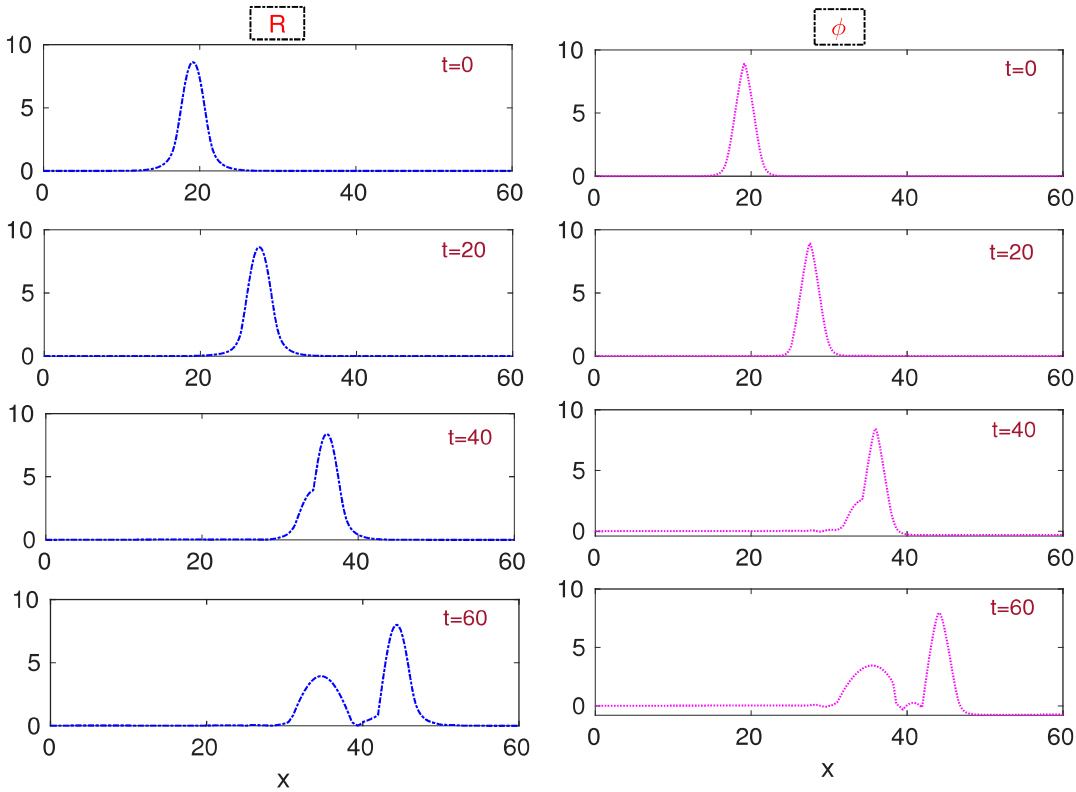

Figure 2.3: Evolution of vector potential (R) and scalar potential (ϕ) in left and right columns respectively at different times t=0, 20, 40, 60 electron plasma periods (ω_{pe}^{-1}). The parameters have been choosen as $\beta = 0.42$ and $\lambda = 0.6289599$.

We have plotted the perturbed vector potential for the solutions in Fig. (2.5). This has been generated by taking a difference between numerically observed profile at times $t = 20$ and $t = 60$ electron plasma periods with the exact numerically obtained solution displaced with group speed β in space. The perturbed amplitude of R is observed to start from the front edge of the structure in few plasma period

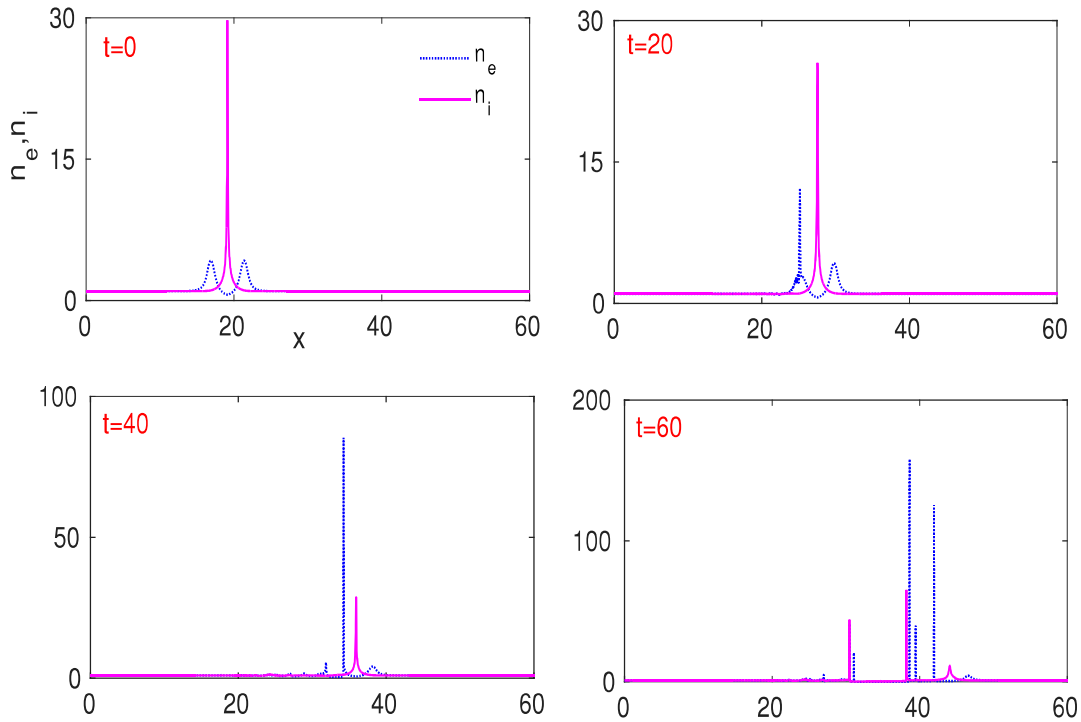

Figure 2.4: Evolution of electron density n_e(blue solid line) and ion density n_i(red solid line) with $\beta = 0.42$ and $\lambda = 0.6289599$ at four different times t=0, 20, 40, 60 electron plasma periods (ω_{pe}^{-1}).

and grows towards the trailing edge from where it is emitted outside the structure. As from the earlier work [58, 80], we know that, whenever electromagnetic light interacts with the plasma, either it decays in two purely electrostatic modes or one electromagnetic and one electrostatic mode. On the basis of the decomposition of the laser pulse, different kinds of instabilities come into the picture. If both the modes are electrostatic, then they get finally absorbed in the plasma and leading to the absorption of the light pulse. Secondly, if one mode is electrostatic and another is electromagnetic in nature, then it can escape from the plasma. In all these cases the phase matching condition can be represented by $\omega_L = \omega_1 + \omega_2$. Where ω_L, ω_1, and ω_2 represent the frequency of a laser light, frequency of mode-

1, and the frequency of mode-2 respectively. One of the basic phenomena in laser plasma interaction is known as Raman scattering. In this interaction the incident light of frequency (ω_0) decay into the scattered light of frequency ($\omega_0 \pm \omega_p$) and a plasma wave of frequency (ω_p). This scattered light gets coupled with the incident light for exciting the plasma wave. It modulates the plasma density. This plasma density modulation again causes the modulation of the incident laser pulse. It results in the form of further scattering and produces an instability as presented in the schematic diagram (2.5).

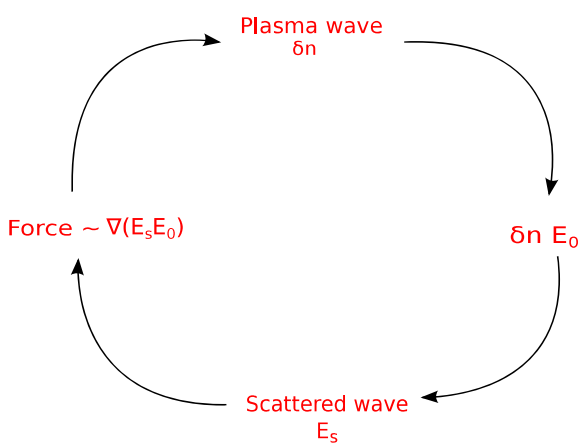

Figure 2.5: Parametric instability feedback loop.

In this section, we compare the numerically estimated growth rates of the instability with the theoretically known growth rates for the forward and backward stimulated Raman scattering. The analytical expression for growth rate [80–82] of the relativistic Forward Raman scattering instability is

$$\Gamma_{rfs} = \frac{1}{2\sqrt{2}\omega} \frac{A_0}{\left(1 + \frac{A_0^2}{2}\right)}$$

The backward Raman scattering instability growth rate for relativistic condition $\frac{v_{osc}}{c} < (\frac{\omega_{pe}}{\omega})^{\frac{1}{2}}$ is,

$$\Gamma_{brs} = \frac{\sqrt{\omega}}{4} \frac{A_0}{(1 + A_0^2)^{\frac{5}{8}}}$$

for $\frac{v_{osc}}{c} > (\frac{\omega_{pe}}{\omega})^{\frac{1}{2}}$ is,

$$\Gamma_{brs} = \sqrt{3} \left(\frac{\omega}{16}\right)^{\frac{1}{3}} \frac{A_0^{\frac{2}{3}}}{(1 + A_0^2)^{\frac{1}{2}}}$$

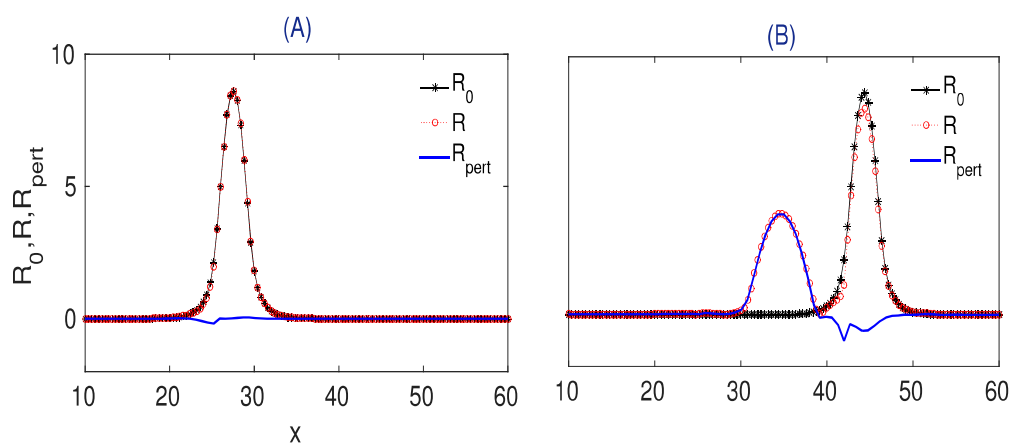

Figure 2.6: Evolution of Vector potential (R) at (a) 20 electron plasma period (ω_{pe}^{-1}) and (b) 60 electron plasma period (ω_{pe}^{-1}). R_0(black solid line) is vector potential at t=0, R(red dashed line) is vector potential after time t evolution and R_{pert}(green dotted-dashed line) is the perturb vector potential for $\beta = 0.42$ and $\lambda = 0.6289599$.

Here, ω is the electromagnetic wave frequency, A_0 is the maximum amplitude of the vector potential and Γ is the growth rate.

Table 2.1, gives the comparison of numerically obtained growth rates with ana-

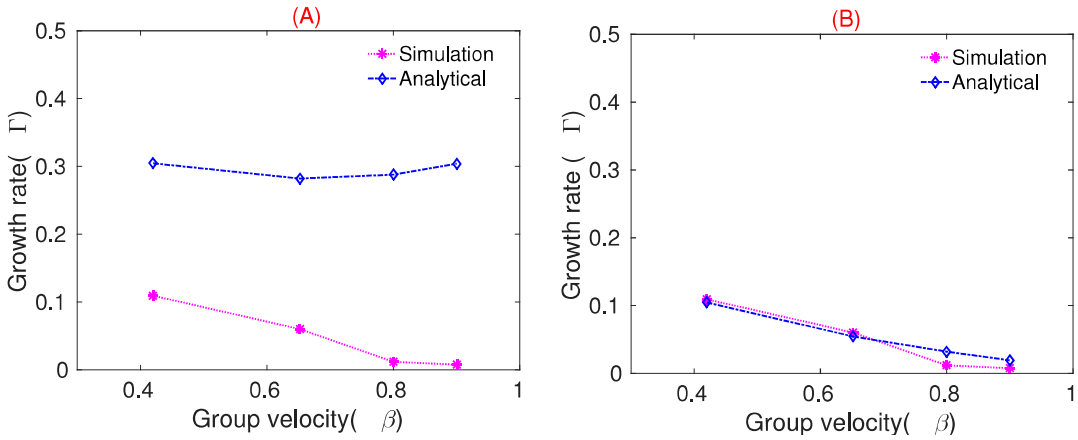

Figure 2.7: Growth rate(blue diamonds) comparison with simulation growth rate(pink stars) for (a) backward Raman instability and (b) forward Raman instability.

lytically estimated growth rates for both forward and backward Raman scattering. This growth rates calculated for four cusp solution which differed from each other by group speed, frequency parameters λ and A_{max} peak amplitude of the vector potential. From these values there are two very important things to be noticed- (1) The threshold value of electron density is larger than the minimum density of the electron in the cavity of the solitary structure, $n_{th} > n_{emin}$. (2) Growth rate values obtained from simulation is very closed to the growth rate calculated from the analytical expression given for the forward Raman scattering as compared to the backward Raman scattering growth rate values and this is also clear from the Fig. (2.7).

Table 2.1: Numerically observed growth rates comparison with analytically estimated growth rates.

β	λ	ω	A_0	u_{emax}	ϕ	n_{emin}	n_{th}	Γ_{brs}	Γ_{frs}	Γ_{sim}
0.420	0.628959900	0.7636715	8.604	0.321	8.899	0.6249	1.33	0.304	0.104	0.109
0.652	0.544000000	0.946258	13.57	0.604	24.04	0.3952	3.82	0.282	0.054	0.060
0.800	0.4570000953	1.269444	17.19	0.765	39.03	0.5238	10.77	0.287	0.032	0.012
0.900	0.3402846592	1.7909718	20.57	0.868	54.72	0.5356	14.75	0.304	0.019	0.007

2.5 Summary

To summarize, this chapter deals with the consolidation of soliton solutions when the ions are dynamical. This results in new variety of solutions which have no counterpart in the immobile ion case. The possibility of ion density hitting the wave breaking amplitude is a new feature. The longitudinal velocity of ions maximize at the center of the soliton. When this velocity becomes equal to the group velocity of the structure, the ion density profile becomes singular. There are no solutions possible beyond this value of the group velocity, β. However, solutions which are poised at the wave breaking point acquire interesting form. The singular ion density produces a cusp in the scalar potential. We have provided an approximate analytical description of the cusp electromagnetic envelope solitons which form at the ion wave breaking limit. The analytical form of the solution is shown to match the exact numerical form of the structure. The time evolution studies have also been carried out which show that these structures survive for several plasma

periods. However, they ultimately break away due to forward Raman scattering process.

3

The stability of 1-D soliton in transverse direction

In this chapter we study the development of transverse structure in the coupled 1-D laser plasma solutions by carrying out 2-D numerical simulations. We have restricted here to the study of solitonic structures which form in the presence of electron response only. It is observed that all the solutions are unstable to the development of transverse filamentation instability. This includes the single and paired structures which have been shown to be robust and stable in 1-D simulations in earlier studies [55].

3.1 Introduction

Out of all the 1-D coupled laser plasma structures, the single peak and the paired peak structures are found to be stable and long-lived in one-dimensional evolution. Solutions having multiple peaks of the vector potential are unstable due to Raman

forward scattering instability [56]. In this chapter, we have shown with the help of 2-D fluid simulation that the single peak and the paired peak soliton get destabilized by the transverse filamentation instability. The numerical growth rates obtained from simulation is found to match well with the analytical values. We have also observed that the multiple peak soliton first undergo the regular forward Raman scattering instability. Subsequently, they develop transverse structure and destabilize through transverse filamentation instability. This is evident from the plot of the perturbed energy in which first growth rate matches with the analytical estimates of the Raman forward scattering instability. The second growth in perturbed energy which comes at the later stage is found to compare well with the analytical estimates of the transverse filamentation instability.

This chapter has been organized as follows. Section (3.2) covers the brief description the fluid simulation. Section (3.3) discusses the numerical results on the observed transverse filamentation instability of the structures. In section (3.4), we provide a comparison of the numerically evaluated growth rates with the analytical estimates obtained for the filamentation instability of the structures. Section (3.5) discusses the nonlinear stage of the instability. Section (3.6) presents the summary and discussions.

3.2 Fluid simulation on 2-D study of electromagnetic solitons

The equations (2.1-2.6), form the complete set of equations to study the propagation of an intense electromagnetic radiation in a cold plasma for electron response, $\alpha = 0$. Now to incorporate the variation along the transverse direction

y, we would have $\nabla = (\frac{\partial}{\partial x}, \frac{\partial}{\partial y}, 0)$ in the set of equations (2.1-2.6) of chapter (2). This particular set of the equations is employed to study the evolution of the well-known 1-D laser plasma soliton solutions for the two-dimensional case. The simulation box is chosen to be in the $x - y$ plane. A 2-D fluid code based on flux-corrected transport scheme of Boris et al. [75]. It has been developed using the LCPFCT suite of subroutines to solve the evolution equations. The basic principle of LCPFCT scheme is based on the generalization of two-step Lax-Wendroff method [83]. We have solved the equations (2.1-2.6) in "$x - y$" plane with periodic boundary conditions using this method. The one-dimensional LCPFCT routines have been used repetitively to construct a 2-D solver by time step splitting into the different (x and y) directions. At every time step, it is checked that the results satisfy equations (2.5) and (2.6). The 1-D solitons have been chosen to have a spatial structure dependent on the x coordinate which is also the direction of their propagation. Thus initially the structures have no y dependence. The exact analytical form of the localized solutions of the above set of equations in the limit of small amplitude is known [39]. The analytical form of stationary solutions with arbitrary amplitude has also been obtained by Esirkepov et al. [52] for the one-dimensional case which can be employed as an initial condition to study their propagation. For arbitrary amplitude propagating structures, we obtain the form numerically by solving the nonlinear eigenvalue problem. These are then employed for initialization of fields in our simulation to study the evolution of structures in a 2-D spatial domain.

3.3 Numerical observations of transverse instability

We choose to study the evolution of all the three classes (namely: single peak, paired and multiple peak structures) of 1-D solitonic structures found in the context of coupled light plasma system. Many solutions with different values of the light frequency λ and the group velocity β were studied.

3.3.1 Single peak structures

Saxena et al. [55] has examined the stability of one-dimensional solitons and found that the single peak solutions exist in a continuum band in the parameter space of β and λ.

It has been observed that single peak solutions are stable and robust in one dimension. For a specific choice of a solution with $\lambda = 0.93$ and $\beta = 0.05$, the stability in 1-D simulations has been illustrated in Fig. (3.1) which shows the snapshots at various times (t =0, 200, 440 and 520) of the light field amplitude R, electrostatic potential ϕ and electron density n profiles. Here, the field R is defined as $R = (A_y^2 + A_z^2)^{1/2}$, where A_y and A_z are the $\hat{y}$ and the $\hat{z}$ components of the vector potential respectively. It should be noted that for the solitonic structures chosen in the simulations, the light wave is all circularly polarized. Consequently, A_y and A_z initially have a phase difference of $\pi/2$. The profile of the various fields at different times in Fig. (3.1) clearly shows that there is no change/distortion in the structures in a 1-D simulation.

The structures merely get translated by the group speed of $\beta = 0.05$ from their original location in these 1-D simulations. The same structure in a 2-D simulation,

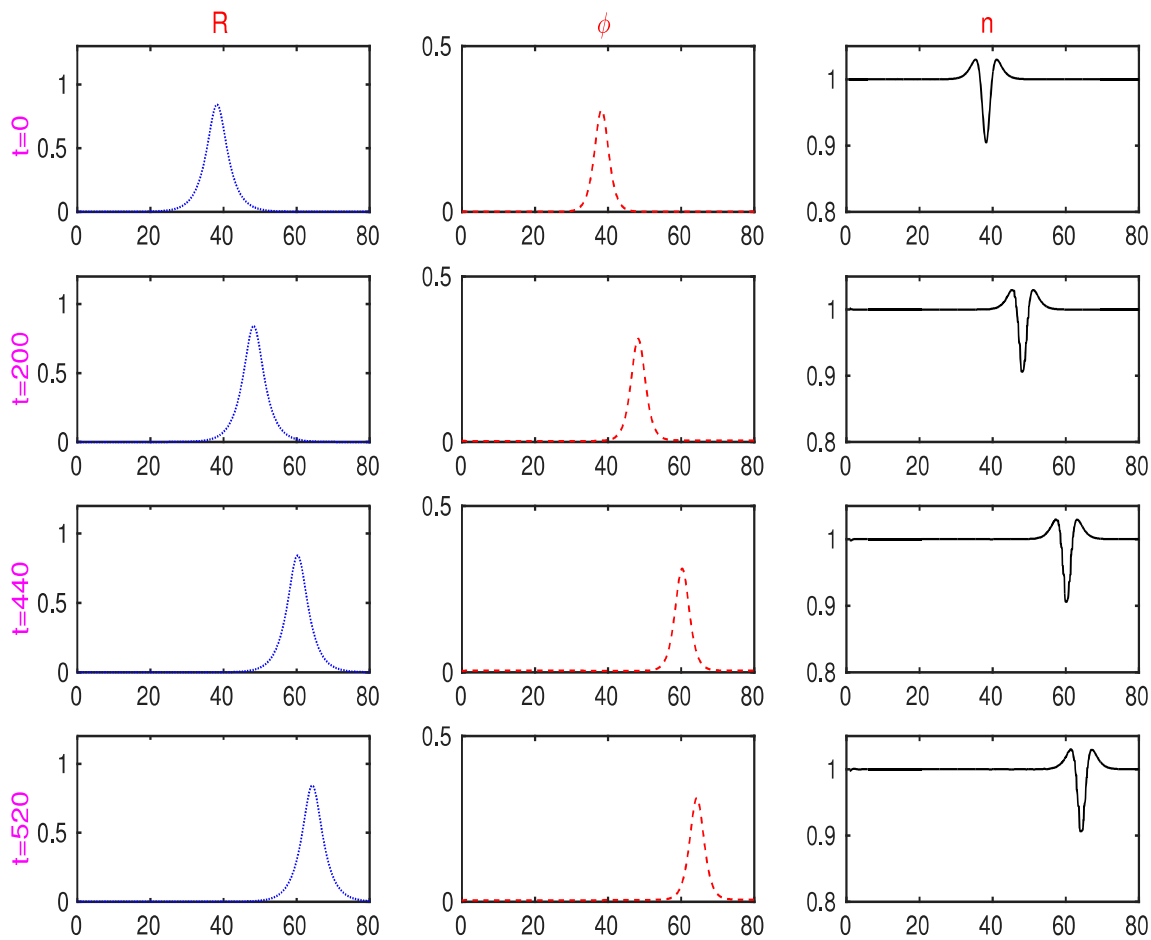

Figure 3.1: 1-D plot of a vector potential R, scalar potential (ϕ) and electron density (n) of a single peak soliton moving with group velocity β=0.05 and λ=0.93 at different times.

however, breaks up in the transverse direction as is evident from Fig. (3.2), where the profile of R and n have been shown at various times. The observed transverse structures have a typical scale length of the order of a few skin depths c/ω_{pe}. The

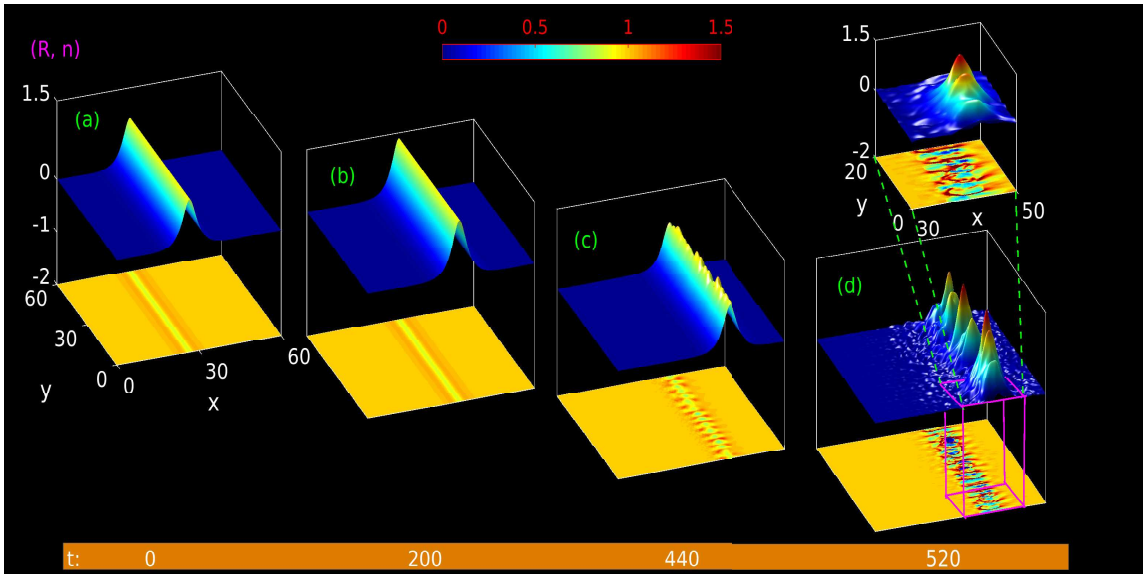

Figure 3.2: A surface plot of vector potential (R) and corresponding profile of electron density (n) shown in "$x - y$" plane at $z = -2$ for single peak soliton moving with group velocity β=0.05 and λ=0.93 at different times.

transverse filamentation of the structure can be understood by realizing that a small initial variation in transverse direction expels the electrons from the high-intensity region by ponderomotive force, thereby changing the refractive index. The change in the refractive index is such as to accentuate the modulation thus triggering the instability.

In Fig. (3.3) the evolution of perturbed field energy (FE_{pert}) has been plotted

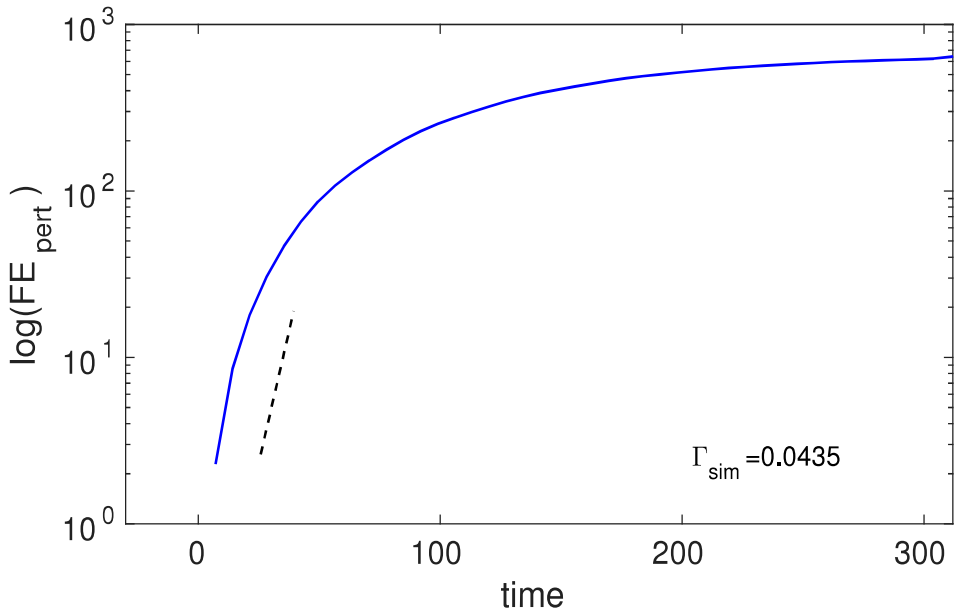

Figure 3.3: Plot of a perturbed field energy vs. time for a single peak soliton moving with group velocity β=0.05 and λ=0.93.

for this simulation. The expression for the perturbed field energy is given as-

$$FE_{pert} = \frac{1}{2}\int\int[\tilde{E}^2 + \tilde{B}^2]dxdy$$

Here $\tilde{E} = E(x, y, t) - E_0(x + \beta t, y)$ and $\tilde{B} = B(x, y, t) - B_0(x + \beta t, y)$. Where the suffix 0 stands for the chosen soliton solution. The Fig. (3.3) shows a linear rapid rise in the perturbed energy which ultimately saturates in the nonlinear regime. The growth rate estimated from the slope of this curve is 0.0431. The growth rate has been obtained from the simulation studies of various single peak solutions having different values of λ and β. This has been summarized in Table -3.1.

3.3.2 Paired solitonic structures

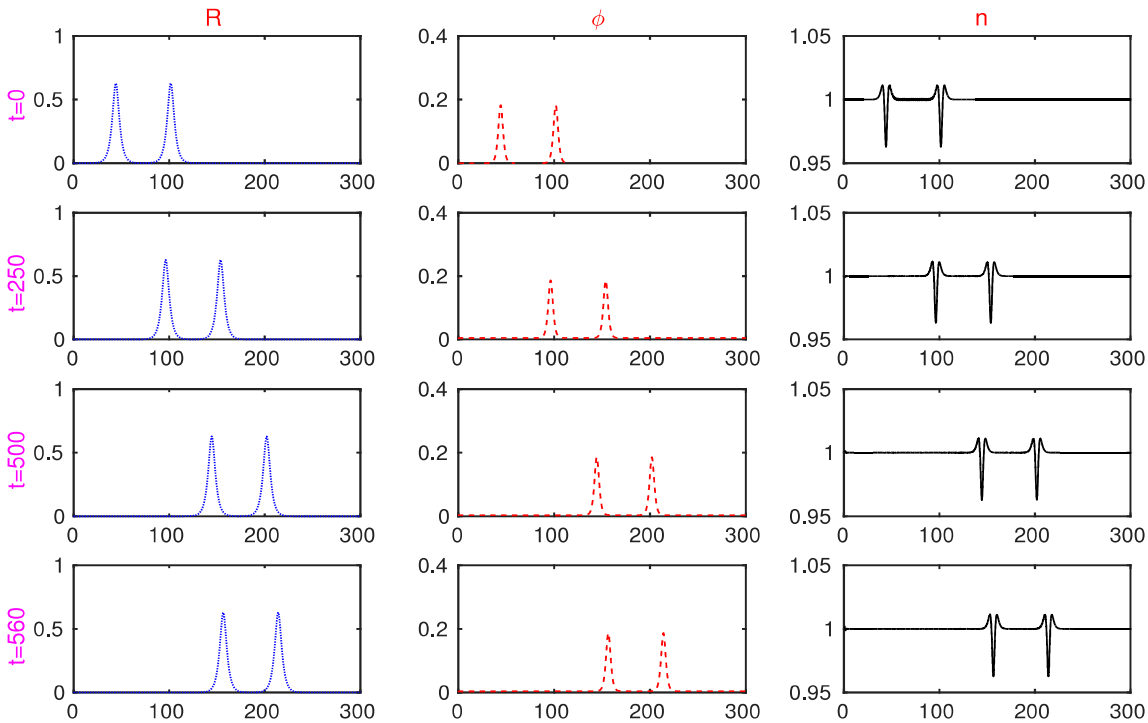

Figure 3.4: 1-D plot of a vector potential R, scalar potential (ϕ) and electron density (n) of a paired peak soliton moving with group velocity β=0.2 and λ=0.938455 at different times.

The paired structures are also observed to be stable in 1-D simulations as represented in Fig. (3.4). We have also examined their stability in the 2-D context with the help of numerical simulations. In Fig. (3.5) we show the profile of R and n for a specific paired solutions with a value of $\beta = 0.2$ and $\lambda = 0.938455$. These solutions also show a development of transverse modulations with time. In Fig. (3.6) the

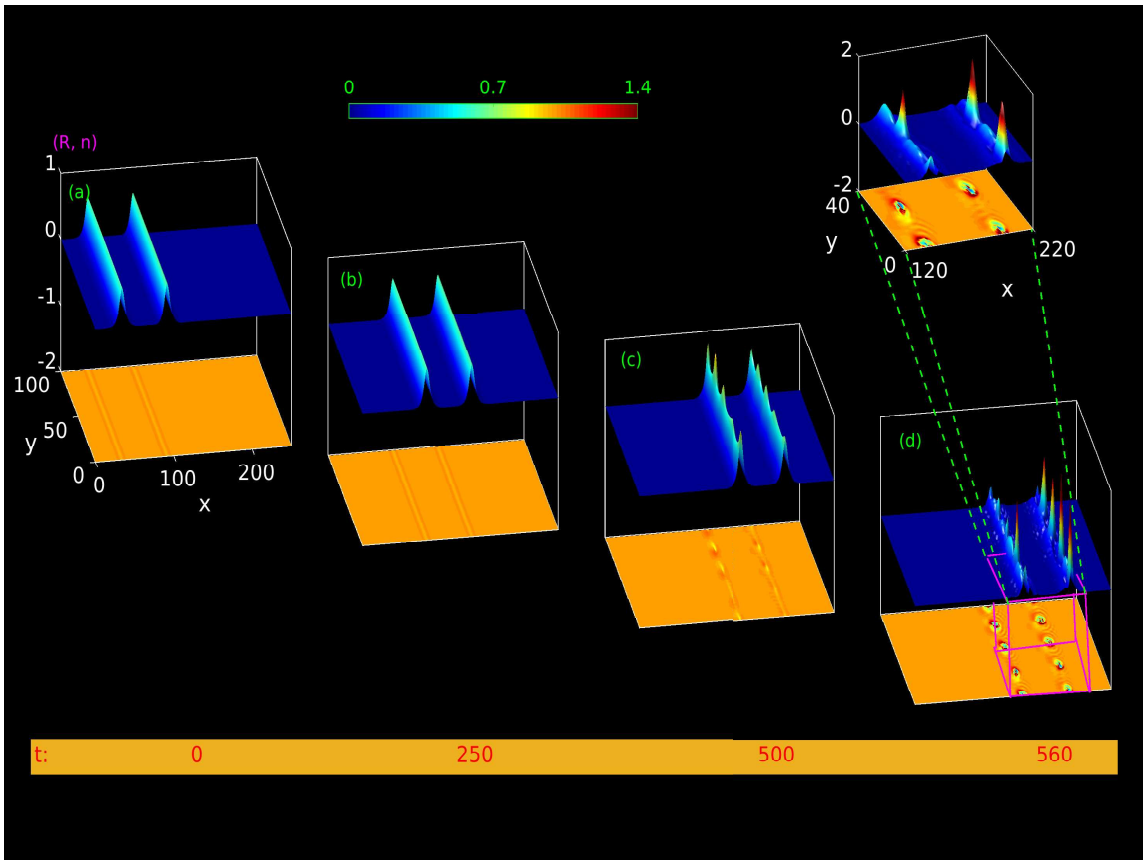

Figure 3.5: A surface plot of vector potential (R) and corresponding profile of electron density (n) shown in "$x - y$" plane at $z = -2$ for paired peak soliton moving with group velocity β=0.2 and λ=0.938455 at different times.

plot of perturbed field energy has been displayed. The perturbed energy grows till $t = 100$ and ultimately shows saturation. The numerical growth rate for various paired structures has been summarized in Table 3.2.

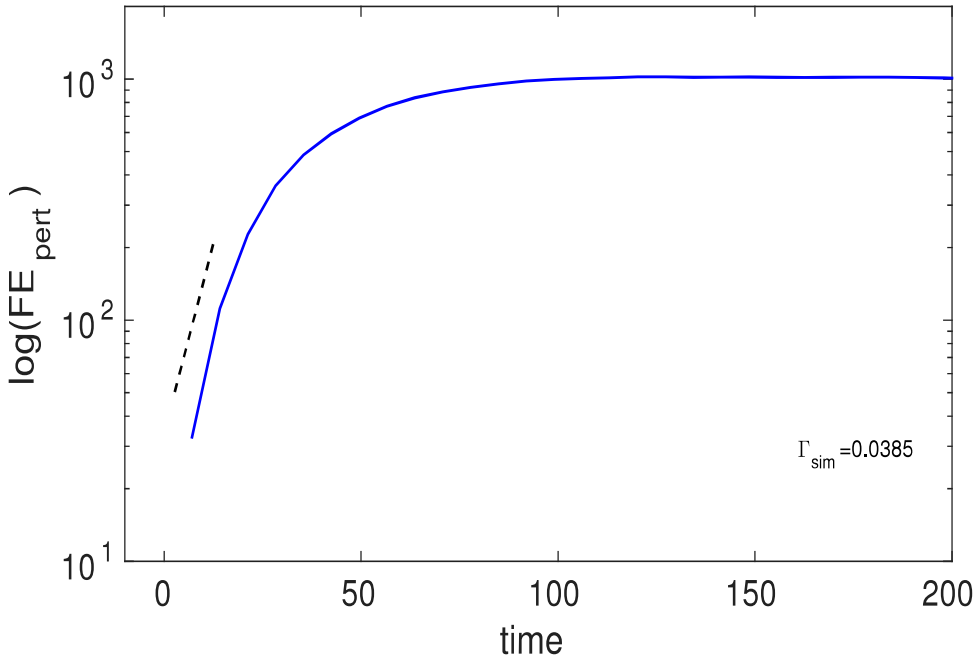

Figure 3.6: Plot of a perturbed field energy vs. time for a paired peak soliton moving with group velocity β=0.2 and λ=0.938455

3.3.3 Multiple peak structures

The evolution of multiple peak solutions have been shown in Fig. (3.8) for $\lambda = 0.714457$ and $\beta = 0.5$. Unlike the single and paired solutions the multiple peak solutions, in fact, are seen to destabilize in the longitudinal direction of propagation in the beginning (like the 1-D evolution shown in Fig. (3.7). This is later followed up with transverse modulations. The distinctive nature of the two destabilization process is captured very clearly in the plot of perturbed field energy evolution

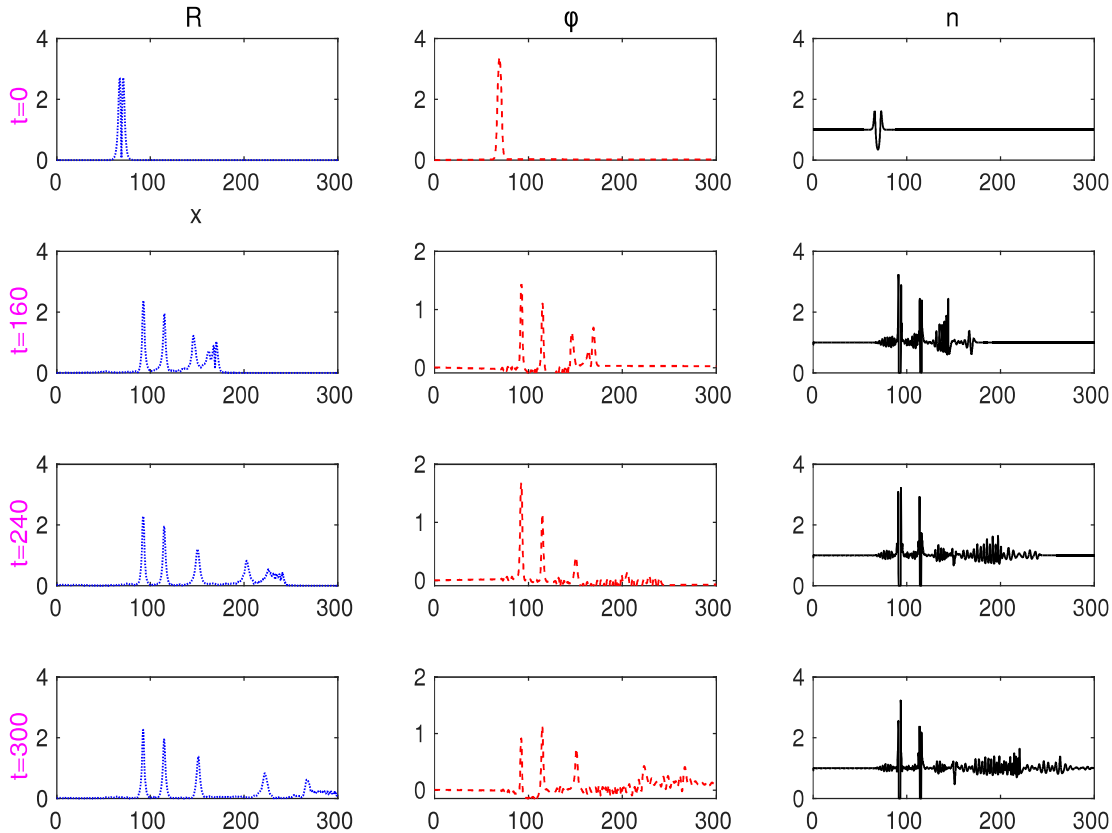

Figure 3.7: 1-D plot of a vector potential R, scalar potential (ϕ) and electron density (n) of a multi peak soliton moving with group velocity β=0.5 and λ=0.714457 at different times.

shown in Fig. (3.9).

It can be seen that there is a rapid growth of energy till $t = 17$, followed by a saturated regime. Around $t = 62$ another rise in energy can be clearly seen. For comparison, the plot of perturbed field energy for the 1-D simulations have been shown alongside. The curve corresponding to 1-D shows merely one initial stage of increase. The second phase of an increase can, therefore, be clearly attributed to the 2-D effects. It is also evident from the nature of profiles at the

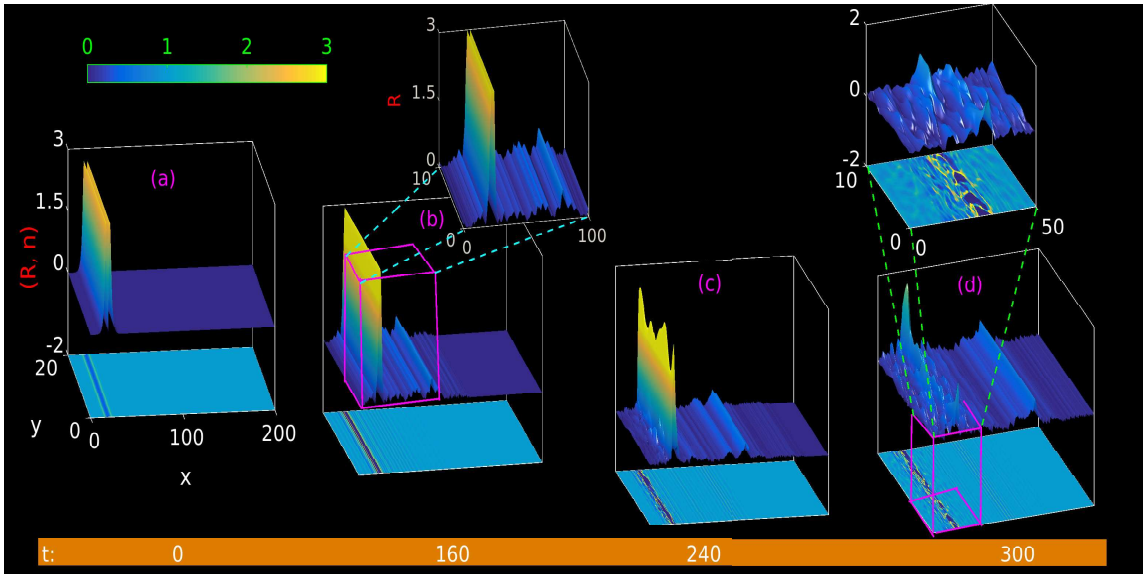

Figure 3.8: A surface plot of vector potential (R) and corresponding profile of electron density (n) shown in "$x - y$" plane at $z = -2$ for multi peak soliton moving with group velocity β=0.5 and λ=0.714457 at different times.

time corresponding to these two phases. The second step is the new instability similar to what the single and paired structures undergo. In Table-3 we provide a summary of our studies carried out for various multipeak solutions.

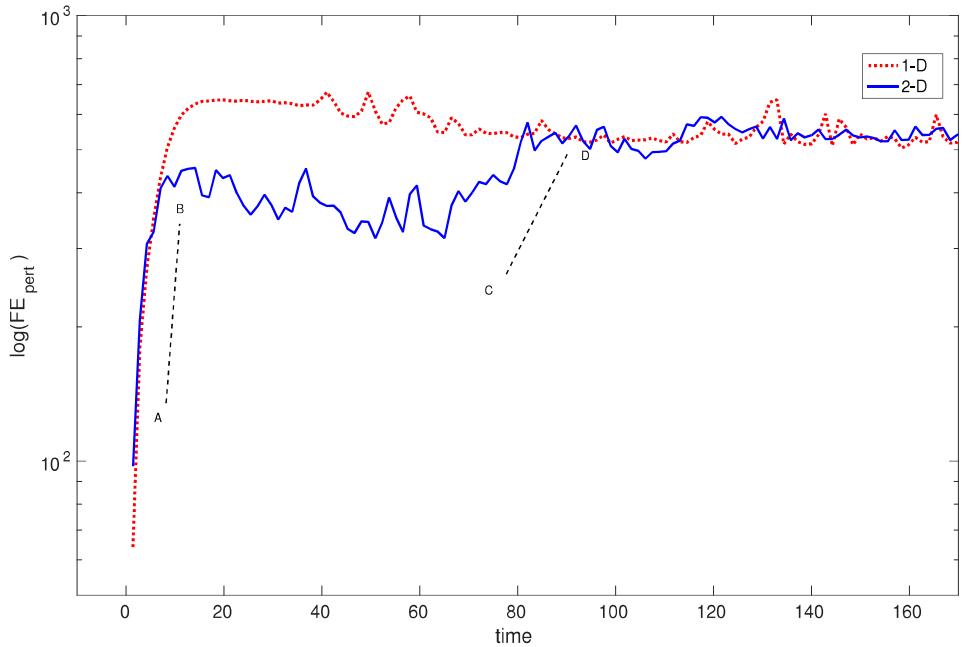

Figure 3.9: Plot of a perturbed field energy vs. time for a multiple peak soliton moving with group velocity β=0.5 and λ=0.714457.

3.4 Comparison of analytical and numerical growth rates

The numerical results clearly demonstrate the presence of an instability in the transverse direction for the single peak and the paired peak structures. For the multiple peak solutions, the forward Raman scattering instability appears first. The transverse filamentation instability then follows it. These instabilities have

been extensively studied by several authors [63–68, 80–82, 84–90]. The analytical expression of the growth rates for the the filamentation/modulational instability and the forward Raman scattering (FRS) instability for the light wave is given by the following expressions respectively [68]:

$$\Gamma_{mi} = \frac{1}{8\omega}\frac{A_0^2}{\gamma^3}, \tag{3.1}$$

$$\Gamma_{rfs} = \frac{1}{\sqrt{8}\omega}\frac{A_0}{\gamma^2} \tag{3.2}$$

These expressions have been obtained for a short laser pulse ($A_0 \sim 1$). Here, ω is the frequency of the light wave with the maximum amplitude of the vector potential as A_0 and γ represents the relativistic factor associated with electrons.

β	λ	ω	A_0	w	Γ_{ana}	Γ_{sim}
0.05	0.93	0.9323	0.8412	56.5	0.0425	0.0431
0.07	0.95	0.9547	0.6728	66.1	0.0339	0.0315
0.1	0.967	0.9768	0.4985	83.2	0.0228	0.0230
0.15	0.96	0.9821	0.5074	81.5	0.0232	0.0235
0.2	0.975	1.0156	0.1996	177.9	0.0046	0.0468
0.3	0.95	1.0440	0.1829	186.8	0.0038	0.0491
0.4	0.91	1.0833	0.2415	141.0	0.0062	0.0163
0.5	0.858	1.1533	0.2769	101.1	0.01	0.0108
0.6	0.797	1.2453	0.1744	163.3.5	0.0029	0.0181
0.8	0.599	1.6639	0.1158	175.1	0.00098	0.0261

Table 3.1: Comparison of numerical and analytical filamentation growth rates for single peak solitary solutions.

In Table - 3.1, Table -3.2 and Table - 3.3, the analytical estimate of the growth rate for modulational instability has been provided by the equation (3.1). It can be

β	λ	ω	A_0	w	Γ_{ana}	Γ_{sim}
0.05	0.91	0.9123	0.9932	137.8	0.0483	0.0431
0.1	0.93047	0.9399	0.8108	114.1	0.0410	0.048
0.2	0.92594	0.9645	0.7345	96.4	0.0366	0.0385
0.3	0.907123	0.9968	0.6896	86.1	0.0333	0.1
0.4	0.89100914	1.0607	0.4974	129.7	0.0209	0.0850
0.5	0.85014	1.1335	0.3966	140.9	0.0139	0.0559
0.6	0.794	1.2406	0.2476	162.3	0.0056	0.06
0.7	0.708993	1.3902	0.2435	187.9	0.0049	0.0768

Table 3.2: Comparison of numerical and analytical filamentation growth rates for paired peak solutions.

observed that the analytically estimated growth rate matches fairly well with the numerically evaluated growth rate of the instability for all the three variety of the structures having smaller width (w) for various values of parameters β and λ. This confirms that the observed instability is the transverse modulational/filamentation instability. In Fig. (3.11) we plot the analytically estimated and numerically evaluated growth rates as a function of the width (w) of solitonic structures for all three kinds of solitons. It can be observed that there is a close agreement between analytical and numerical results when the structure is narrow. The difference between analytical and numerical values increase with increasing width of the structure. This is reasonable as the analytical expressions for the growth rate Γ in equation (3.1) is valid only for short laser pulse envelope. Ina previous study Saxena et al. [56] has already made the comparison of numerical and analytical growth rate for forward Raman scattering instability for the multiple peak solutions for 1-D simulations. The growth rate for the FRS instability obtained from our 2-

β	λ	ω	A_0	w	$\Gamma_{ana_{mi}}$	$\Gamma_{sim_{mi}}$	$\Gamma_{rfs_{ana}}$	$\Gamma_{rfs_{sim}}$
0.1	0.61440192	0.6206	7.305	34.3	0.0268	0.0364	0.0564	0.0620
0.2	0.6640659	0.6917	5.519	35.9	0.0312	0.0238	0.0673	0.0605
0.3	0.699742	0.7689	4.257	33.2	0.0352	0.024	0.0880	0.0732
0.4	0.718307	0.8553	3.338	36.7	0.0385	0.0204	0.1176	0.0907
0.5	0.714457	0.9526	2.707	34.6	0.04	0.03	0.1174	0.16
0.6	0.688022	1.0750	2.204	38.9	0.0398	0.0123	0.1317	0.0215
0.7	0.6371499	1.2493	1.77	38.1	0.0373	0.0039	0.1407	0.0768
0.8	0.554374	1.5399	1.371	32.5	0.03	0.0117	0.1338	0.082

Table 3.3: Comparison of numerical and analytical filamentation and raman forward scattering growth rates for multi peak solitary solutions.

D simulations provides similar estimates. We have also made a comparison of the growth rate for FRS and the transverse filamentation/modulational instability and observe that the FRS growth rate is comparatively higher. It is for this reason that the multiple peak solutions are first unstable to FRS and after that, the 2-D filamentation instability appears.

3.5 Nonlinear development of the instability

It is clear from our simulation and analysis that the stable solitonic structures of 1-D are susceptible to filamentation instability in the transverse direction. For the single peak and the paired peak structures, the filamentation instability leads to the formation of the structures in the transverse direction which are typical of the order of skin depth. However, these structures, subsequently, in the nonlinear phase of the instability coalesce and form bigger structures (e.g. Fig. (3.10)). This phenomenon appears similar to the process of an inverse cascade that is observed

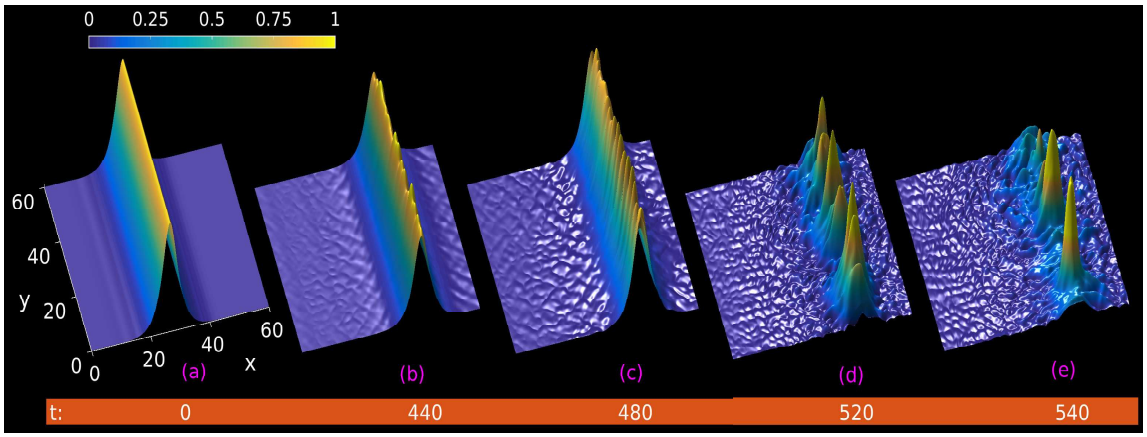

Figure 3.10: Surface plot of vector potential R for single peak soliton moving with group velocity β=0.05 and λ=0.93 at different times.

typically in the 2-D fluid systems. It should, however, be noted that the multiple peak solutions which suffer first the forward Raman instability and subsequently disintegrates along the transverse direction do not seem to display the long scale coalescence in the nonlinear regime. The fields typically in this case remain at short scales and are fairly random in nature.

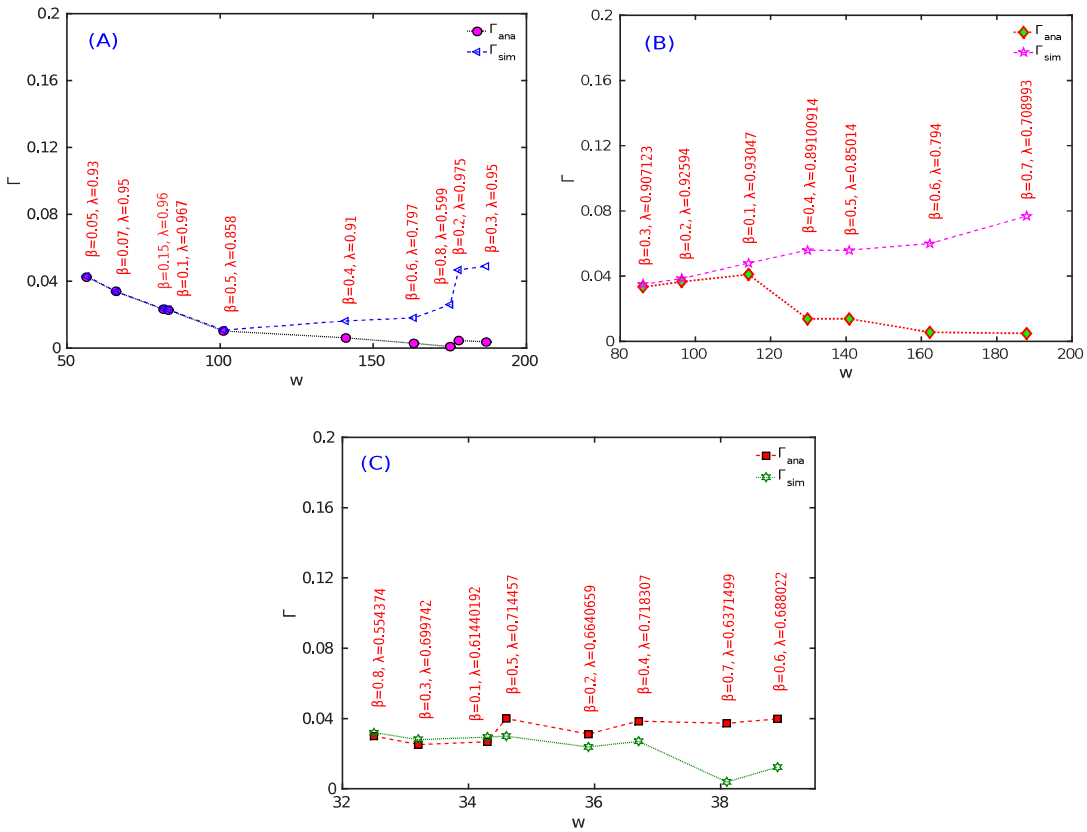

Figure 3.11: Analytical and simulation growth rate plot vs width (w) of the solitonic structures for (A)Single peak soliton (B) Paired soliton and (C) Multipeak soliton.

3.6 Summary

The coupled light plasma system permits various kinds of localized solutions. In particular, for the case when the ion dynamical response can be ignored (treating ions merely as merely a neutralizing stationary background) three varieties of solitary structures have been shown to exist. They correspond to the single peak, paired and multiple peak structures of the light wave amplitude. The multiple peak solutions have been shown to be unstable to forward Raman scattering instability

in previous 1-D simulations [56]. The other two, single and paired structures, however, were found to be stable in the 1-D runs. We have shown here with the help of 2-D simulations that these two structures are unstable when 1-D restrictions are removed to permit 2-D perturbations. The resulting instability was identified as the transverse filamentation instability by comparing the numerically observed growth rate with the analytical expression for the growth rate of filamentation instability of short pulses. The multiple peak solutions in 2-D first undergo the forward Raman instability process. Subsequently, they destabilize in the transverse direction through the filamentation instability. The growth rate of both the instability can be identified clearly from the slope of the perturbed energy. In the nonlinear regime, the transverse structures of the single and paired solutions show the phenomena of merging and form longer scales solutions, akin to the inverse cascade process. However, the multiple peak structures which suffer disintegration both in longitudinal and transverse directions by two consecutive instabilities, in the nonlinear regime continue to have short random scale field structure.

4

Observation of time-dependent 1-D localized structures in laser plasma system with fluid simulations

In this chapter, we report the observation of a variety of time dependent localized structures in the coupled laser plasma system through 1-D fluid simulations. Such structures are seen to survive as coherent entities for a long time up to several hundreds of plasma periods. A detailed study to understand the context of their formation and their dynamical characteristic have been carried out. It is observed that typically these structures form as a result of collision amongst certain exact solutions. The other variety constitutes of emitted remnants of unstable exact 1-D solutions which exhibit time dependence in their shape while remaining robust and preserving their identity. It is shown that such time dependence can also be artificially recreated by significantly disturbing the delicate balance between the radiation and the density fields required for the exact solution. The

ensuing time evolution is an interesting interplay of plasma oscillation (associated with electron density) and oscillations of the electromagnetic fields. However, the plasma oscillations are invariably found to acquire high amplitude ultimately and undergo wave breaking process with a consequent drop in total energy shown in fluid simulations. Even after wave breaking, compact coherent structures with trapped radiation inside high-density peaks, continue to exist. Since fluid simulations cannot be trusted beyond the wave breaking point, we have in the next chapter carried Particle - In - Cell simulations.

4.1 Introduction

As mentioned in the chapter (2) and (3), the coherent structures are important in many ways. For instance, they can be used as a means for transporting energy in plasma medium [91]. They can also be utilized for particle and photon acceleration purposes [41]. However, the precarious spatial balance of electrostatic and electromagnetic fields required for their formation can be difficult to satisfy in a realistic situation. It is shown in this chapter that there also exist time-dependent localized structures which do not require any such delicate balance between the various fields. The structures though time dependent, survive as a single entity for a very long duration e.g. for several hundreds of plasma periods. The energy leakage is minimal. We feel that such versatile long-lived structures are also well suited for many applications including the transport of energy. The context of the formation of such time-dependent structures, the behavior they exhibit during evolution etc., has been examined in considerable detail using fluid simulation in this chapter (4).

This chapter has been organized as follows. The next section (4.2) contains a description of the numerical simulation technique used to study time-dependent localized structures in LP (laser plasma) systems. In section (4.3), we provide a description of certain spontaneously formed time-dependent structures. For instance, in the collisional interaction between high but unequal amplitude single peak structures, the remnant structure displays interesting oscillatory behavior. These remnants are observed to invariably have a high amplitude (exceeding the upper limit of radiation for static single peak solutions [52]) static oscillating profile. In some previous time, evolution studies of the multiple peak solutions of the laser plasma coupled system are found to be unstable to forward Raman scattering instability. As a result of this instability, they eject radiation and density bunches from their wake which are found to be very robust and survive as a coherent entity even though their profile changes with time. In section (4.4), we recreate the nature of time dependence observed in these spontaneously formed structures by deliberately disturbing the delicate balance between the radiation and the electron density profile of exact solutions. Despite the significant disturbance, the structure does not disintegrate but exhibits similar traits of time dependence as observed in section (4.3) for spontaneously formed structures. A detailed study of these system shows that the energy alternates between field and kinetic forms. The excess radiation introduced in the system tries to leak out of the structure and in the process excites electron density oscillations. These typically represent excitation of plasma wave in an inhomogeneous medium which subsequently acquires large amplitudes forming density peaks and undergoes wave breaking. The radiation gets entrained inside two density peaks forming coherent entities with compact support. These structures are found to retain their identity in fluid simulations for

a long time. However, keeping in view the reservations on fluid simulations beyond wave breaking time, PIC studies have also been performed and are presented in the next chapter (5). The PIC study confirms the fluid simulation observations even beyond the wave breaking phenomena. This shows that the structures with entrained radiation inside two density peaks hovering around the wave breaking limit are realistic. Section (4.5) contains the summary and discussion.

4.2 Numerical simulation technique

In this section, we study the properties of those structures which get ejected from an unstable 1-D solitons and/or are remnant of various interactions amidst the exact solutions by solving equations (2.1-2.6) by considering the case of a laser pulse which is propagating along the x-direction inside a plasma. We have purposefully also disturbed the precarious balance between the various fields that the exact solutions have to satisfy and studied their evolution.

Various diagnostics such as the energies associated with field (FE) and kinetic (KE) along with total energy (TE) of the plasma has been tracked in time. These energies are evaluated numerically by the following expressions:

$$FE(t) = \frac{1}{2}\sum_i [E_i^2(t) + B_i^2(t)]\Delta x_i$$

$$KE(t) = \sum_i n_i(t)[\gamma_i(t) - 1]\Delta x_i$$

$$TE(t) = KE(t) + FE(t)$$

where $i = 1, 2, 3, ...N_x$ and N_x is the number of spatial grid points having a width of Δx_i. $E_i(t)$, $B_i(t)$, $n_i(t)$ and $\gamma_i(t)$ are the values of electric field, magnetic field, electron density and relativistic factor respectively at the $i-$th grid point at time t.

4.3 Evolution of spontaneously formed structures

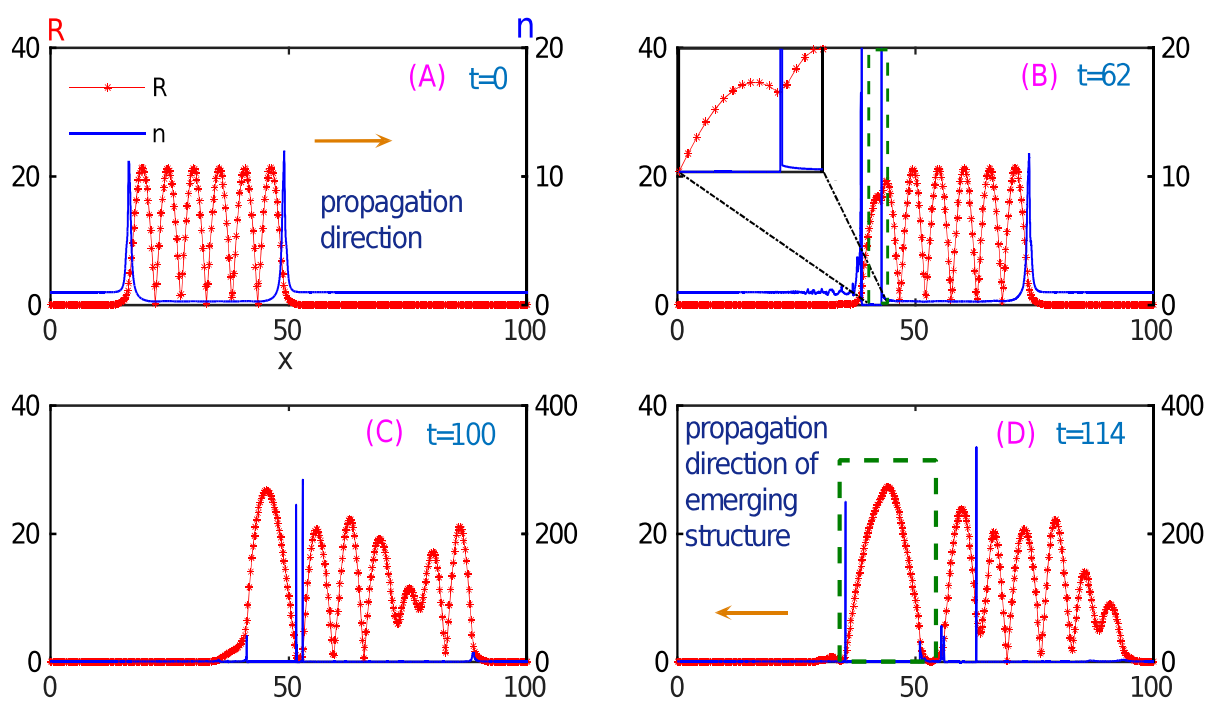

Figure 4.1: Vector potential (R) and density (n) for moving soliton at group velocity (β=0.4) for multi peak soliton.

In some previous studies [55, 56], it was observed that the unstable multipeak solitons emit certain structures from their rear edge as they evolve. These emitted structures have peaked densities within which radiation is trapped. In Fig. (4.1) such a destabilization process has been shown. An ejected structure (identified by the green dashed lines in Fig. (4.1D)) of radiation trapped between two adjacent density peaks have been chosen to study for its time evolution separately and observed that the structure propagates in a backward direction to the original solution from which it has been emitted. It also changes its shape with time. However, it retains its coherent identity during the entire course of evolution studied in the present simulation.

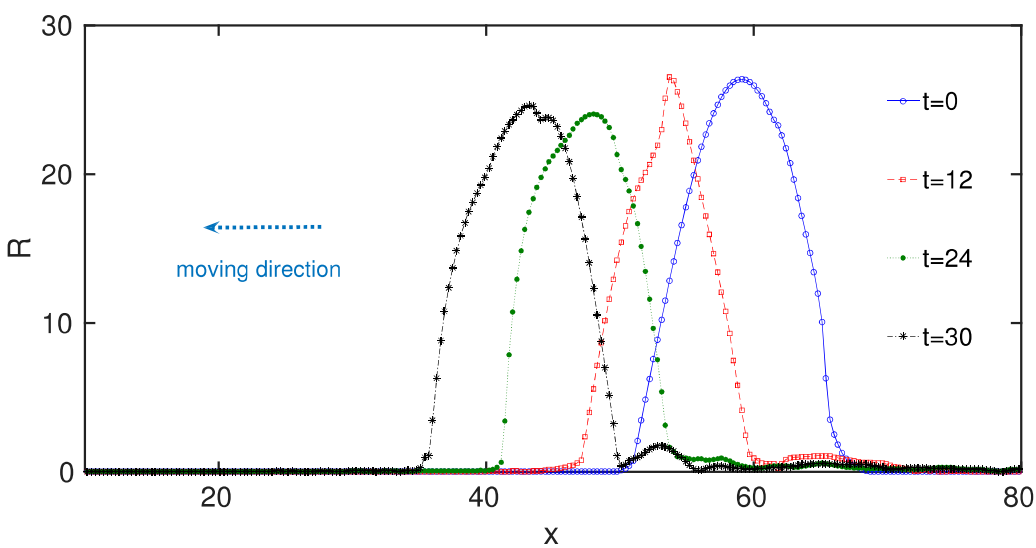

Figure 4.2: Vector potential (R) profile at different time t=0, 12, 24, 30.

The snapshots of $R = \sqrt{A_y^2 + A_z^2}$ at different times showing various phases of evolution has been depicted in Fig. (4.2). It is clear that the structure takes a

series of different shapes as it propagates. Some energy also keeps getting leaked from the structures. The density peaks at the two edge show interesting out of phase oscillations wherein as the amplitude of the density peak at the front of the structure diminish, the peak at the back of the structure increases and vice versa. a closer look shows that as the density at the back of the structure increases, it pushes the radiation towards the front. This introduces a disturbance in the profile of R which seems to propagate from the back of the structure towards the front. The structure seems to show many complex dynamical processes that work simultaneously e.g. propagation, shape evolution, energy leak, electron density oscillations etc. However, amidst all these processes the overall integrity of the structure seems to remain intact for several tens of plasma periods.

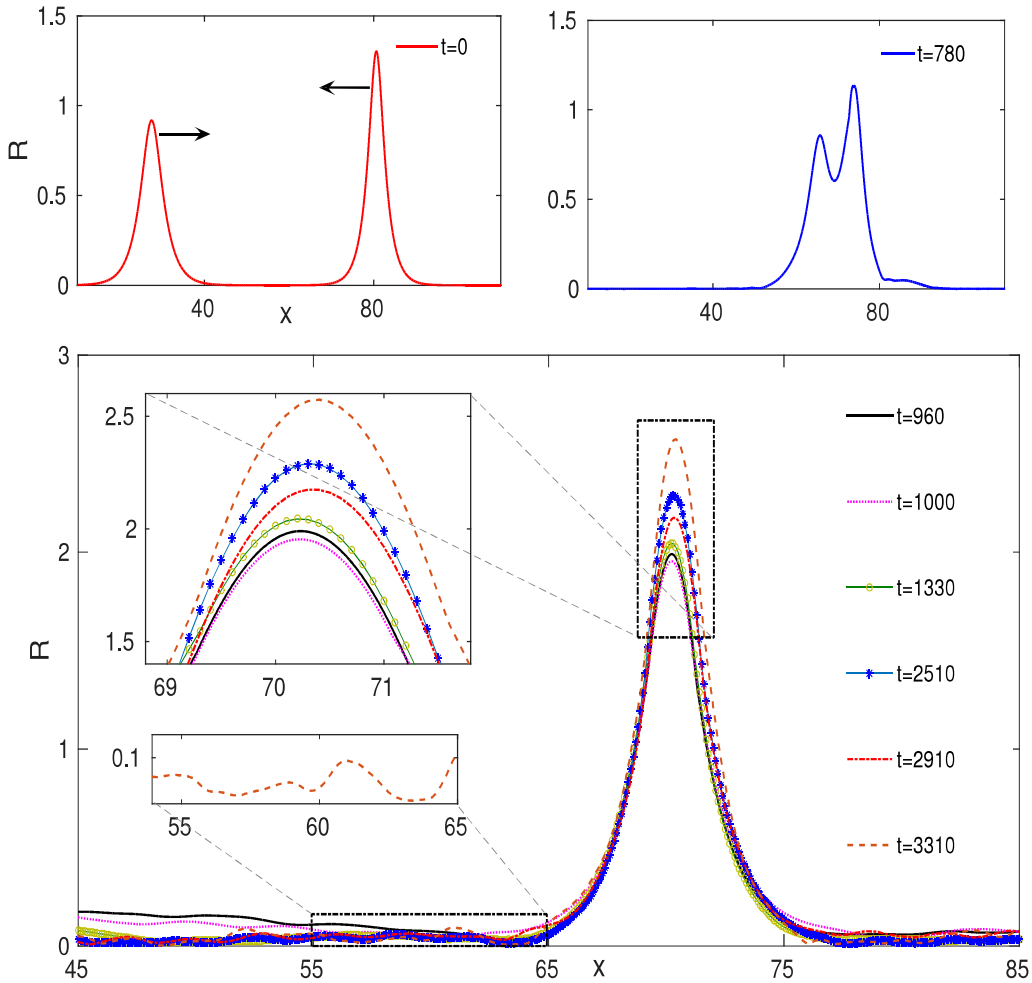

Figure 4.3: Collision of two single peak of soliton moving at group velocity $\beta = -0.01$ and $\beta = 0.05$.

Another example of time-dependent robust structures are found is the case when two high but unequal amplitude oppositely moving exact single peak structures suffer collision as shown in Fig. (4.3). It is observed that the two structures, in this case, merge into a large amplitude non-propagating structure. The ampli-

tude of R in this case, however, exceeds the upper permissible limit of static exact solutions (Esirkepov et al., [52]) for which the density is completely evacuated from the center. The amplitude of this spontaneously formed structure shows oscillations in time and there is also evidence of the radiation leaking out from it. However, the overall structure seems to persist for a long time. This raises several questions- Does the laser plasma system permit a new variety of time-dependent solutions, where the time dependence is not merely restricted to steady propagation. There is a need to explore more to understand the complex interplay between density and radiation fields in more detail and if possible develop a physical understanding of it. To gain further understanding, we explore the time dependence in the context of stable exact solutions in the next section by deliberately disturbing the delicate balance between the various fields by a known amount.

4.4 Evolution of significantly perturbed stable structures

We have chosen several exact single peak solutions and enhanced the radiation trapped inside the density cavity significantly. For instance, we considered enhancing the amplitude of R by a constant factor and have also considered asymmetrically changing the value of R about the central region of the structure. In the first case, the trapped radiation pressure is in excess than that required for the balance. In the second case, at one of the edges the radiation pressure dominates and at other the electrostatic force dominates. The dynamics for both kinds of changes introduced in the initial profiles have been investigated thoroughly. Furthermore, we choose to evolve both kinds of solutions (after introducing these

significant perturbations), namely the static (for which the group velocity $\beta = 0$) and propagating (for which the value of β is finite). The two subsections below discuss them in detail.

4.4.1 Evolution of perturbed static structures

In this subsection, we consider the stationary solutions i.e. those with group velocity, $\beta = 0$ for our studies. Esirkepov et al. [52] have obtained an exact analytical form for the stationary solitonic structures. We take the analytical form of the solution and express it in terms of the initial conditions for electric, magnetic and velocity fields. These fields are then evolved in our simulations. The initial density of the electron is chosen to satisfy the analytical form of the solution.

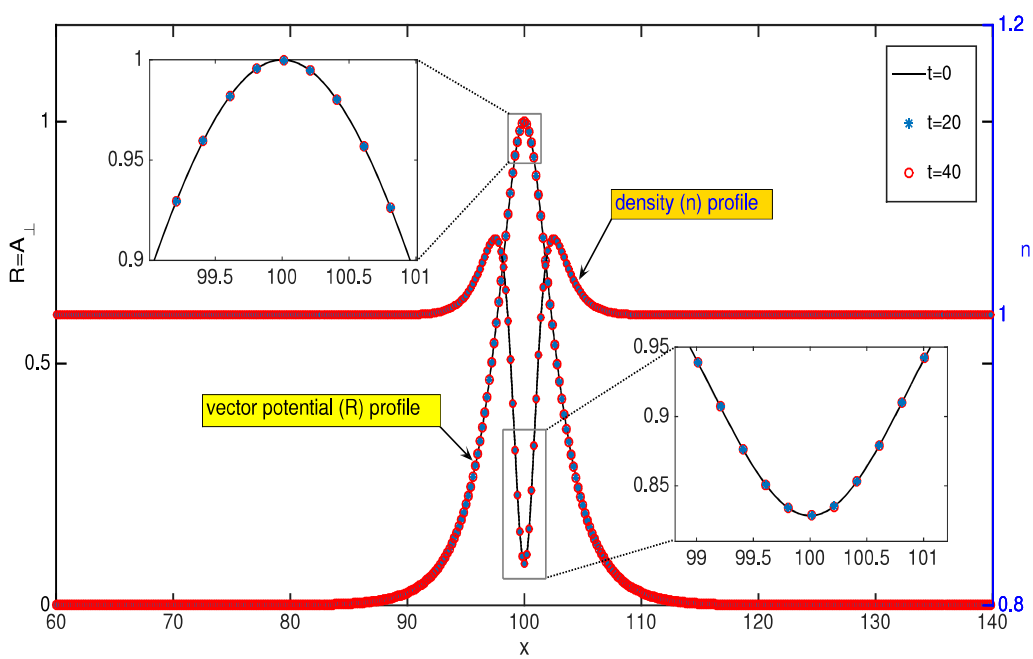

Figure 4.4: Single peak soliton with group velocity $\beta = 0$ and $A_0 = 1$.

The stationary solitary solutions in our simulation was chosen for a value of $A_0 = 1$; where A_0 is the peak value of R of the solution. The frequency of laser has been derived from, $\omega = \sqrt{2\sqrt{1+A_0^2} - 2}/A_0 \simeq 0.9102$. We have initiated our simulation and followed the time evolution of this structure. In Fig. (4.4), we show the plots of the profile of R at various times obtained from the simulation. It can be observed that the plots even when zoomed in and expanded, fall exactly on top of each other at various times. All other fields also show no evolution. The kinetic and field energy associated with the structure show no variations and remain constant throughout the period of evolution. This is exactly how the stable static solutions obtained by Esirkepov et al. [52] are expected to behave. This validates the numerical code and also verifies the correctness of the choice of the initial condition.

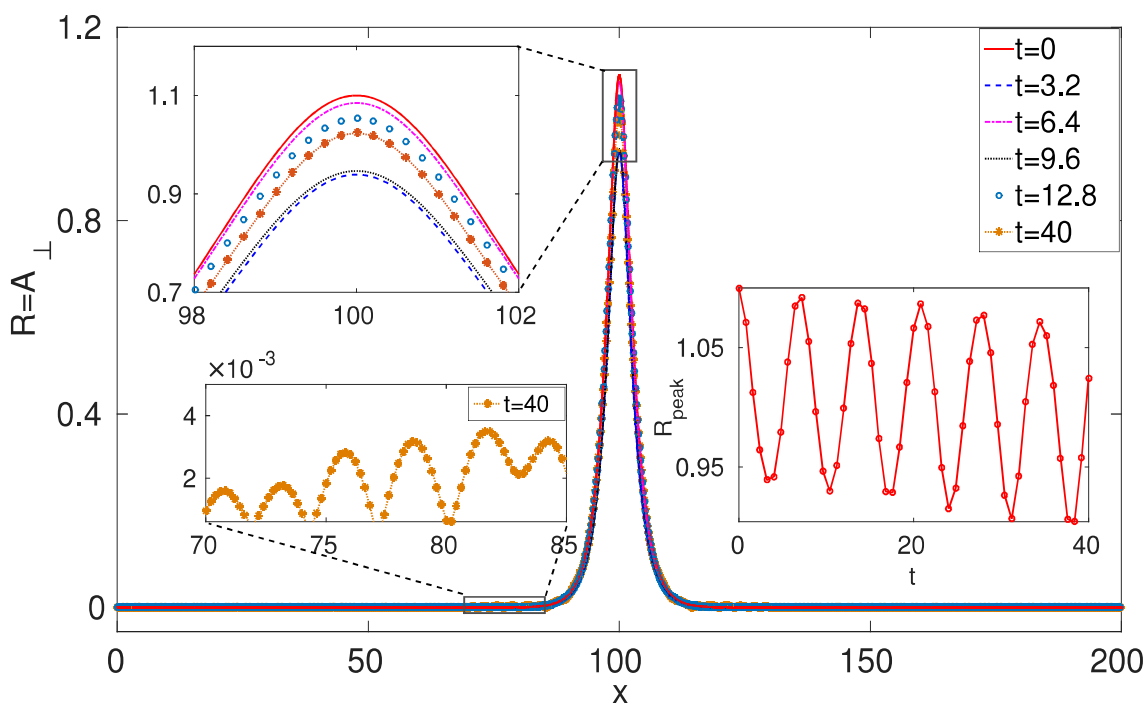

Figure 4.5: Vector potential (R) for stationary ($\beta = 0$) single peak soliton of amplitude $R = 1.1R0$ at different times.

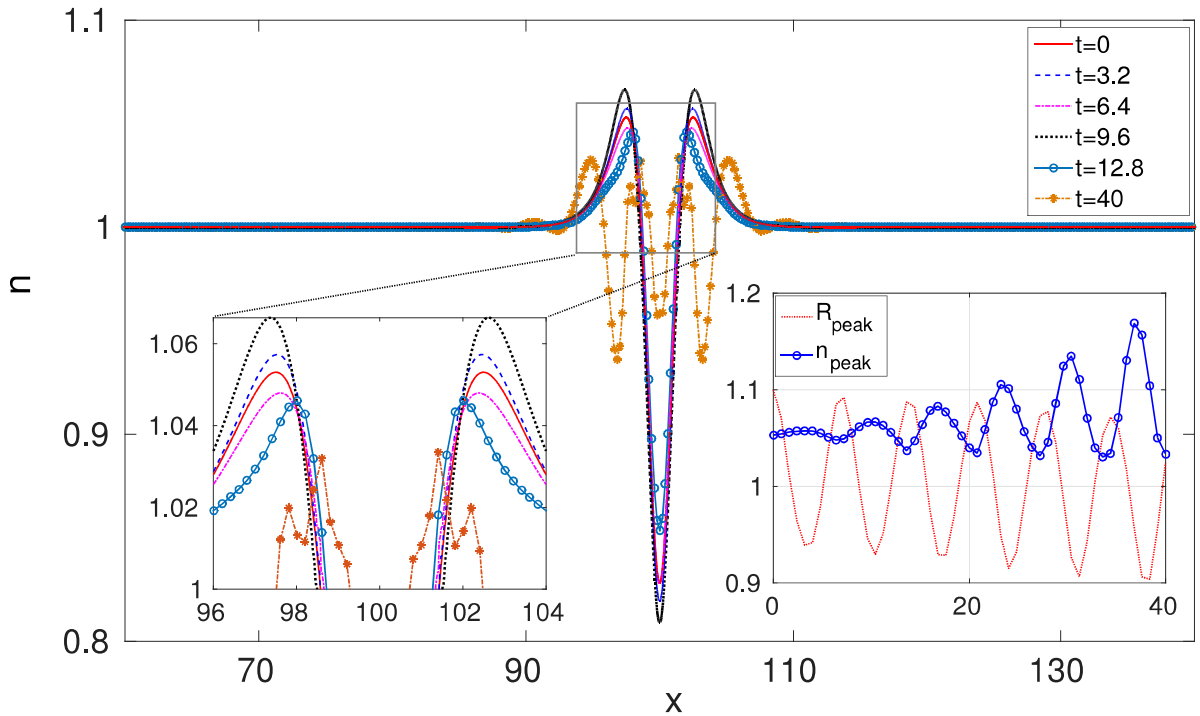

Figure 4.6: Desnity (n) profile for stationary ($\beta = 0$) single peak soliton of amplitude $R = 1.1R0$ at different times.

We now take the same solution, keep all the fields identical but enhance the trapped radiation inside by a multiplicative factor of 1.1. This disturbs the balance between the electrostatic and ponderomotive forces leading to time dependence. The question is how the trapped excess radiation readjusts, whether it simply tries to leak out of the structure to retain its original identity or does it evolve towards some other coherent localized form or does it simply disintegrate? The evolving profiles for R and n are shown in Fig. (4.5) and Fig. (4.6) respectively. Both show regular oscillations. In one of the subplots of Fig. (4.6), we show the evolution of the peak of both density n and R fields. It should be noted that the oscillations of the two fields are always out of phase in time. It can be understood by realizing that the excess radiation trapped inside the structure offers excess

ponderomotive pressure due to which the electron density is pushed out and starts getting enhanced at the edge. As the density cavity gets deeper at the center, the radiation expands and its peak starts dropping down. This explains the out of phase changes in the oscillations corresponding to radiation and density peaks. The electron inertia leads to the excitation of plasma oscillations of the density perturbations that get forced due to excess radiation pressure. These oscillations are of forced character as the oscillation frequency evaluated from the plot (time period $T \sim 6.98$) closely corresponds to the frequency of laser $\omega \sim 0.9$ for the solution.

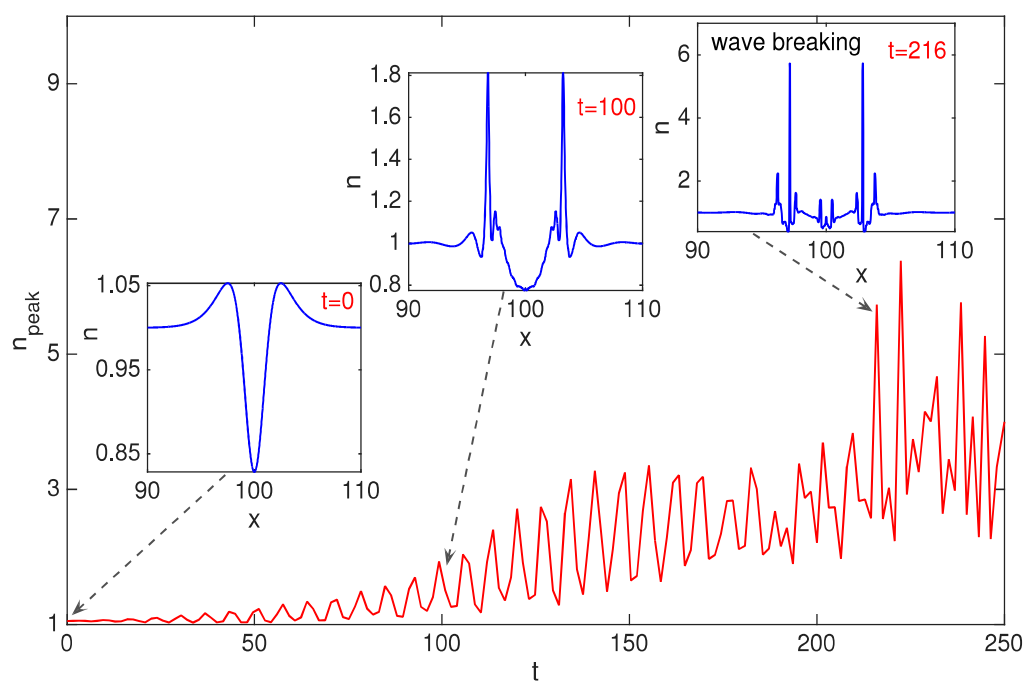

Figure 4.7: Density peak n_{peak} oscillation as a function of time t.

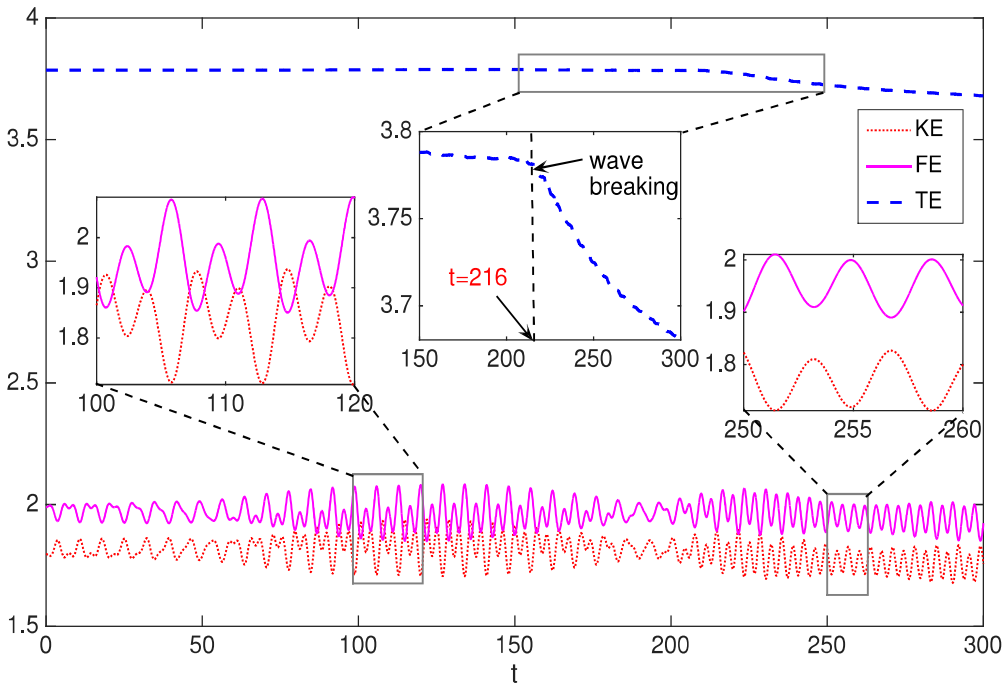

Figure 4.8: Kinetic energy (KE), field energy (FE), total energy (TE) as a function of time t for fluid.

From the time evolution of the peak of the radiation field R, it can be observed that it steadily decreases. This happens as a result of steady leakage of the radiation from the edges (see inset of Fig. (4.5), where the edge portion of the structure has been zoomed in at $t = 40$) indicating clearly that the density profile is unable to confine the excess radiation. The peak of density oscillations, however, are observed to steadily increase with time. In fact, the density profile is observed to generate several peaked sharp structures. The excess radiation puts a

ponderomotive pressure on the electrons and triggers plasma oscillation. The electron density peaks monotonically increase with time. Around $t \sim 216$ as shown in Fig. (4.7), the density acquires a very spiky form. This, in fact, is a signature of wave breaking phenomena. We have tracked the total energy (TE) evolution in Fig. (4.8) which is conserved all throughout but shows a very small dip exactly at $t \sim 216$, when the density spike is observed to form. Despite changing the grid size the energy dip typically occurs around the same time. In the next chapter (5), it is reported that in the PIC simulations too exactly around this time the density spikes appear. At the wave breaking point in the fluid code, there is a loss of small amount of energy to the grid. In PIC simulations where the total energy incorporates the individual particle energy, the energy remains constant but shows up as particle heating with the width of the distribution increasing. It is interesting to note that the FE and KE continue to remain out of phase before as well as after and also during the wave breaking process as can be viewed from the enhanced inset of the Fig. (4.8)

The radiation profile has also been perturbed asymmetrically about the center so as to have excess radiation at one of the edge and a reduced value at the other. The objective being to basically mimic the 'out of phase oscillations' of the density peaks observed in the context of structures emitted spontaneously from an unstable multi-hump solution discussed in section (4.3). Thus one chooses the perturbed profile as-

$$R = R_0 + R_{amp} \sin k(x - x_0)$$

For a typical width of L_W of the soliton, $k = 2\pi/L_W$ was chosen, x_0 is the

location of the center of the structure. Furthermore, the perturbation was chosen to be finite over only one wavelength adjusted within the structure. Thus $R_{amp} = 0.1$ if $\mid x - x_0 \mid < L_W$, otherwise $R_{amp} = 0$. This choice ensures that at one of the edges radiation pressure dominates whereas at the other edge scalar potential is the dominating force.

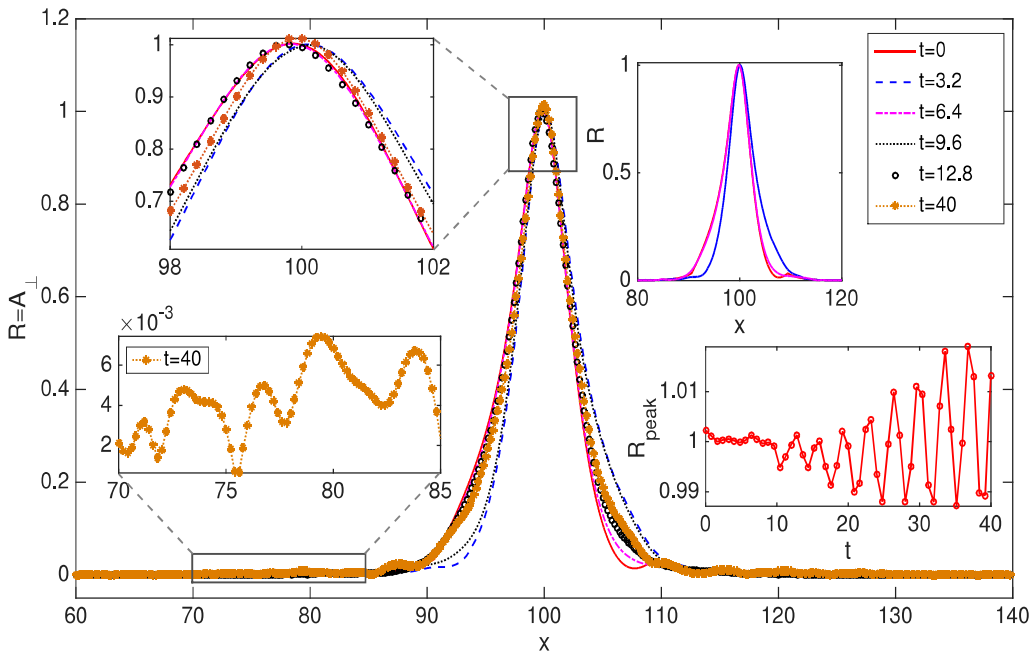

Figure 4.9: Vector potential (R) for stationary ($\beta = 0$) single peak soliton of amplitude $R = R0 + 1.1\sin(kx)$ at different times.

As from Fig. (4.9), one observes that the structures show asymmetric oscillations with one edge expanding while the other contracts. Basically, the edge where the radiation pressure exceeds the equilibrium value, the radiation tends to expand out. At the other edge, where the R is lower than equilibrium value, it is pushed in. Some amount of radiation is observed again to leak out.

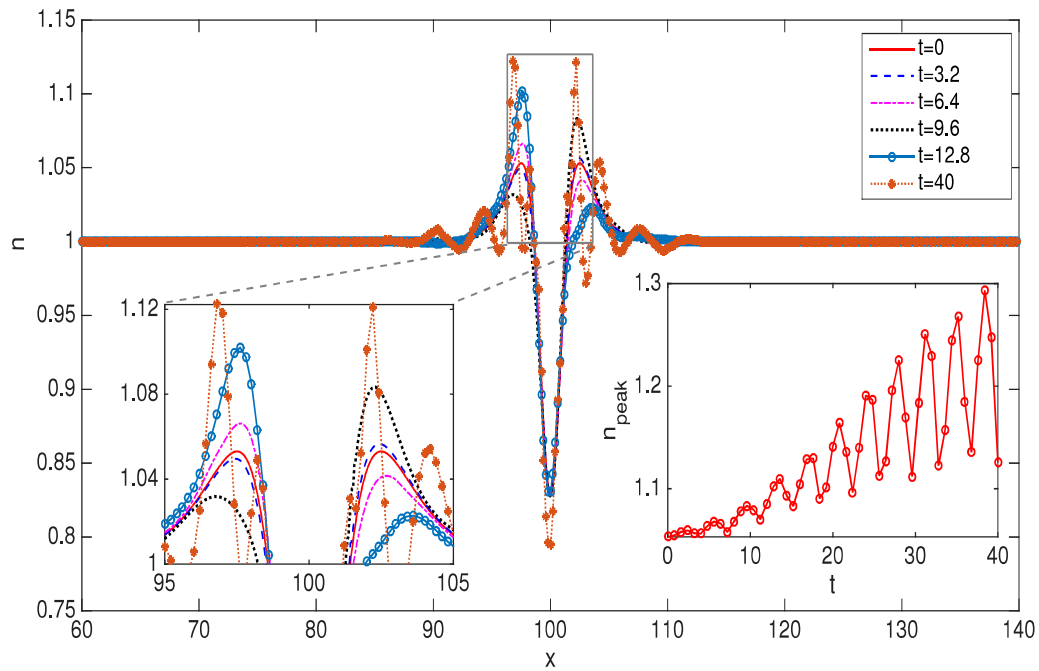

Figure 4.10: Desnity (n) profile for stationary ($\beta = 0$) single peak soliton of amplitude $R = R0 + 1.1\sin(kx)$ at different times.

The plasma oscillations also get excited and the amplitude of density keeps growing as can be seen from Fig. (4.10). Ultimately wave breaking occurs at about $t \sim 184$ which is tracked by the formation of density spikes (see Fig. (4.11)) and a dip in the value of the total energy which can be seen from Fig. (4.12).

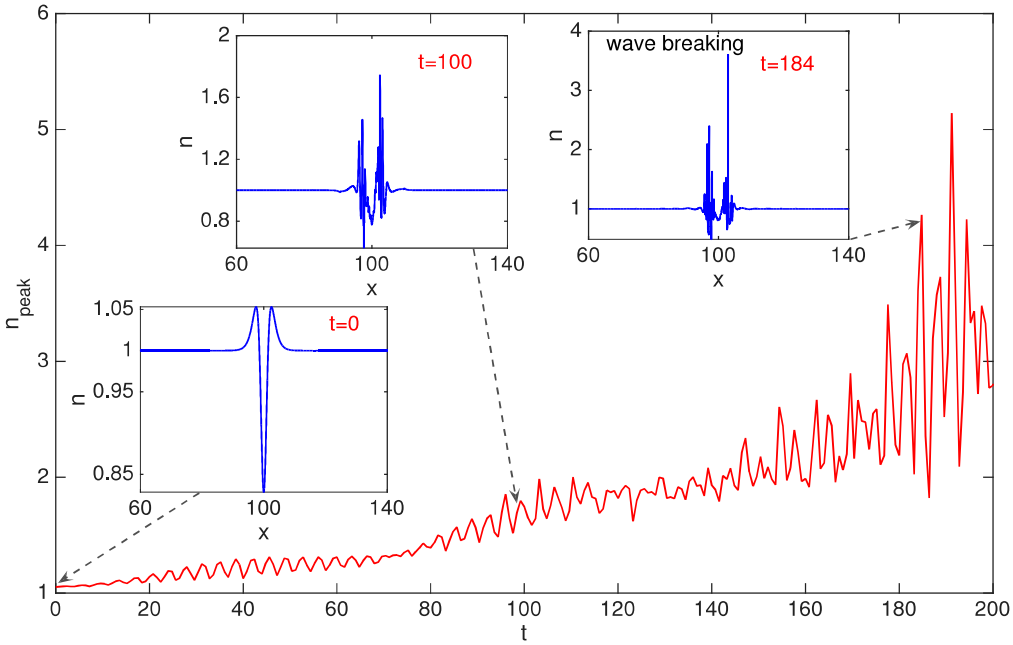

Figure 4.11: Density peak n_{peak} oscillation as a function of time t after incorporation of asymmetric perturbation of $R = R0 + 1.1\sin(kx)$ in vector potential.

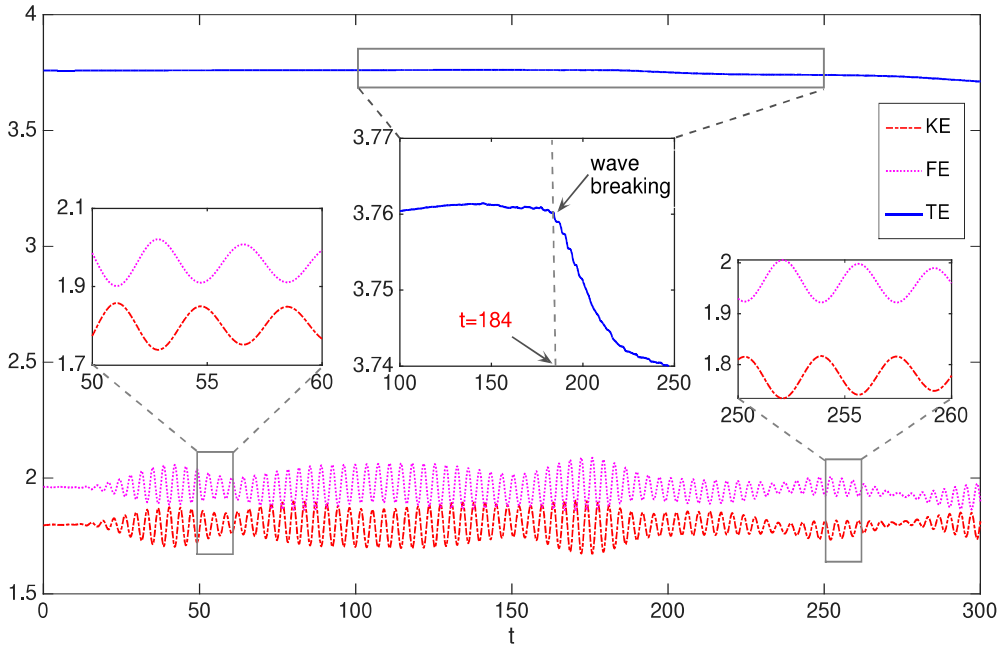

Figure 4.12: Kinetic energy (KE), field energy (FE), total energy (TE) as a function of time t for for asymmetric perturbation.

Thereafter one again ends up with structures in which radiation trapped between density peaks survives for a long duration. It should be noted that the oscillatory phase of structures (in both cases when the trapped radiation is enhanced and/or it is asymmetrically perturbed), resembles the structures which form as an aftermath of a collisional interaction of two unequal high amplitude solitons discussed in section (4.3). However, subsequent to wave breaking, the resultant form wherein trapped radiation between sharp density peaks evolves resembles the emitted structures observed during the destabilization process of the Raman forward instability.

4.4.2 Evolution of perturbed propagating structures

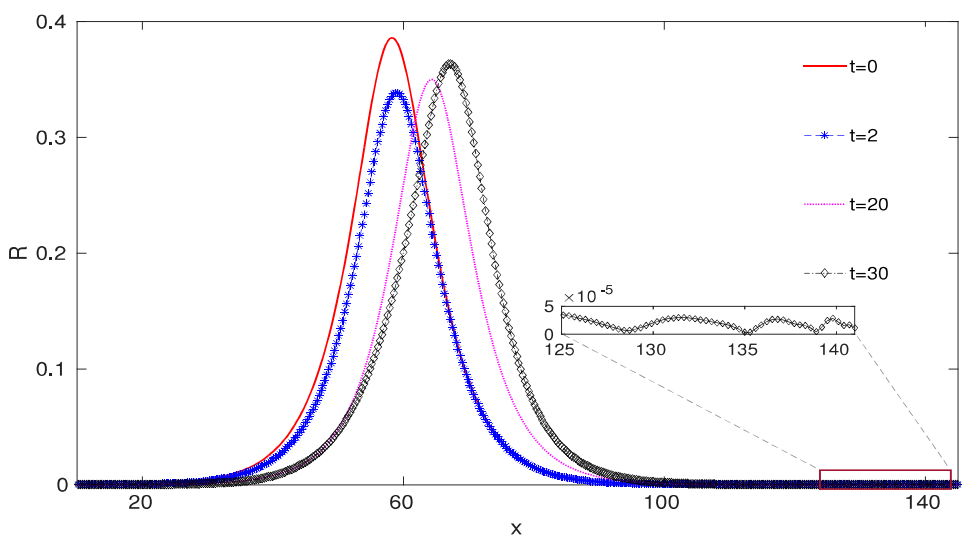

Figure 4.13: Vector potential (R) profile of moving single peak soliton with group velocity ($\beta = 0.3$) with excess perturbation in vector potential of form $R = 1.1R_0$ at different times.

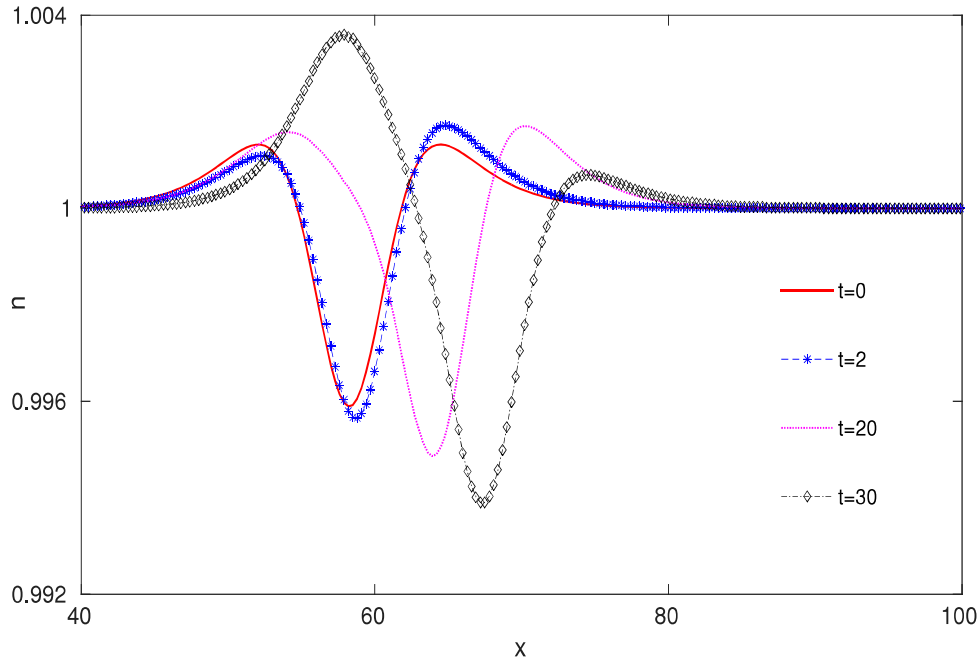

Figure 4.14: Density (n) profile of moving single peak soliton with group velocity ($\beta = 0.3$) with excess perturbation in vector potential of form $R = 1.1R_0$ at different times.

Similar observations are made when the delicate balance between radiation and the electrostatic field is disturbed for a propagating structure with a group speed of β. We have chosen moving single peak soliton with the parameters ($\lambda = 0.94$, $\beta = 0.3$) to illustrate this, where $\lambda = \omega(1 - \beta^2)$. This is a stable single peak propagating structure as shown by Vikrant et al [55]. We perturb this structure by increasing the amplitude of vector potential with a multiplicative factor so that $R = 1.1R_0$. The results are plotted in Fig. (4.13) and (4.14) in terms of vector potential and density respectively.

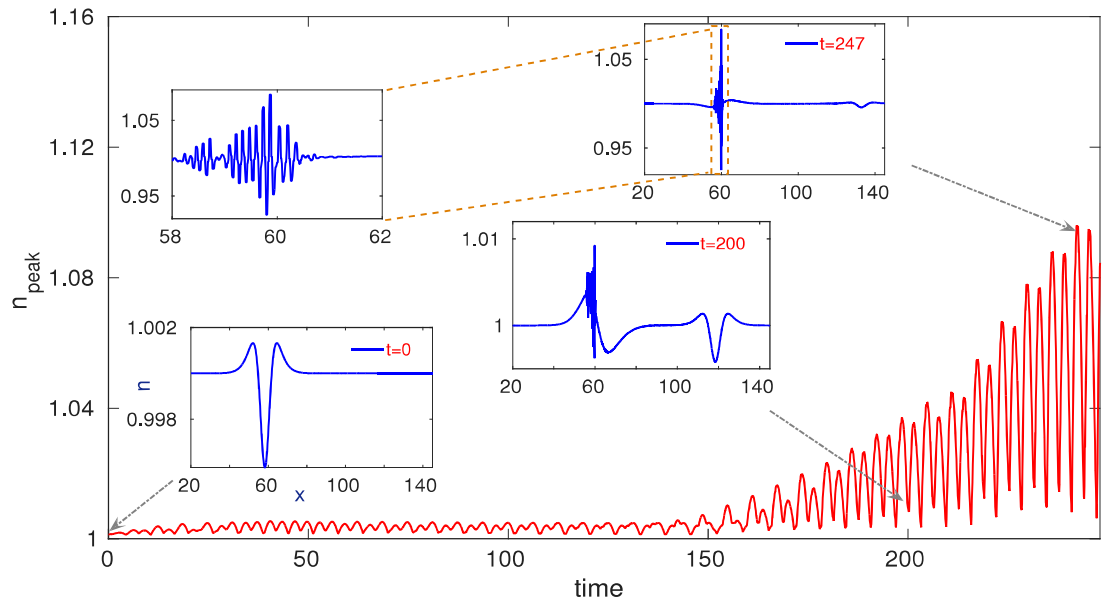

Figure 4.15: Density peak n_{peak} oscillation as a function of time t after incorporation of symmetric perturbation $R = 1.1R0$ in vector potential.

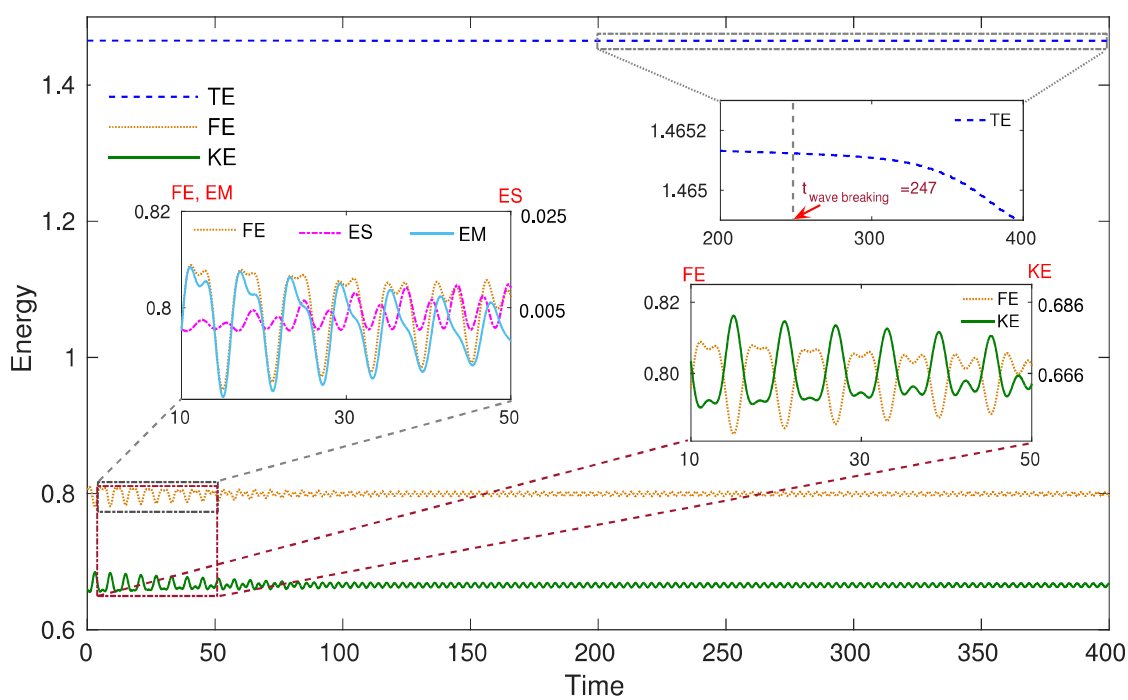

Figure 4.16: Kinetic energy (KE), field energy (FE), and total energy (TE) as a function of time t for moving single peak soliton with group velocity ($\beta = 0.3$) after trapping of excess radiation of the form $R = 1.1R_0$.

In the case of moving structures, we observe that the excess radiation introduced in perturbation gets emitted from its trailing edge. The finite group velocity ensures that the emitted radiation gets separated from the original structure which continues to propagate stably. The emitted structure left behind shows signatures of formation of peak density perturbations eventually suffering wave breaking (see Fig. (4.15)) at t = 247 process which shows up in the evolution of energy (See Fig. (4.16)). On the other hand, the original structures after emission keep propagating ahead. A comparison of the original structure with the perturbed structure at various times have been shown in Fig. (4.17). While at $t = 0$, the amplitude of the perturbed profile of R (shown by the solid brown line) is higher than the original solution (shown by *) the scenario changes at later times after emission.

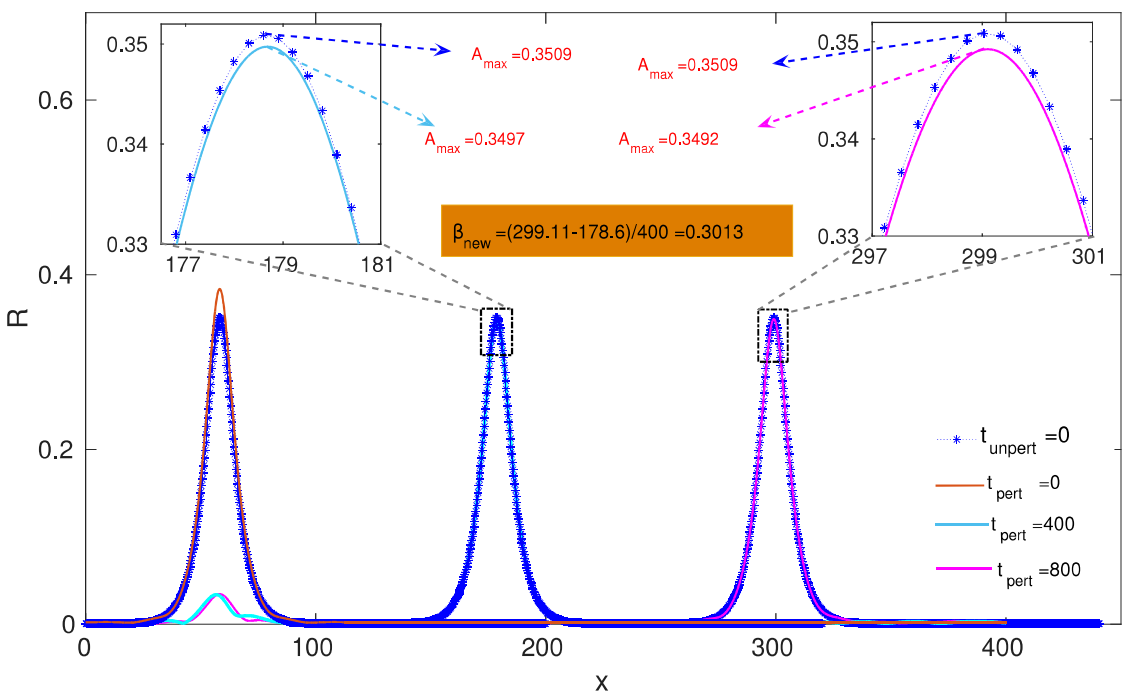

Figure 4.17: The Localized structure get accelerated from $\beta = 0.3$ to $\beta_{new} = 0.301$, $R = 1.1R_0$.

For instance, the zoomed in plots comparing original and the evolved structures at $t = 400$ and $t = 800$ show that at these times the amplitude of R is smaller than the original stable structure. The structure undergoes very little change between $t = 400$ to $t = 800$ and seems to asymptotically approach another stable solution. a numerical estimate of the group velocity β for the new solution has been made and is seen to be higher than the group speed of the original structure. It thus appears that a propagating perturbed stable solution after emission seems to approach another stable form. Basically, a finite propagation speed helps to get the structure separated from the emitted fields. This insulates the structure from the disturbances which are left behind in the form of emitted fields and their evolution. On the other hand, the static structure which is fixed in space continues to remain the part of the disturbance. The plot of kinetic energy, field energy and total energy with time is shown in Fig. (4.16). Similar to the non-propagating structures, here too there is an exchange between kinetic and field energies. The total energy of the system, however, remains conserved. At $t \sim 247$ the wave breaks and the total energy shows a dip and the density profile becomes spiked (see Fig. (4.15)).

4.4.2.1 The frequency Spectra

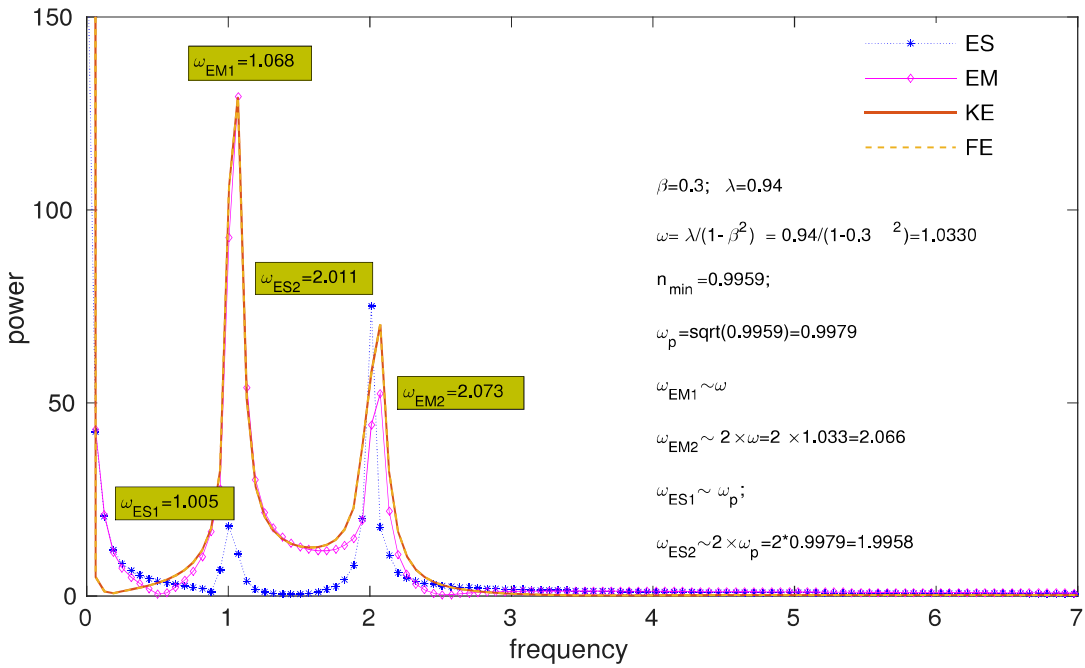

Figure 4.18: Frequency spectrum for the moving localized structure, $\beta = 0.3$.

The regular oscillations observed in the field and kinetic energies prompted us to study their frequency spectra. In Fig. (4.18), we have plotted one such power spectrum in the frequency domain for the field and kinetic energies of one of the cases. As expected, the power spectra for field and kinetic energy show a perfect overlap (yellow dashed line and brown solid line in the color plot of this figure). The exchange between kinetic and field energies thus decides the entire dynamical process. The power spectrum shows a zero frequency part along with two additional peaks. The second peak appears to be at twice the frequency of the first. We also investigated the division between electrostatic (ES) (line with *) and

electromagnetic (EM) (line with diamond) parts of the field energies. Interestingly, the ES and EM spectra show differences. The peak at the higher frequency is at twice the frequency of the lower one. But the peaks in the spectra of EM and ES fields are located at different frequencies. The EM peaks occur at light frequency ω and its harmonic at 2ω. The presence of these frequencies in EM field energy clearly shows that the light field in the disturbance does not remain circularly polarized anymore. The peaks occurring in ES spectra, however, can be identified with the plasma frequency and its harmonic evaluated from the minimum density n_{min}. The zero frequency DC part, in this case, has much smaller power compared to the EM energy. The dynamics thus constitutes of an evolution of clearly identifiable and distinguishable electrostatic and electromagnetic disturbances. There can also be some amount of coupling between the ES and EM modes as the spectral peaks in ES and EM disturbances appear broadened and overlap with each other although their maxima are clearly distinguishable.

4.5 Summary and Discussion

We report observations of a variety of time-dependent (in addition to mere propagation) localized structures in the 1-D fluid simulations of coupled laser plasma system. Interesting variations in the shape of the profile of radiation has been observed. Despite such a time dependence the structures are found to be fairly robust in a sense that they survive by retaining their identity for several hundred of plasma periods.

Such time-dependent structures can form either spontaneously or can also be recreated by disturbing the delicate balance between various fields required in the context of exact solutions. For instance, the emitted radiation from the wake of

the unstable multiple peak exact solutions shows interesting shape evolution along with propagation. The collision amidst two high but different amplitude exact solutions also leads to the formation of a static structure with oscillating amplitudes. When deliberately excess radiation is introduced in a structure, tries to shed it by triggering electromagnetic and electrostatic oscillations in the medium. Propagating structures often shed the excess part and move away evolving into other stable structures. The static structures, on the other hand, remain embroiled with the ensuing evolution of the disturbances which is constituted of very regular oscillations in R and density fields. These oscillatory disturbances can be clearly identified in terms of their associated frequencies in electrostatic and electromagnetic parts. The electrostatic plasma oscillations typically acquire high amplitudes with time in the presence of underlying density inhomogeneity of the structure which ultimately leads to wave breaking phenomena. These time-dependent structures have also been observed in Particle - In - Cell (PIC) simulations. These will be presented in the next chapter 5.

It should be noted that while the exact solutions require a very delicate balance between the radiation and density fields for the time-dependent structures, it is not necessary to satisfy such a stringent condition. Thus while it would be rather difficult to form the exact solutions experimentally for implementing any application. We feel that in contrast, these time-dependent structures which form spontaneously and retain their identity for a long time would be more easily amenable in experimental observations and hence suitable for applications.

5

Time-dependent 1-D localized structures in laser plasma system: Insight from particle-in-cell simulations

The existence of time-dependent robust 1-D localized structures was shown in a chapter (4), with the help of fluid simulations. These structures are important as they do not require the delicate balance between the spatial profiles of various fields to be satisfied as in the case with exact solitonic structures. It was shown in a chapter (4) that such time-dependent structures can be deliberately created by disturbing the precarious balance of the exact solutions significantly. They are also observed to form spontaneously as an aftermath of an instability which the exact solutions undergo, and/or when certain exact solutions suffer collisional interaction. The time dependence was primarily identified as an interplay between field and kinetic energy of the coupled laser plasma system. The light and the plasma waves excitation around the background of exact solution were observed.

The inhomogeneity of the background structures was seen to invariably lead to plasma wave breaking through phase mixing process. The fluid simulations, however, shows that even after the wave breaking process interesting time-dependent structures with radiation trapped between two high-density peaks are observed to survive. Fluid simulations, however, cannot be relied for understanding the existence of such structures dithering around the wave breaking amplitude. We, therefore, employed Particle - In - Cell (PIC) simulations in this chapter for studying the time-dependent structures.

5.1 Introduction

In chapter (4), we have investigated the behavior of the localized structures using 1-D numerical fluid simulation techniques where the delicate balance between the outward ponderomotive force and inward electrostatic force was significantly disturbed. For instance, an excess and/or modified radiation profile was introduced as an initial condition and its evolution was studied numerically via fluid simulations. The excess and/or asymmetrical profile of the radiation induces oscillations in vector potential at the light frequency. As the radiation tries to leak out from the density cavity, it pushes the electron density at the edges triggering plasma oscillations in the system. The interplay of light and plasma oscillations then define the subsequent evolution. The plasma wave is ultimately seen to keep achieving higher amplitude and subsequently shows signatures of wave breaking phenomena. This has been identified by the drop in total energy when spiked density structures appear. Since fluid simulations cannot be trusted after wave breaking, we have in this chapter studied the phenomena through Particle - In - Cell (PIC) simulation. It has been shown that the PIC studies compare exactly with the fluid simulations

prior to the wave breaking point. Thereafter the PIC studies show quantitative deviation from the fluid results, though the qualitatively, the observations remain similar. Furthermore, the total energy, in this case, remains conserved all throughout the simulation as expected. The energy loss in the system observed in the case of fluid simulation, observed as particle heating in PIC.

The chapter has been organized as follows. Section (5.2), present a brief description of PIC simulation techniques. Section (5.3) covers numerical results obtained from particle-in-cell simulation. Here, we have also provided a comparison between the results obtained from fluid and PIC simulations. Finally, section (5.4) provides the brief summary of this chapter.

5.2 Description of PIC Simulation for 1-D study

We have developed 1-D particle-in-cell (PIC) simulation code to understand the evolution of the coupled laser plasma structures. The PIC essentially uses the equation of motion (Lorentz force equation) for the evolution of particle velocity and position. The Maxwell's equations are used to evolve electric and magnetic fields self-consistently. The methodology of the PIC simulations has been described in detail in many review articles [92] and books [93].

The box length of the system (L_x), cell size (Δx) and time step (Δt) are chosen similar for both fluid and PIC simulations. The time step fulfills the Courant-Friedrich-Levy condition, [94]. We have chosen to consider only the evolution of electrons. Ions provide, merely, a smooth neutralizing background. The particle positions initially are chosen in such a fashion as to define the requisite electron density of the structure of choice. There are well-known prescriptions for the

same [95]. The charge density and the current density defined at the grids are used for evolving the electric and magnetic fields. The electric and magnetic fields, in turn, are interpolated at the particle locations for advancing the velocity and the location of the particles by well-known schemes [93]. The results from PIC simulations are in general quite noisy. A choice of about 50 to a maximum of about 250 particles per cell in our simulations showed a considerable reduction in noise. We present the results in terms of same normalizations as adopted in Chapter (4). The boundary condition of the system has been taken to be periodic to perform this simulation.

We have initiated our simulation using the profiles of density, velocity, electric field and magnetic field for various kind of structures that were experimented within Chapter (4). The profiles of density, velocity, electric field and magnetic field with time is recorded. The total field energy (FE) and total kinetic energy (KE) as a function of time for the system is evaluated as follows:

$$FE(t) = \frac{1}{2}\sum_i (E_i^2 + B_i^2)\Delta x \tag{5.1}$$

$$KE(t) = \sum_i \gamma_i (n_i - 1) \tag{5.2}$$

Where $i = 1, 2, ...N_x$, representing the index associated with the cell. Here N_x is the number of grids.

5.3 Results

The PIC code has been verified by reporducing the observations of exact solutions. For instance, we chose the analytical form of the exact solution with $\beta = 0$, provided by Esirkepov et al. [52]. We have plotted the profiles of these solutions in terms of vector potential and density in Fig. (5.1) and (5.2) respectively at different times obtained from the PIC studies. It is clear from these figures that the solutions are stable and long-lived. The plots of kinetic energy (KE), field energy (FE) and total energy (TE) with time from the particle-in-cell simulation has been shown in Fig. (5.3). The energies show no variation with time. It also matches well with the fluid observations.

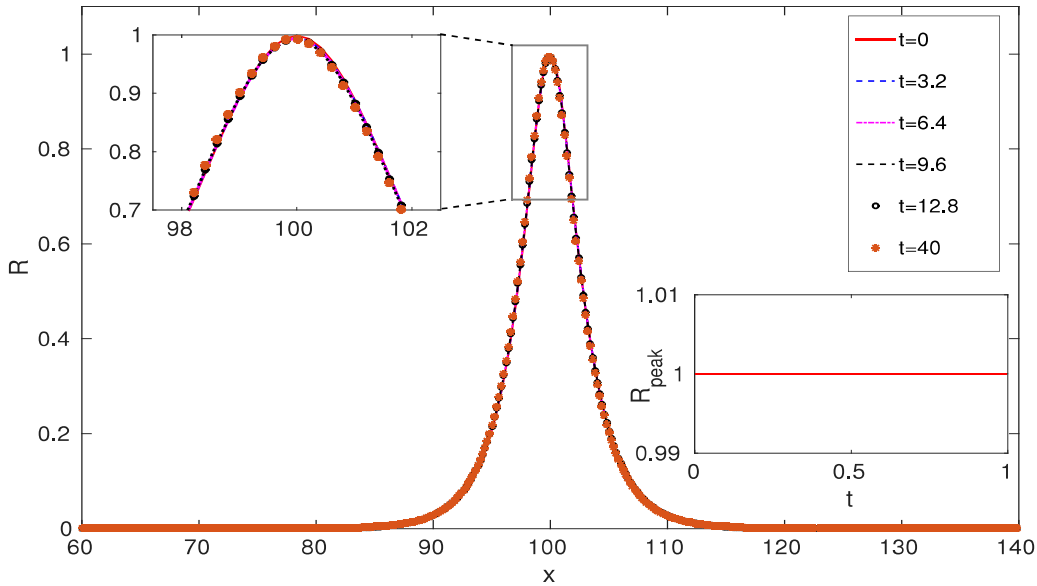

Figure 5.1: Vector potential (R) for stationary (β=0) single peak soliton of amplitude $A_0 = 1$ at different times.

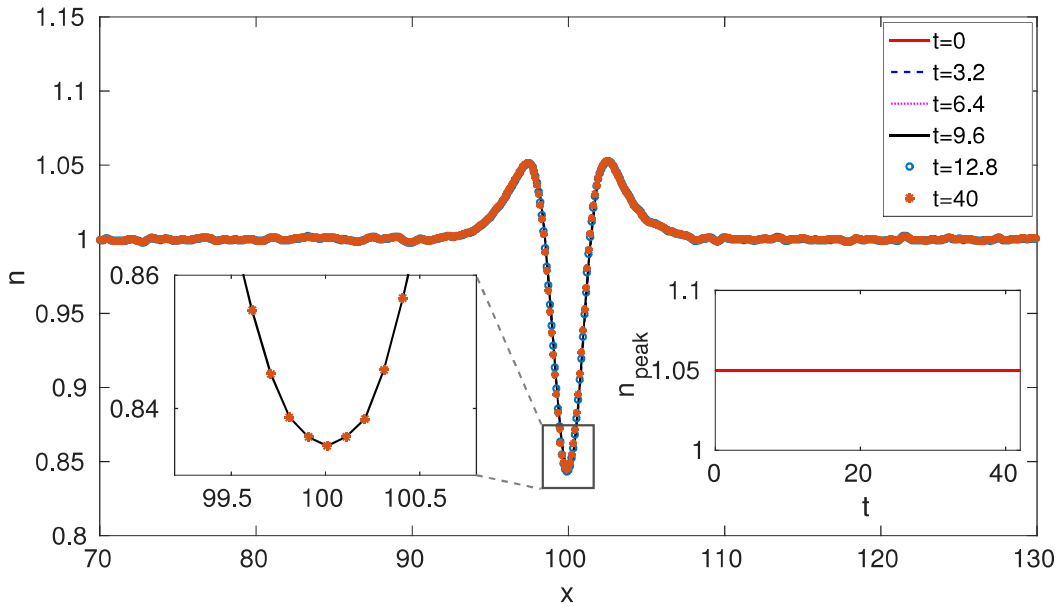

Figure 5.2: Density (n) for stationary (β=0) single peak soliton at different times.

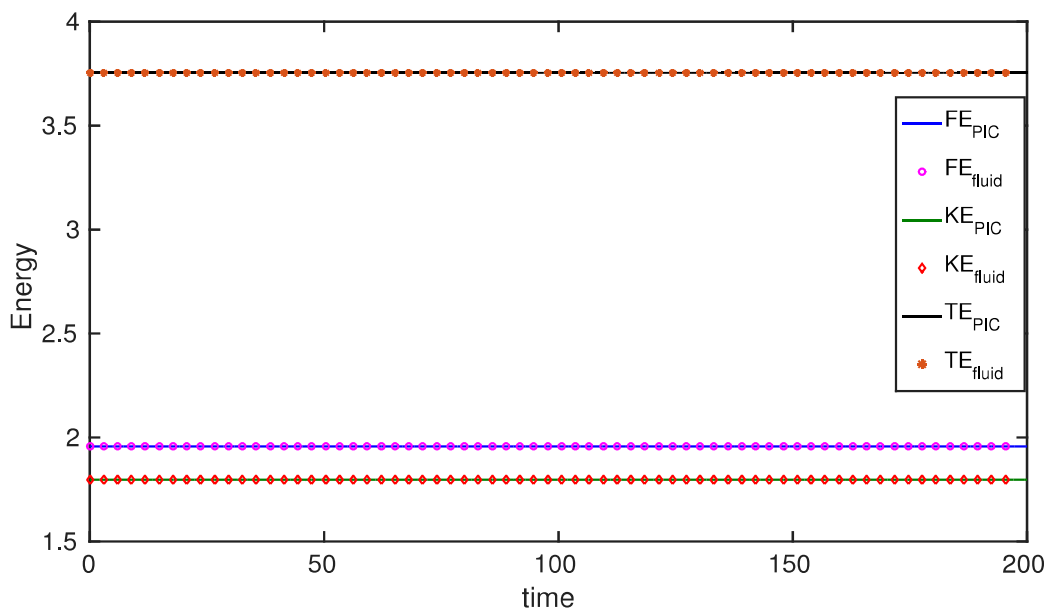

Figure 5.3: Kinetic energy, Field energy, Total energy as a function of time t for fluid(marker)and PIC(solid line) for stable stationary single peak soliton.

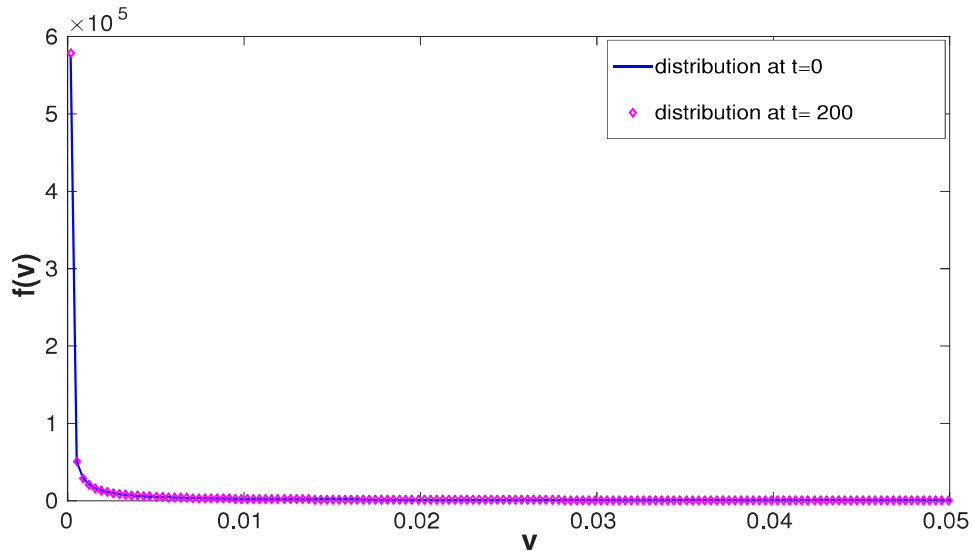

Figure 5.4: Distribution function for stable soliton solution at time $t = 0$ and $t = 200$.

In Fig. (5.4), we present the velocity distribution of the particles at time t=0 and 200. There occurs no broadening in the velocity of the particles. Thus the choice of temperature; $T = 0$ initially continues to be satisfied subsequently. We also performed other preliminary tests to reproduce the known observations with the help of PIC studies. These tests verify the correctness of the code.

We next take up the problem of investigating time dependence in structures. Various cases of significantly modified static as well as moving solutions have been chosen for the study.

5.3.1 Time dependent observations for stationary localized structure in Particle-in-cell simulation

We now choose to enhance the radiation trapped inside the $\beta = 0$ solutions provided by Esirkepov et al. [52] by a certain factor (say 1.1). The space-time evolution of the vector potential and density profiles of these structure illustrated in Fig. (5.5) and (5.6) respectively.

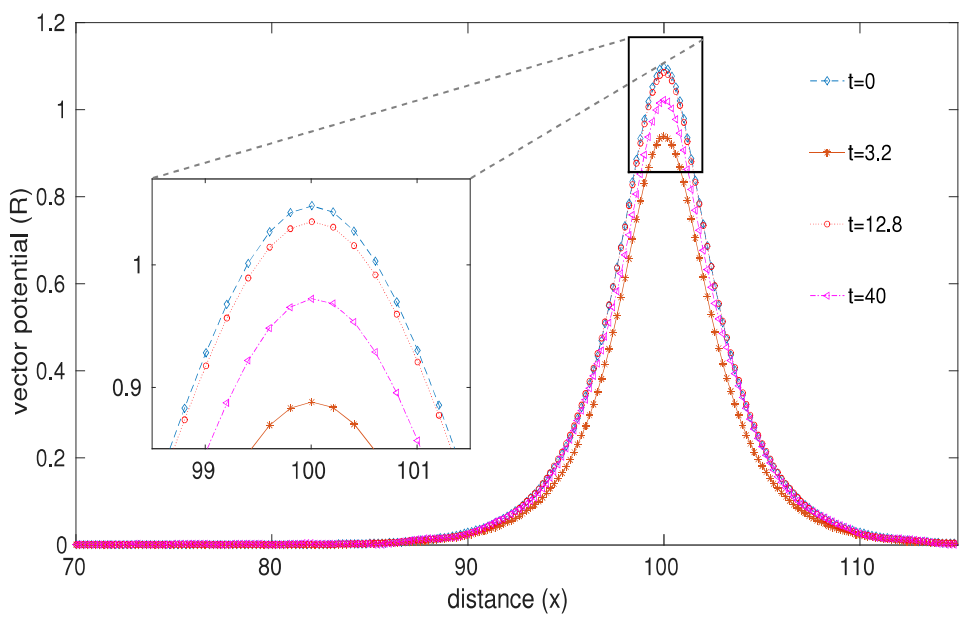

Figure 5.5: Vector potential (R) for stationary (β=0) single peak soliton of amplitude $R = 1.1R_0$, confine an excess radiation 10% of R_0 in electron density cavity at different times.

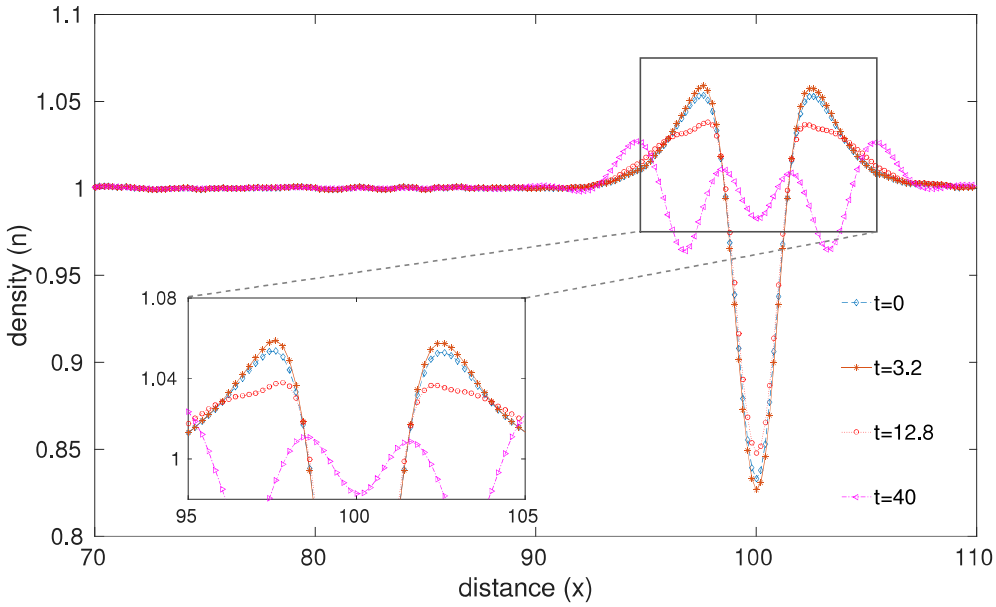

Figure 5.6: Plot of density (n) for stationary (β=0) single peak soliton associated with an excess radiation of amount 10% of R_0 at different times.

It is clear that the amplitude of the structure oscillates with time. Basically as explained in Chapter (4), the excess radiation tries to leak out and in an effort pushes out the two density peaks at the edge triggering plasma oscillations. Fig. (5.7), represents the variation of the field energy (FE), the kinetic energy (KE) and the total energy (TE) as a function of time t. We have provided a comparison with the evolution of energies in the fluid simulation for the identical case.

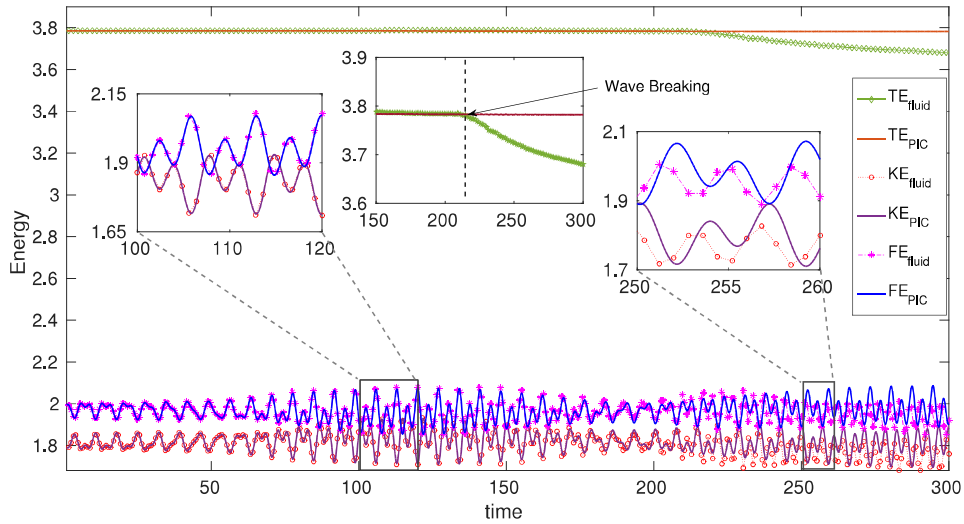

Figure 5.7: Kinetic energy (KE), Field energy (FE) and total energy (TE) for the confinement of a symmetric excess radiation (of amount 10%) of stable vector potential in electron cavity as a function of time t from fluid(marker with dashed) and PIC(solid line).

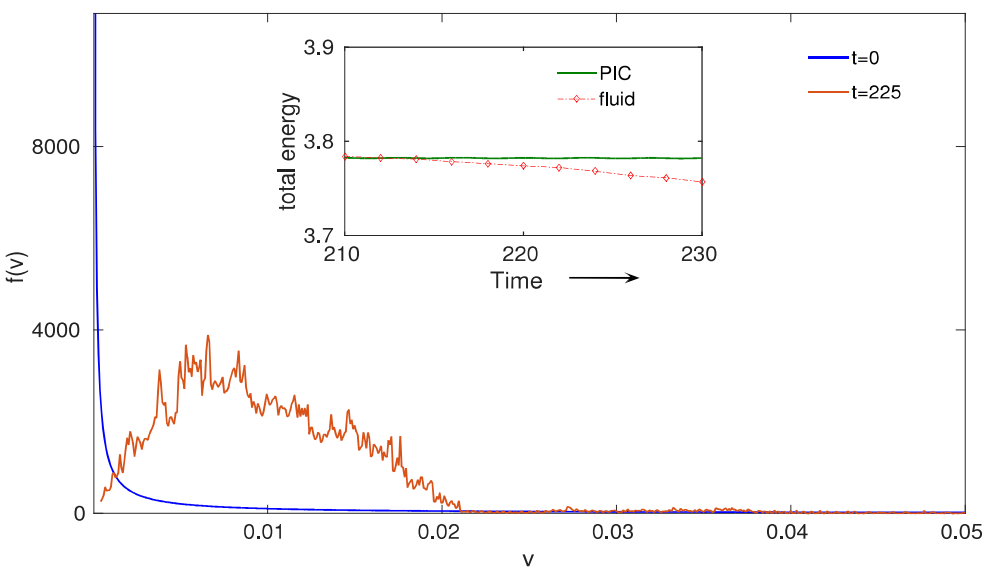

Figure 5.8: Distribution function of the particles for the confinement of a symmetric excess radiation (of amount 10%) of stable vector potential in electron cavity at time $t = 0$ and $t = 225$.

In the PIC simulation, it can be observed that the total energy remains conserved throughout the simulation. The TE for the fluid simulation, however, shows a dip at around $t = 216$ which is the signature of the wave breaking phenomena. In PIC, the energy remains conserved as wave breaking leads to increase in the thermal energy of the particles. The FE and KE show out of phase oscillation which is identical in both fluid and PIC till the wave breaking time, $t = 216$. Thereafter, there appears a slight phase shift in the FE and KE oscillations for fluid and PIC simulations. However, the character of the two oscillations continues to remain identical. For instance, even after wave breaking, the KE and FE oscillations remain out of phase. We have plotted the particle velocity distribution function at time $t = 0$ and $t = 225$ respectively. It can be seen from the Fig. (5.8) that though initially there was no width in the velocity distribution of the particles corresponding to T=0. However, after the wave breaking particles get randomized. The full width at half maxima provides an estimate of the effective temperature T, at time $t = 225$. This thermal kinetic energy is acquired by the particles during wave breaking phenomena due to which the TE in PIC simulation remains conserved. In fluid simulations, on the other hand, there is no way to keep track of the effective heating that a wave breaking phenomena would cause. The grid dissipation is, therefore, responsible for the task. We have also chosen to add an asymmetric perturbation in the radiation so as to enhance the radiation at one edge and diminish the radiation at the other edge of the solutions as done in the fluid case in the chapter (4).

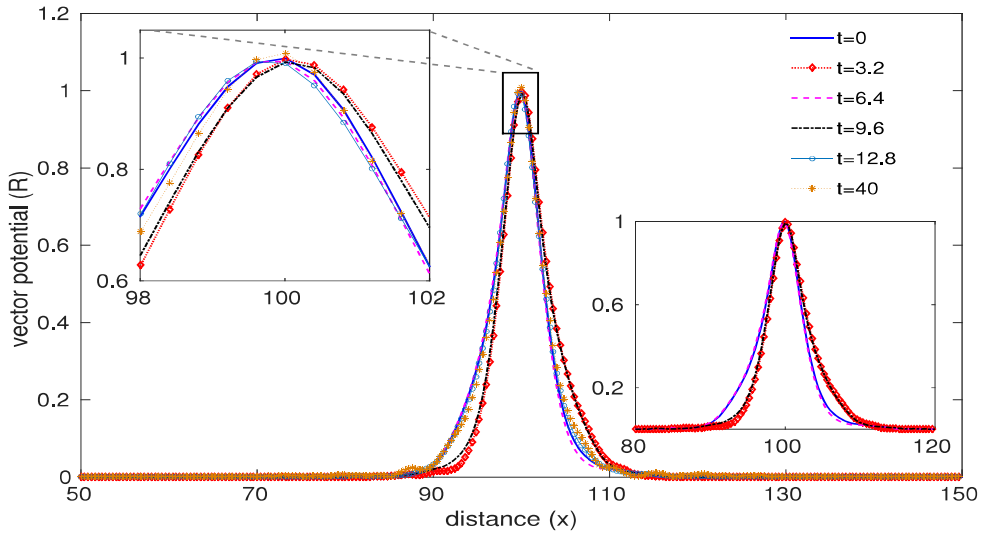

Figure 5.9: Vector potential (R) profile having an asymmetricity of 10% in the laser pulse from its stable solution.

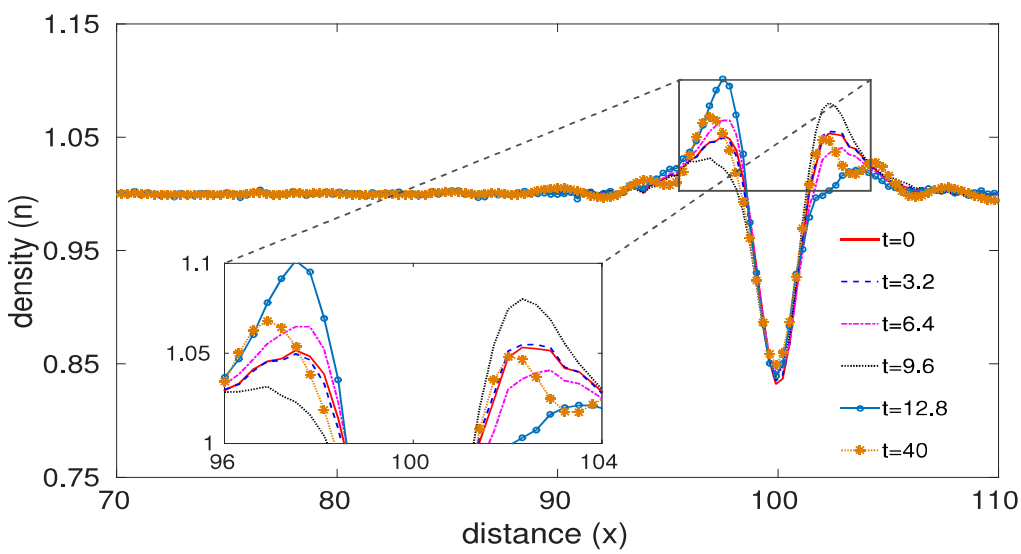

Figure 5.10: Density (n) for stationary ($\beta = 0$) single peak soliton associated with an asymertic radiation at different times.

The profiles of vector potential (R) and density (n) have been plotted at various

times in Fig. (5.9) and (5.10) respectively. They behave again identical to the fluid simulations (see Fig. (4.9) and (4.10) of Chapter (4)). The time evolution of field energy (FE), kinetic energy (KE) and total energy (TE) of the localized structure with time t have been shown in Fig. (5.11).

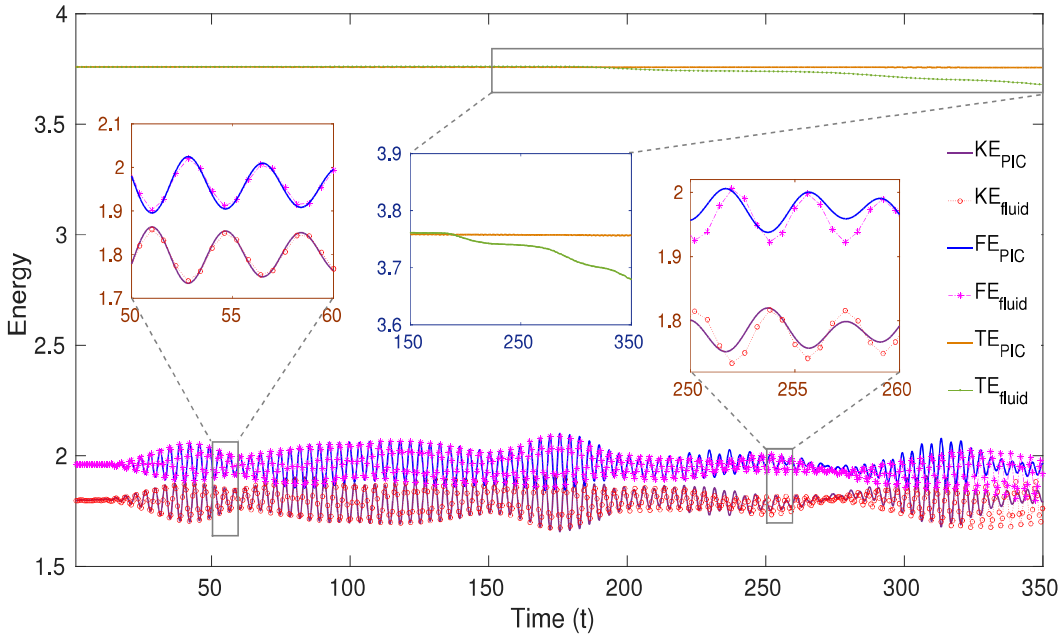

Figure 5.11: Kinetic energy (KE), Field energy (FE) and total energy (TE) for the confinement of a asymmetric excess radiation (of amount 10%) of stable vector potential in electron cavity as a function of time t obtained from fluid(marker with dashed)and PIC(solid line).

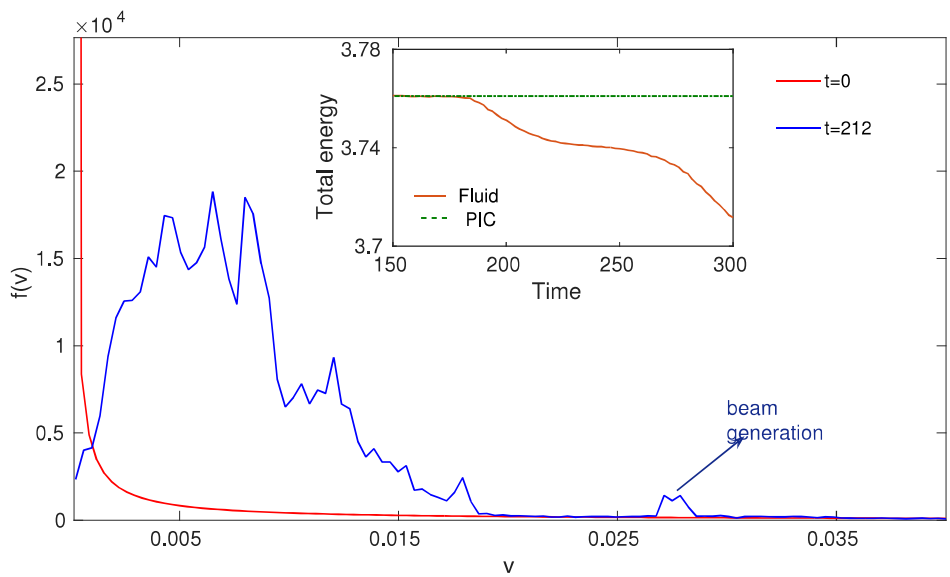

Figure 5.12: Distribution function of the particles for the confinement of a asymmetric excess radiation (of amount 10%) of stable vector potential in electron cavity at time $t = 0$ and $t = 212$.

Here too, the total energy estimated from the fluid simulation and from the PIC simulation matches well till ($t \sim 180$), the wave breaking time where the fluid simulation shows a drop in TE. The temperature of the random kinetic energy attained by the particles has been estimated again by the FWHM of the velocity distribution function. This is about arise at time $t = 212$ (see Fig. (5.12)).

5.3.2 Time dependent observations for moving localized structure in Particle-in-cell simulation

We now consider moving single peak solutions which are known to be stable. We have initiated the profiles obtained by solving equation (2.14-2.17) for the parameters, $\lambda = 0.94$ and $\beta = 0.3$ in our PIC simulation.

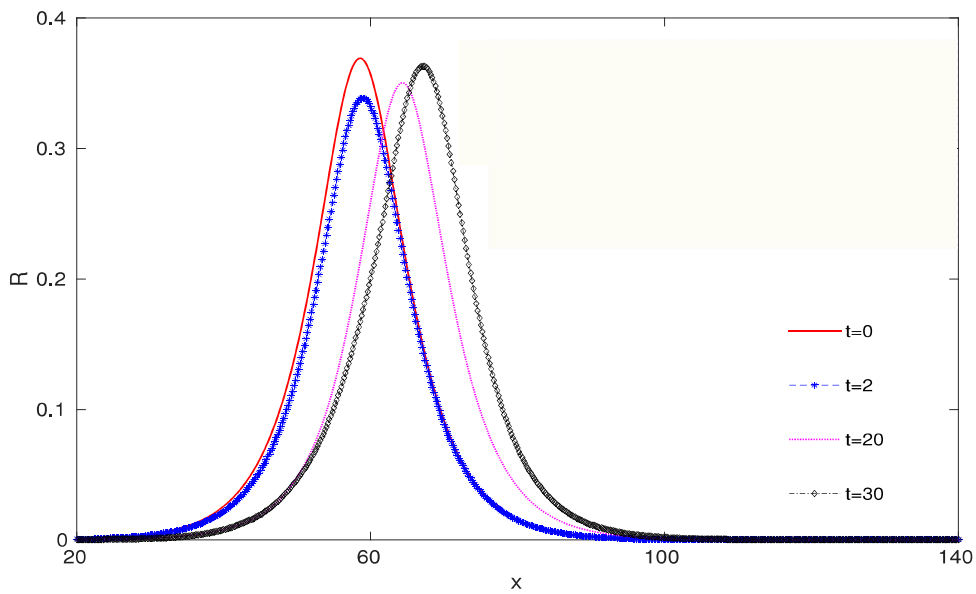

Figure 5.13: Vector potential (R) for moving single peak soliton for group velocity $\beta = 0.3$ and $\lambda = 0.94$ having an 10% excess radiation confinement in electron density cavity at different times.

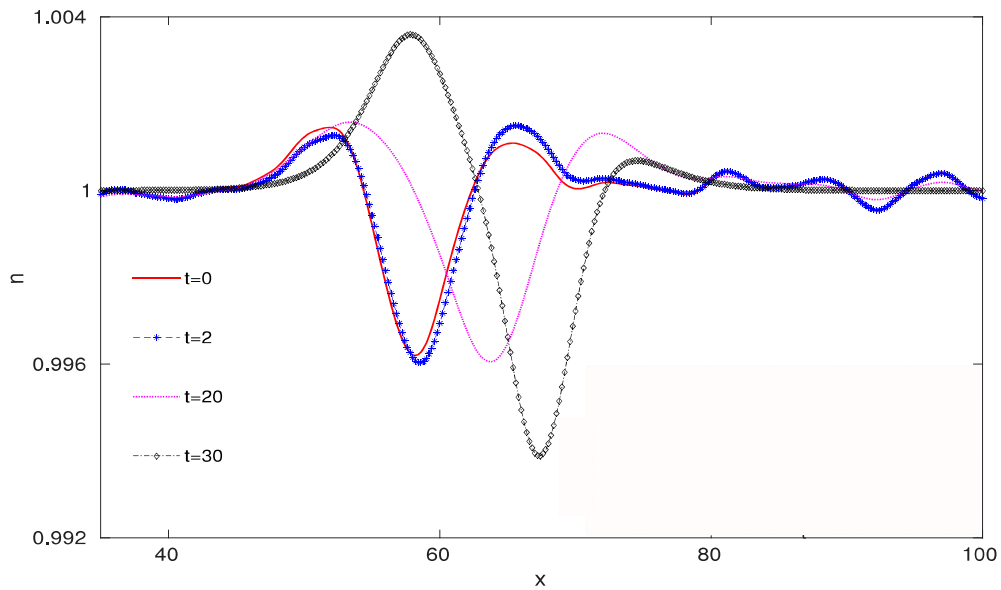

Figure 5.14: Density (n) for moving single peak soliton for group velocity $\beta = 0.3$ and $\lambda = 0.94$ having an 10% excess radiation confinement in electron density cavity at different times.

We have shown the time evolution of the spatial profile of such structures in terms of vector potential (R) and density (n) as given in Fig. (5.13) and (5.14) respectively. It is observed that the perturbed soliton moves forward as a stable form and tries to get rid of the excess radiation as it evolves. In this case, since the disturbances are left behind, the structure appears to evolve towards a new stable solution in the neighborhood.

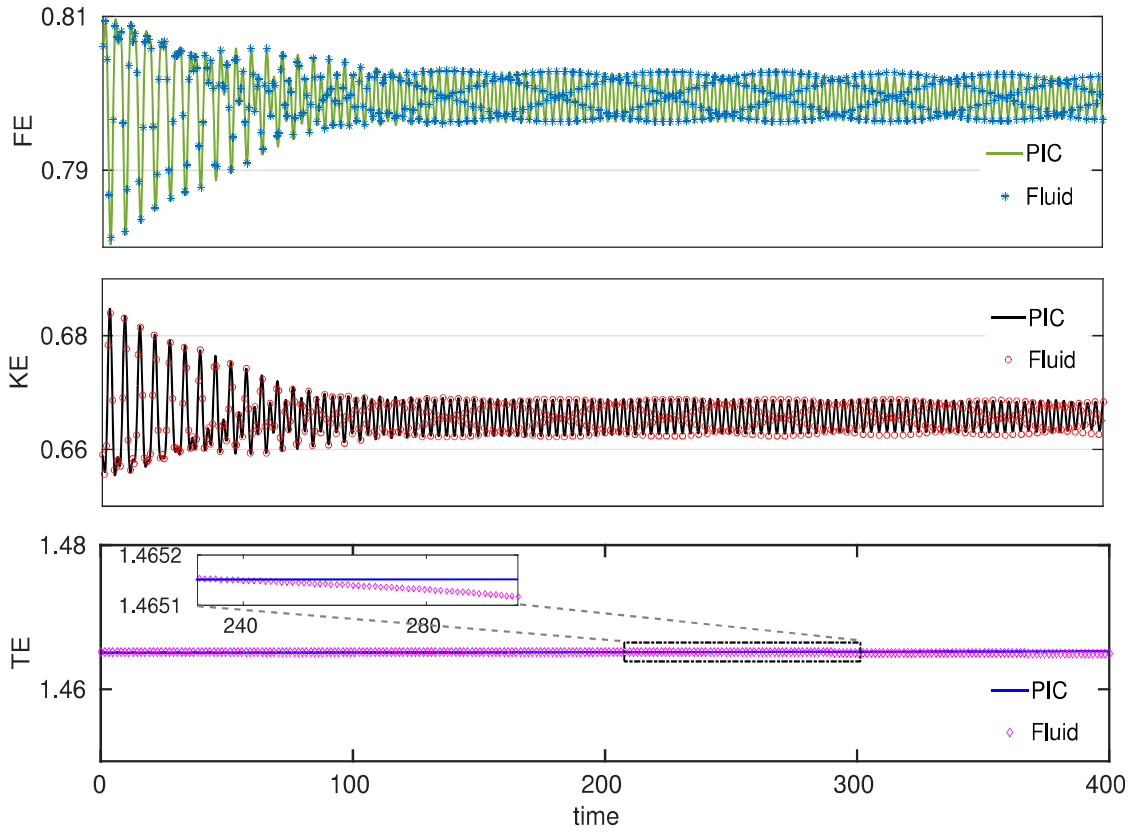

Figure 5.15: Kinetic energy (KE), Field energy (FE) and total energy (TE) for the confinement of a symmetric excess radiation (of amount 10%) of stable vector potential in electron cavity for moving single peak soliton with group velocity $\beta = 0.3$ and $\lambda = 0.94$ as a function of time t for fluid(marker with dashed)and PIC(solid line).

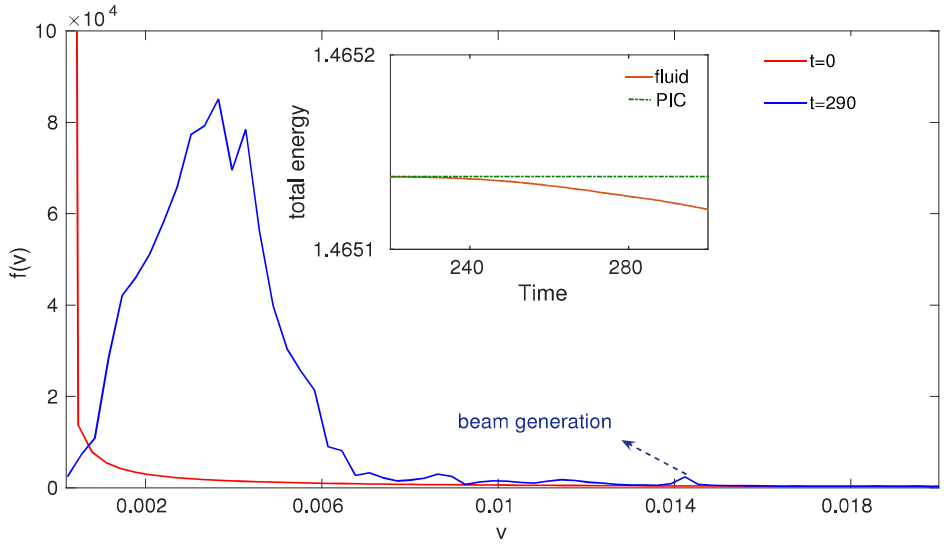

Figure 5.16: Distribution function of the particles for the confinement of a symmetric excess radiation (of amount 10%) of stable vector potential in electron cavity at time $t = 0$ and $t = 290$.

This is also evidenced from the time evolution of the energy as shown in the Fig. (5.15). The dip in total energy for the moving single peak soliton at a time, $t = 247$ is extremely small. When the results obtained from the fluid and PIC simulations compared, even after this dip, there is almost negligible phase shifts occurs in the oscillations of the FE and KE. The acquired random thermal energy of the particles are also quite small as evidenced from the plot of the distribution function as shown in the Fig. (5.16).

In the fluid simulations, we had chosen to evolve a remnant that was ejected out of the multiple peak solitonic structures while they underwent for the forward Raman scattering instability. They had a compact support as radiation was trapped inside two high-density peaks and the evolution displayed complex interesting features. We explore the evolution of these structure through PIC simulation. It can be seen from the Fig. (5.17) that the complex features observed in fluid simulations in the evolution of these structures are also reproduced in the PIC studies. The energy evolution also shows out of phase oscillations amidst KE and FE (see Fig. (5.18)).

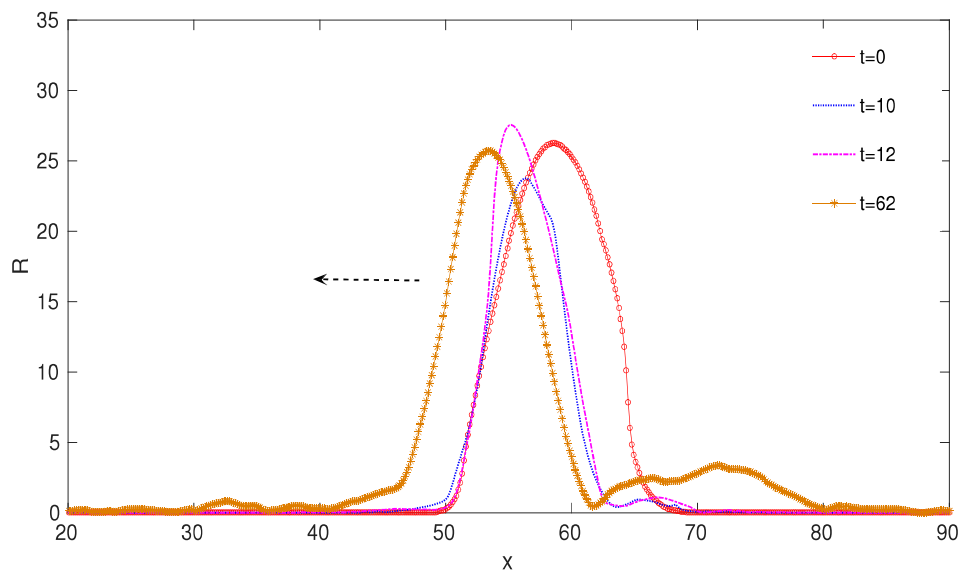

Figure 5.17: Vector potential for self generated compact localized solution moving in -ve x direction.

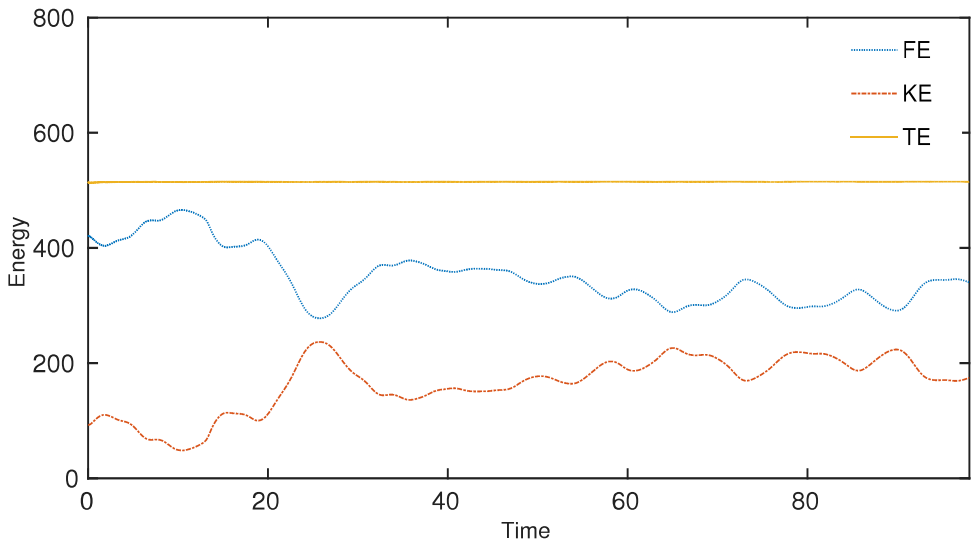

Figure 5.18: Kinetic energy, field energy and total energy as a function of time for localized compact structure.

It is, therefore, clear that structures showing complex time dependence are permitted by the coupled laser plasma set of equations. It would be worthwhile if one could provide a simplified analytical description of the same.

5.4 Summary

In this chapter (5), we presented the observation of the time-dependent localized structure by using PIC simulation in 1-D. We have introduced time dependence by significantly modifying the delicate balance of these structures. It is observed that the PIC observations support the inferences gathered from fluid simulations as presented in chapter 4. There is total agreement in fluid and PIC observations till the time, density acquires sharp form and reaches wave breaking point which can be discerned from a drop in total energy TE of the fluid simulations. In the PIC simulations, the energy gets irreversibly converted into random thermal

kinetic energy of the particles. One observes out of phase oscillations in the field and kinetic energies in both kinds of simulations. Even after wave breaking, the differences between fluid and PIC, observations are minor and in terms of a phase shifted oscillations amidst field and kinetic energies.

Some spontaneously formed structures have been observed to display complex time evolution and are yet found to remain robust and preserve their identity. For instance, the ejected structures from the multiple peak solutions as an aftermath of Raman forward scattering instability shows many compact structures with radiation trapped inside two high-density peaks. Their evolution in fluid simulations had displayed complex shape variations with time. We reproduced those complex behavior using PIC studies in this chapter.

6

Conclusion and future work

This chapter summarizes the main observations of the thesis. A few salient features pertaining to the coherent 1-D solutions of the coupled laser plasma system has been investigated in this thesis. These include: (i) A suitable analytical description of the cusp solitonic structures formed at the ion wave breaking point. (ii) A 1-D evolution study showing the destabilization process of cusp structures. (iii) Transverse destabilization of solitonic structures by carrying out 2-D simulations. For this thesis, we restricted to that class of solutions for the study of transverse destabilization which comprises of electron dynamical response only (iv) An entirely new variety of robust time-dependent (apart from mere propagation) structures were shown to exist both with the help of fluid and PIC simulations in 1-D.

A brief summary of main observations on these issues has been provided in this chapter which is then followed up by the future scope of the research work in the area.

6.1 Salient features of the thesis

This thesis is dedicated to the study of the localized structures in a coupled laser plasma system. The formations and existence of such structures for longer durations are important from various perspectives. These solutions and their evolution can be described by the coupled set of relativistic fluid Maxwell equations. The existence of many varieties of localized structures and the stability studies in 1-D of some of them have been explored earlier. In this thesis, we have addressed the following specific issues pertaining to them

6.1.1 Cusp solitary structure

- Variety of new soliton structures were found to exist in the system once the ion dynamical response included. On the basis of the shape of the potential, these solitary structures are classified as- single peak, paired peak, high amplitude, flat top, multipeak and cusp. Detailed investigation of the single peak, paired peak and the multipeak soliton has been performed by Saxena et al. [55, 56]. The semi-analytical model of the flat-top soliton has been given by Sundar et al. [58]. They have also mentioned that theses flat top structures suffers through Brillouin's scattering which makes them unstable.

- In chapter 2, we have derived an analytical expression for the scalar potential in terms of group velocity β and the maximum amplitude of vector potential A_{max} for the cusp structure (which forms at the ion wave breaking limit). The analytical expression shows good agreement with the exact solution, for the given value of a group velocity (β), frequency (λ) and vector potential (R).

- Stability of a cusp solution has been studied by evolving it in a fluid-Maxwell model based on the flux corrected scheme. These cusp structures found to be unstable as they start emitting radiation from the trailing edge of the cusp soliton. The origin of such a radiation is found to be due to the forward Raman scattering and is eventually responsible for destabilizing the structure.

6.1.2 Stability of 1-D soliton in transverse direction

- The stability of a variety of one-dimensional solitons were discussed earlier. The single peak and paired peak solitons are found to be stable. Whereas, multipeak solitary structures are emitting radiation due to the Raman forward scattering. The typical time-scale for the growth of the instability is of the order of a few hundred of plasma period. To visualize the effect of the 2-D on the evolution of theses 1-D structures, we extended the geometry from one to two dimensions. At the moment we have concentrated only on studying the transverse stability of the structures with electron response only.

- In chapter 3, we have shown that the single peak and paired peak solitons ultimately get destabilized by the filamentation instability in the transverse direction. The transverse profile gets gradually modulated and finally breaks into filamentary structures. We have also calculated the numerical growth rate from the fluid simulations and found them to be matching well with the analytical value of the filamentation instability.

- Multiple peak solutions in two-dimension first undergo the regular one-dimensional

forward Raman scattering instability. The filamentation instability with a slower growth rate has been shown to appear at a later stage of the evolution for the multipeak solutions.

6.1.3 Observation of time-dependent localized structures in a one-dimensional laser plasma system.

- Soliton forms due to the precarious balance between the ponderomotive force and the electrostatic force which finally leads to a configuration where the electrons are piled up at the edge and prevents the leakage of radiation. in chapter 4, we have investigated the time-dependent behavior using 1-D numerical fluid simulation for structures in which the delicate balance between the ponderomotive and electrostatic forces has been disturbed.

- It has been observed that despite significantly altering the delicate balance of the two forces, the structure continues to retain its identity and does not get disintegrated.

- The time-dependent structures have also been observed to form spontaneously. For instance, it was shown that when a multiple peak solitonic structures evolve, they undergo a destabilization due to forward Raman scattering process. As a result of this instability, some structures get ejected from the trailing edge of the solutions. The ejected structures essentially have a compact spatial profile of radiation trapped inside two high electron density peaks. These structures have been shown to display interesting complex shapes during evolution.

Another variety of structures which were observed to form spontaneously

during the course of collisional interaction of certain exact solutions. They are essentially non-propagating, have oscillatory amplitude and a small amount of radiation is observed to leak out of the structures.

- Such time-dependent structures can also be recreated by introducing excess radiation inside an exact solution. The excess radiation puts pressure at the edge densities and triggers plasma oscillations. An interesting interplay between field and kinetic energies are observed. These two energies oscillate out of phase. Against the inhomogeneous background, the plasma oscillations ultimately get phase mixed and generate density spikes resulting into wave breaking.

- Even after wave breaking, the structures have been observed to retain their identity. However, keeping in view that kinetic effects would be important after wave breaking, PIC simulations have been performed.

6.1.4 Kinetic studies of time-dependent localized structures in a one-dimensional laser plasma system.

- The PIC studies quantitatively reproduce the fluid simulations prior to the wave breaking phenomena. This includes the exact reproduction of the spatial profiles and the energy evolution.

- The wave breaking point in fluid simulations of the time-dependent structures are discerned by a small dip in the total energy which happens as the density acquires a very sharp form. Thereafter, the PIC and fluid studies show a slight difference. There appears a slight phase shift between the fluid and PIC observations in the oscillatory behavior of field and kinetic energies.

The total energy remains conserved all throughout the PIC simulations. It is observed that the wave breaking leads to acquiring a random thermal kinetic energy of the particles.

- The estimation of the drop in the total energy in the fluid simulation has been found to typically compare well with the thermal spread acquired by the particles in the PIC studies.

6.2 Future directions

The thesis covers certain aspects pertaining to localized structures in the coupled laser plasma medium. Some directions in which further explorations can be carried out have been listed below.

- We have provided an analytical description of the cusp structures which form at the ion wave breaking point. A PIC study aimed at understanding their role in ion acceleration would be important.

- The transverse destabilization has been investigated in the context of solutions having only the electron dynamical response in the present thesis. The role of transverse dimension for the other variety of solutions which form in the presence of ion response need to be carried out.

- An extension of evolution studies to a full 3-D geometry would be fruitful. It may lead to the final 3-D form of the light plasma structures.

- In the present thesis, observations pertaining to the existence of robust yet complex time-dependent structures have been made. An analytic model description of such structures needs to be carried out.

- The role of inhomogeneous densities in the propagation of many of these structures can be investigated.
- The application of these solutions for energy transport can be investigated in detail.
- The upcoming advancements in laser system would soon push the regime of laser intensities in the domain where novel effects such as radiation reaction, pair production etc., would become important. It would be, therefore, an important exercise to seek possible localized solutions in the presence of these effects.

Bibliography

[1] B. Liu, H. Y. Wang, J. Liu, L. B. Fu, Y. J. Xu, X. Q. Yan, and X. T. He. Generating overcritical dense relativistic electron beams via self-matching resonance acceleration. *Phys. Rev. Lett.*, 110:045002, Jan 2013.

[2] C. Joshi. The development of laser- and beam-driven plasma accelerators as an experimental fielda). *Physics of Plasmas*, 14(5), 2007.

[3] M. I. K. Santala, Z. Najmudin, E. L. Clark, M. Tatarakis, K. Krushelnick, A. E. Dangor, V. Malka, J. Faure, R. Allott, and R. J. Clarke. Observation of a hot high-current electron beam from a self-modulated laser wakefield accelerator. *Phys. Rev. Lett.*, 86:1227–1230, Feb 2001.

[4] T. Tajima and J.M. Dawson. Laser electron accelerator. *Phys. Rev. Lett.*, 43, 1979.

[5] A. Modena. *Nature*, 377, 1995.

[6] L. M. Gorbunov and V. I. Kirsanov. *SOY. Phys. JETP*, 66:1527–1530, 1987.

[7] and A. S. Sakharov S. V. Bulanov, V. I. Kirsanov. *JETP Lett.*, 50, 1989.

[8] P. Sprangle, E. Esarey, and A. Ting. Nonlinear theory of intense laser-plasma interactions. *Phys. Rev. Lett.*, 64:2011–2014, Apr 1990.

[9] G. Malka and J. L. Miquel. Experimental confirmation of ponderomotive-force electrons produced by an ultrarelativistic laser pulse on a solid target. *Phys. Rev. Lett.*, 77:75–78, Jul 1996.

[10] S. C. Wilks, J. M. Dawson, W. B. Mori, T. Katsouleas, and M. E. Jones. Photon accelerator. *Phys. Rev. Lett.*, 62:2600–2603, May 1989.

[11] V. A. Mironov, A. M. Sergeev, E. V. Vanin, and G. Brodin. Localized nonlinear wave structures in the nonlinear photon accelerator. *Phys. Rev. A*, 42:4862–4866, Oct 1990.

[12] R. L. Savage, C. Joshi, and W. B. Mori. Frequency upconversion of electromagnetic radiation upon transmission into an ionization front. *Phys. Rev. Lett.*, 68:946 – 949, Feb 1992.

[13] M. I. K. Santala, M. Zepf, I. Watts, F. N. Beg, E. Clark, M. Tatarakis, K. Krushelnick, A. E. Dangor, T. McCanny, I. Spencer, R. P. Singhal, K. W. D. Ledingham, S. C. Wilks, A. C. Machacek, J. S. Wark, R. Allott, R. J. Clarke, and P. A. Norreys. Effect of the plasma density scale length on the direction of fast electrons in relativistic laser-solid interactions. *Phys. Rev. Lett.*, 84:1459–1462, Feb 2000.

[14] J. D. Kmetec, C. L. Gordon, J. J. Macklin, B. E. Lemoff, G. S. Brown, and S. E. Harris. Mev x-ray generation with a femtosecond laser. *Phys. Rev. Lett.*, 68:1527–1530, Mar 1992.

[15] P. P. Rajeev, P. Taneja, P. Ayyub, A. S. Sandhu, and G. Ravindra Kumar. Metal nanoplasmas as bright sources of hard x-ray pulses. *Phys. Rev. Lett.*, 90:115002, Mar 2003.

[16] A. S. Sandhu, A. K. Dharmadhikari, P. P. Rajeev, G. R. Kumar, S. Sengupta, A. Das, and P. K. Kaw. Laser-generated ultrashort multimegagauss magnetic pulses in plasmas. *Phys. Rev. Lett.*, 89:225002, Nov 2002.

[17] Donald Umstadter. Review of physics and applications of relativistic plasmas driven by ultra-intense lasers. *Physics of Plasmas*, 8(5), 2001.

[18] Max Tabak, James Hammer, Michael E. Glinsky, William L. Kruer, Scott C. Wilks, John Woodworth, E. Michael Campbell, Michael D. Perry, and Rodney J. Mason. Ignition and high gain with ultrapowerful lasers*. *Physics of Plasmas*, 1(5), 1994.

[19] A.J. Kemp, F. Fiuza, A. Debayle, T. Johzaki, W.B. Mori, P.K. Patel, Y. Sentoku, and L.O. Silva. Laser plasma interactions for fast ignition. *Nuclear Fusion*, 54(5):054002, 2014.

[20] V. Malka et al. *Nat. Phys.*, 4, 2008.

[21] M. Honda, A. Nishiguchi, H. Takabe, H. Azechi, and K. Mima. Kinetic effects on the electron thermal transport in ignition target design. *Physics of Plasmas*, 3(9):3420–3424, 1996.

[22] Andrey Komarov, Konstantin Komarov, Alioune Niang, and Fran çois Sanchez. Nature of soliton interaction in fiber lasers with continuous external optical injection. *Phys. Rev. A*, 89:013833, Jan 2014.

[23] A. S. Davydov. Solitons in molecular systems. *Phys. Scr.*, 20:3–4, 1979.

[24] Y. Tarik et al. Heavy solitons in a fermionic superfluid. *Nature*, 499:426–430, 2013.

[25] I. S. Aranson and L. Kramer. The world of the complex ginzburg-landau equation. *Rev. Mod. Phys*, 74:99–143, 2002.

[26] A. J. Heeger et al. Solitons in conducting polymers. *Rev. Mod. Phys*, 60:781–850, 1988.

[27] Trines et al. Spontaneous generation of self-organized solitary wave structures at earth's magnetopause. *Phys. Rev. Lett.*, 99:205006, Nov 2007.

[28] Sanat Kumar Tiwari, Amita Das, Abhijit Sen, and Predhiman Kaw. Molecular dynamics simulations of soliton-like structures in a dusty plasma medium. *Physics of Plasmas*, 22(3), 2015.

[29] P. Bandyopadhyay, G. Prasad, A. Sen, and P. K. Kaw. Experimental study of nonlinear dust acoustic solitary waves in a dusty plasma. *Phys. Rev. Lett.*, 101:065006, Aug 2008.

[30] P. K. Shukla and B. Eliasson. Nonlinear dynamics of large-amplitude dust acoustic shocks and solitary pulses in dusty plasmas. *Phys. Rev. E*, 86:046402, Oct 2012.

[31] P K Shukla and A A Mamun. Solitons, shocks and vortices in dusty plasmas. *New Journal of Physics*, 5(1):17, 2003.

[32] A. Barkan, R. L. Merlino, and N. DAngelo. Laboratory observation of the dust-acoustic wave mode. *Physics of Plasmas*, 2(10), 1995.

[33] Dust-acoustic waves in dusty plasmas. *Planetary and Space Science*, 38(4):543 – 546, 1990.

[34] J. Heinrich, S.-H. Kim, and R. L. Merlino. Laboratory observations of self-excited dust acoustic shocks. *Phys. Rev. Lett.*, 103:115002, Sep 2009.

[35] K. Stasiewicz. Theory and observations of slow-mode solitons in space plasmas. *Phys. Rev. Lett.*, 93, 2004.

[36] J.S. Pickett et al. Furthering our understanding of electrostatic solitary waves through cluster multispacecraft observations and theory. *Advances in Space Research*, 41(10):1666 – 1676, 2008.

[37] George I. Melikidze, Janusz A. Gil, and Avtandil D. Pataraya. The spark-associated soliton model for pulsar radio emission. *The Astrophysical Journal*, 544(2):1081, 2000.

[38] M. Borghesi, S. Bulanov, D. H. Campbell, R. J. Clarke, T. Zh. Esirkepov, M. Galimberti, L. A. Gizzi, A. J. MacKinnon, N. M. Naumova, F. Pegoraro, H. Ruhl, A. Schiavi, and O. Willi. Macroscopic evidence of soliton formation in multiterawatt laser-plasma interaction. *Phys. Rev. Lett.*, 88:135002, Mar 2002.

[39] P. K. Kaw, A. Sen, and T. Katsouleas. Nonlinear 1d laser pulse solitons in a plasma. *Phys. Rev. Lett.*, 68:3172–3175, May 1992.

[40] A. G. Litvak V. A. Kozlov and E. V. Suvorov.

[41] D. Jung, L. Yin, B. J. Albright, D. C. Gautier, R. Hörlein, D. Kiefer, A. Henig, R. Johnson, S. Letzring, S. Palaniyappan, R. Shah, T. Shimada, X. Q. Yan, K. J. Bowers, T. Tajima, J. C. Fernández, D. Habs, and B. M. Hegelich. Monoenergetic ion beam generation by driving ion solitary waves with circularly polarized laser light. *Phys. Rev. Lett.*, 107:115002, Sep 2011.

[42] N. M. Naumova, S. V. Bulanov, T. Zh. Esirkepov, D. Farina, K. Nishihara, F. Pegoraro, H. Ruhl, and A. S. Sakharov. Formation of electromagnetic postsolitons in plasmas. *Phys. Rev. Lett.*, 87:185004, Oct 2001.

[43] D. Strickland and G. Mourou. Compression of amplified chirped optical pulses. *Opt. Commun.*, 56:219–221, 1985.

[44] Thomas Katsouleas. Accelerator physics: Electrons hang ten on laser wake. *Nature*, 431:515–516, Sep2004.

[45] S. P. D. Mangles et al. Monoenergetic beams of relativistic electrons from intense laser-plasma interactions. *Nature*, 431:535–538, Sep2004.

[46] C. G. R. Geddes et al. High-quality electron beams from a laser wakefield accelerator using plasma-channel guiding. *Nature*, 431:538–541, Sep2004.

[47] J. Faure et al. A laser-plasma accelerator producing monoenergetic electron beams. *Nature*, 431:541–544, Sep2004.

[48] Xiaoming Wang et al. Quasi-monoenergetic laser-plasma acceleration of electrons to 2 gev. *Nature Communications*, 2013.

[49] A. Modena et al. Observation of raman forward scattering and electron acceleration in the relativistic regime. *IEEE TRANSACTIONS ON PLASMA SCIENCE*, 24:289– 95, 1996.

[50] W. B. Mori. The physics of the nonlinear optics of plasmas at relativistic intensities for short-pulse lasers. *IEEE JOURNAL OF QUANTUM ELECTRONICS*, 33:1942–1953, 1997.

[51] MORDECAI D. ROSEN and ROGER W. FALCONE MARGARET M. MURNANE, HENRY C. KAPTEYN. Ultrafast x-ray pulses from laser-produced plasmas. *Scienece*, 251:531–536, 1991.

[52] T. Zh. Esirkepov, F. F. Kamenets, S. V. Bulanov, and N. M. Naumova. Low-frequency relativistic electromagnetic solitons in collisionless plasmas. *Journal of Experimental and Theoretical Physics Letters*, 68(1):36–41, 1998.

[53] D. Farina and S. V. Bulanov. Relativistic electromagnetic solitons in the electron-ion plasma. *Phys. Rev. Lett.*, 86:5289–5292, Jun 2001.

[54] S. Poornakala, A. Das, P. K. Kaw, A. Sen, Z. M. Sheng, Y. Sentoku, K. Mima, and K. Nishikawa. Weakly relativistic one-dimensional laser pulse envelope solitons in a warm plasma. *Physics of Plasmas*, 9(9), 2002.

[55] Vikrant Saxena, Amita Das, Abhijit Sen, and Predhiman Kaw. Fluid simulation studies of the dynamical behavior of one-dimensional relativistic electromagnetic solitons. *Physics of Plasmas*, 13(3), 2006.

[56] Vikrant Saxena, Amita Das, Sudip Sengupta, Predhiman Kaw, and Abhijit Sen. Stability of nonlinear one-dimensional laser pulse solitons in a plasma. *Physics of Plasmas*, 14(7), 2007.

[57] Daniela Farina and Sergei V Bulanov. Dynamics of relativistic solitons. *Plasma Physics and Controlled Fusion*, 47(5A):A73, 2005.

[58] Sita Sundar, Amita Das, Vikrant Saxena, Predhiman Kaw, and Abhijit Sen. Relativistic electromagnetic flat top solitons and their stability. *Physics of Plasmas*, 18(11), 2011.

[59] Maurizio Lontano, Matteo Passoni, and Sergei V. Bulanov. Relativistic electromagnetic solitons in a warm quasineutral electron-ion plasma. *Physics of Plasmas*, 10(3), 2003.

[60] Predhiman K. Kaw, Kyoji Nishikawa, Yugo Yoshida, and Akira Hasegawa. Two-dimensional and three-dimensional envelope solitons. *Phys. Rev. Lett.*, 35:88–91, Jul 1975.

[61] J. Denavit, N. R. Pereira, and R. N. Sudan. Two-dimensional stability of langmuir solitons. *Phys. Rev. Lett.*, 33:1435–1438, Dec 1974.

[62] George Schmidt. Stability of envelope solitons. *Phys. Rev. Lett.*, 34:724–726, Mar 1975.

[63] C. Joshi, T. Tajima, J. M. Dawson, H. A. Baldis, and N. A. Ebrahim. Forward raman instability and electron acceleration. *Phys. Rev. Lett.*, 47:1285–1288, Nov 1981.

[64] C. J. McKinstrie and R. Bingham. Stimulated raman forward scattering and the relativistic modulational instability of light waves in rarefied plasma. *Physics of Fluids B*, 4(8), 1992.

[65] V. K. Tripathi and C. S. Liu. Raman backscattering in laser wake-field and beat-wave accelerators. *Physics of Fluids B*, 3(2), 1991.

[66] T. W. Huang, C. T. Zhou, A. P. L. Robinson, B. Qiao, H. Zhang, S. Z. Wu, H. B. Zhuo, P. A. Norreys, and X. T. He. Mitigating the relativistic laser beam filamentation via an elliptical beam profile. *Phys. Rev. E*, 92:053106, Nov 2015.

[67] S. Guerin, G. Laval, P. Mora, J. C. Adam, A. Heron, and A. Bendib. Modulational and raman instabilities in the relativistic regime. *Physics of Plasmas*, 2(7), 1995.

[68] Decker et al. The evolution of ultra-intense, short-pulse lasers in underdense plasmas. *Physics of Plasmas*, 3(5), 1996.

[69] W. B. Mori, C. Joshi, J. M. Dawson, D. W. Forslund, and J. M. Kindel. Evolution of self-focusing of intense electromagnetic waves in plasma. *Phys. Rev. Lett.*, 60:1298–1301, Mar 1988.

[70] T. Katsouleas and W. B. Mori. Wave-breaking amplitude of relativistic oscillations in a thermal plasma. *Phys. Rev. Lett.*, 61:90–93, Jul 1988.

[71] H. H. Kuehl and C. Y. Zhang. One-dimensional, weakly nonlinear electromagnetic solitary waves in a plasma. *Phys. Rev. E*, 48:1316–1323, Aug 1993.

[72] R. N. Sudan, Y. S. Dimant, and O. B. Shiryaev. One-dimensional intense laser pulse solitons in a plasma. *Physics of Plasmas*, 4(5), 1997.

[73] P. Kaw and J. Dawson. *Phys. Fluids*, 13, 1970.

[74] A.I. Akhiezer and R.V. Polovin. *Sov. Phys. JETP*, 3:696, 1956.

[75] J.P. Boris, A.M. Landsberg, E.S. Oran, and J.H. Gardner. Lcpfct - a flux-corrected transport algorithm for solving generalized continuity equations. Technical Report NRL Memorandum Report 93-7192., Navel Research Laboratory, 1993.

[76] H.C. Le, J. Vuillon, D. Zeitoun, W. Marine, M. Sentis, and R.W. Dreyfus. 2d modeling of laser-induced plume expansion near the plasma ignition threshold. *Applied Surface Science*, 96:76 – 81, 1996.

[77] Kyoungjin Kim. Time-dependent one-dimensional modeling of pulsed plasma discharge in a capillary plasma device. *IEEE Transactions on Plasma Science*, 31(4):729 – 735, 2003.

[78] Sanat Kumar Tiwari, Amita Das, Predhiman Kaw, and Abhijit Sen. Observation of sharply peaked solitons in dusty plasma simulations. *NJP*, 14(6):063008, 2012.

[79] Sudip Sengupta Ratan Kumar Bera and Amita Das. Fluid simulation of relativistic electron beam driven wakefield in a cold plasma. *POP*, 22(073109), 2015.

[80] J. F. Drake, P. K. Kaw, Y. C. Lee, G. Schmid, C. S. Liu, and Marshall N. Rosenbluth. Parametric instabilities of electromagnetic waves in plasmas. *Physics of Fluids*, 17(4), 1974.

[81] W. B. Mori, C. D. Decker, D. E. Hinkel, and T. Katsouleas. Raman forward scattering of short-pulse high-intensity lasers. *Phys. Rev. Lett.*, 72:1482–1485, Mar 1994.

[82] A. S. Sakharov and V. I. Kirsanov. Theory of raman scattering for a short ultrastrong laser pulse in a rarefied plasma. *Phys. Rev. E*, 49:3274–3282, Apr 1994.

[83] W. Press et al. Numerical recipes: The art of scientific computing. *Cambridge University Press*, 1992.

[84] Deepa Verma, Amita Das, Predhiman Kaw, and Sanat Kumar Tiwari. The study of electromagnetic cusp solitons. *Physics of Plasmas*, 22(1), 2015.

[85] M. S. Sodha, Tarsem Singh, D. P. Singh, and R. P. Sharma. Growth of laser ripple in a plasma and its effect on plasma wave excitation. *Physics of Fluids*, 24(5), 1981.

[86] M. S. Sodha and V. K. Tripathi. Steady-state self-focusing and filamentation of whistlers in a plasma. *Journal of Applied Physics*, 48(3), 1977.

[87] P. Kaw, G. Schmidt, and T. Wilcox. Filamentation and trapping of electromagnetic radiation in plasmas. *Physics of Fluids*, 16(9), 1973.

[88] Andrew J. Schmitt. Three-dimensional filamentation of light in laser plasmas. *Physics of Fluids B*, 3(1), 1991.

[89] Eduardo M. Epperlein. Kinetic theory of laser filamentation in plasmas. *Phys. Rev. Lett.*, 65:2145–2148, Oct 1990.

[90] Z. M. Sheng, K. Nishihara, T. Honda, Y. Sentoku, K. Mima, and S. V. Bulanov. Anisotropic filamentation instability of intense laser beams in plasmas near the critical density. *Phys. Rev. E*, 64:066409, Nov 2001.

[91] J.F.M. BLAZQUEZ. Application of solitons to the study of laser propagation into a thermonuclear plasma in inertial confinement fusion. *Laser and Particle Beams*, 20:153âĂŞ157, 2001.

[92] John M. Dawson. Particle simulation of plasmas. *Rev. Mod. Phys.*, 55:403–447, Apr 1983.

[93] C.K. Birdsall and A.B Langdon. Plasma physics via computer simulation. 1985.

[94] K. Friedrichs R. Courant and H. Lewy. *Math. Ann*, 100, 1928.

[95] Roger W.; James W. Eastwood Hockney. Computer simulation using particles. 1981.